THE INFLUENCE OF FINITE BANDWIDTH ACTUATORS ON RAIL VEHICLE ACTIVE SUSPENSIONS

by

FORREST T. BUZAN

B.S., University of Illinois, Urbana-Champaign
(1980)

SUBMITTED TO THE DEPARTMENT OF
MECHANICAL ENGINEERING IN PARTIAL
FULFILLMENT OF THE REQUIREMENTS
FOR THE DEGREE OF

MASTER OF SCIENCE IN
MECHANICAL ENGINEERING

at the

MASSACHUSETTS INSTITUTE OF TECHNOLOGY

July 1982

Signature of Author.....
Department of Mechanical Engineering
July 10,1982

Certified by.....
J. Karl Hedrick
Thesis Supervisor

Accepted by.....
Warren M. Rohsenow
Chairman, Departmental Graduate Committee

THE INFLUENCE OF FINITE BANDWIDTH ACTUATORS ON RAIL VEHICLE ACTIVE SUSPENSIONS

by

FORREST T. BUZAN

Submitted to the Department of Mechanical Engineering
on June 8, 1982 in partial fulfillment of the
requirements for the Degree of Master of Science
in Mechanical Engineering.

ABSTRACT

The performance requirements and design of an active suspension system for passenger rail vehicles are investigated. Consideration is given to lateral ride quality, suspension stroke, and active power consumption, using an Amcoach vehicle for a baseline model. Results of field measurements are presented showing the current ride to be dominated by one hertz vibrations attributed to secondary suspension vibrational modes.

Modeling the actuators' dynamics as first order lags, a frequency domain study using a linear, fifteen degree-of-freedom vehicle model shows a three hertz actuator bandwidth to provide sufficient response speed for active ride quality control. This model also provides estimates of the actuators' performance requirements, including peak forces needed and maximum strokes.

A pneumatic actuator suspension system design is presented. Digital simulations of the system's performance show it to imitate an ideal actuator, but predict larger power consumption rates than predicted for a hydraulic actuator.

Thesis Supervisor: J. Karl Hedrick
Title: Associate Professor of Mechanical Engineering

ACKNOWLEDGEMENTS

The author would like to express his deepest appreciation to all those whose friendship and advice made his stay at M.I.T. both educational and enjoyable. Many thanks to:

The U.S. Department of Transportation's Office of University Research who sponsored this work under contract number DTRS5680-C-00018,

Professor J. Karl Hedrick, who supervised this work, ever mindful of the "bottom line" results and concerned with our ability to "say something smart,"

Professor David N. Wormley, who continually amazed me with his working knowledge of everything we tackled and who sacrificed his own flesh to collect data on the Northeast Corridor,

Leslie Regan for typing this thesis and for her insight to life at M.I.T.

Herb Pomeroy and the M.I.T. Festival Jazz Ensemble (the Bebop Professor and his Scientists),

all the members, past, present, and future, of the V.D. Laboratory; especially to:

George Celniker whose work clearly preceded this work and who led me into the world of tennis racket testing,

Long Chain Chen and Dan Cho
good luck in extending this analysis,

Gerald Melsky with whom I shared much coffee, coke, and speculation in the last months of this thesis,

Mark Nagurka, the old man of the lab, whose humor allowed us all to continue...laughing,

Mary Ann Partridge, my "passive" partner in this project who shared the burden of all my traumata here at M.I.T. and tolerated all of our jokes.

Mostly, though, I wish to thank my sisters and brother, and my mother for their love and support and my late father, to whom I dedicate this work on trains.

TABLE OF CONTENTS

LIST OF FIGURES

LIST OF FIGURES (cont.)

LIST OF FIGURES (cont.)

LIST OF TABLES

CHAPTER 1

INTRODUCTION

This thesis presents an analysis of an active suspension system for passenger rail vehicles. It examines the effect of actuator dynamics on the implementation of a lateral suspension active control scheme to an Amcoach passenger rail vehicle, and presents the design and simulation of a pneumatic actuator system.

1.1 Background

The success of any transportation system is dependent on many factors. These include cost, trip time, frequency of operation, and "ride quality". "Ride quality" refers to the physical comfort of the passengers and results from such things as compartment temperature, noise, roominess, and ride roughness [1]. Of these factors, cost, trip time, and ride roughness are all related, at least partially, to suspension design.

The suspension system of a rail vehicle must support the weight of the vehicle and force it to follow the general movement of the track, while isolating it from the track's roughness. Thus enters one of the classic trade-offs of suspension design: while a stiff suspension is preferred for following the guideway, a soft suspension is best to isolate the vehicle from vibrations, which ruin ride quality. This is known as the ride quality-suspension stroke trade-off, since a soft suspension yields low accelerations and a good ride, and a stiff suspension yields small suspension strokes and good tracking [2,3,4].

The elements of the conventional rail vehicle suspension are shown in Figure 1.1.1. This suspension can be broken up into two parts: the primary suspension, which connects the wheelsets to the trucks, and the secondary suspension, between the trucks and the carbody. Modeled as linear springs and dampers, these elements create forces dependent on the relative motion of the masses they connect and can only store and dissipate energy; hence, this is referred to as a "passive" suspension. This work was concerned only with lateral ride quality, thus only those elements which are related to the lateral motion were included.

The desire to increase speeds, and thus reduce trip times, makes the suspension design all the more difficult. At higher speeds the ride becomes harsher and the secondary suspension stroke becomes larger. The ride quality further decreases when the large strokes cause the "bump-stops" to be contacted [5]. These nonlinear elements were designed as safety features to limit the maximum secondary stroke to $1\frac{1}{2}$ inches, thus preventing carbody contact with objects close to the right of way. Their presence increases the need to avoid large secondary strokes.

Attempts to "beat" the ride quality-stroke trade-off at higher speeds led to the proposal of active suspension elements [4,6,7,8,9,10] Active suspensions are not restricted to generating forces in response to local relative displacements and velocities, as are passive suspensions, but can instead be driven by signals from any states or combinations of states that can be measured. Furthermore, they have the capacity to add power to the system, rather than simply store it for latter use or dissipate it [11].

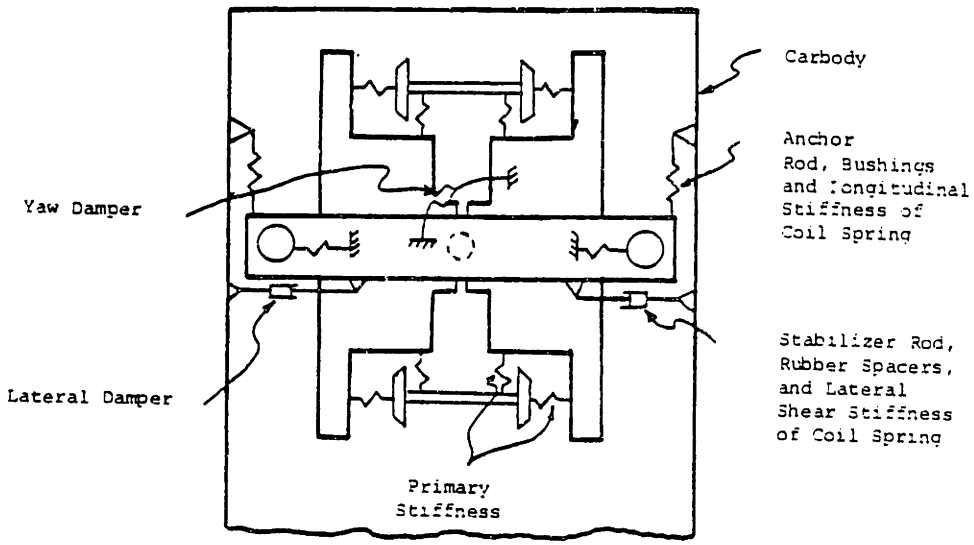

a. Plan View

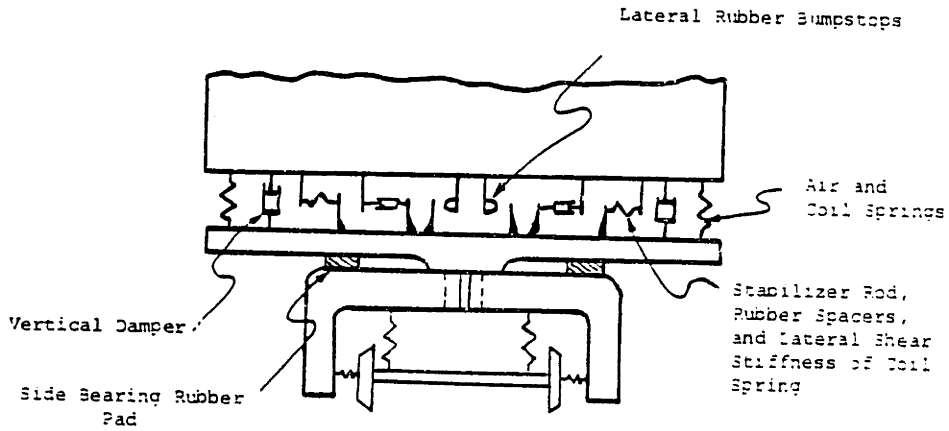

b. Rear View

FIGURE 1.1.1: SUSPENSION ELEMENTS OF PIONEER III TRUCKS

The use of active suspensions requires additional equipment such as sensors, signal processors, actuators, and power sources. A new trade-off is encountered as increased ride quality must be balanced against the active consumption of power.

Celniker [4] developed active feedback schemes for controlling the truck-wheelset hunting mode and the lateral, roll, and yaw carbody vibrational modes by using an active suspension in parallel with a conventional secondary. The stability controller used the lateral and yaw velocities of the trucks as active controller inputs to generate active torques within the secondary suspension to control hunting. His 'local' ride controller generated lateral forces in the secondary proportional to the carbody accelerations and velocities measured over each truck. This controller was used to reduce lateral vibrations of the car. At high speeds (185 mph) both controllers were needed to improve the ride quality, as an uncontrolled hunting motion was sufficiently large to affect the carbody motion. At more moderate speeds (100 mph) the local controller was adequate for ride quality improvement.

1.2 Scope and Objectives

While Celniker's study [4] assumed ideal actuator response, this work addresses the effects of actuator dynamics on the implementation of Celniker's local controller to a rail vehicle. The vehicle model parameters were chosen to match those of an Amtrak vehicle operating on the Northeast Corridor.

Ride quality testing was performed to examine the ride quality and secondary stroke of the baseline vehicle; Chapter 2 presents the details and results of these tests.

Using a high order, linear vehicle model, Chapter 3 evaluates the active system performance with the actuators' dynamics modeled as first order lags. Actuator performance requirements are determined and actuator system types are discussed.

Chapter 4.0 presents the design, modeling, and simulation of a pneumatic actuator system. Nonlinear valve dynamics require time domain, digital simulations; therefore, a low order model with only one vehicle degree of freedom was used.

Implementation concerns are investigated in Chapter 5.0, including power consumption and valve saturation. Failure analysis of the actively controlled vehicle is also presented.

Chapter 6 summarizes the study of actuator dynamics and their effect on the active suspension system performance.

Appendix A contains the equations of motion for the fifteen d.o.f. passive vehicle model. The active element matrices for active augmentation of that model are contained in Appendix B. Appendices C, D, & E presents the FORTRAN subroutines used for the valve simulations of Chapters 4.0 and 5.0.

CHAPTER 2

RIDE QUALITY TESTS

2.1 Introduction

The ride quality of a rail vehicle is typically measured in terms of the vibrational acceleration experienced by the passengers and cargo [1]. Testing was performed for the purpose of identifying the ride quality characteristics of the Amcoach passenger car. Relative motion between the car and leading truck was measured, as well as the lateral and vertical accelerations at several points in the car. The recorded signals were later analyzed for frequency content.

2.2 Test Plan and Equipment

The test, performed on the Northeast Corridor between Washington, D.C. and Boston, Massachusetts, required two days of instrumenting the test vehicle at the Amtrak Maintenance Shop (Figure 2.2.1) in Wilmington, Delaware, and one day of testing. The testing was coordinated through Ed Lombardi; Chief Test Engineer for Amtrak.

The test purpose was to measure the vertical acceleration at the four corners of the car, as well as at the center, and to measure the lateral acceleration at the center and at both ends (Figure 2.2.2). This made the calculation of both linear and angular carbody accelerations possible from the data. Table 2.2.1 lists the major equipment used on the trip. The 3-axis accelerometer package was placed at the center of the car, while the 6-axis accelerometer package was disassembled to allow the accelerometers to be placed at both extremes of

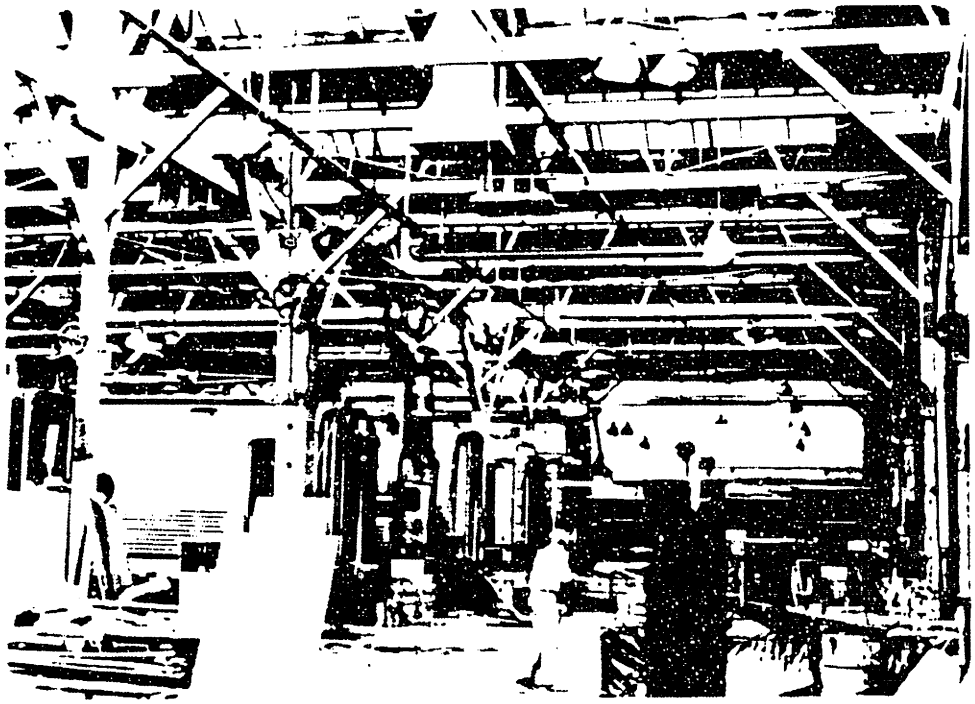

a) Repair Facility

b) Welding of String Pot Brackets

FIGURE 2.2.1: VEHICLE PREPARATION AT AMTRAK MAINTENANCE FACILITY, WILMINGTON, DELAWARE

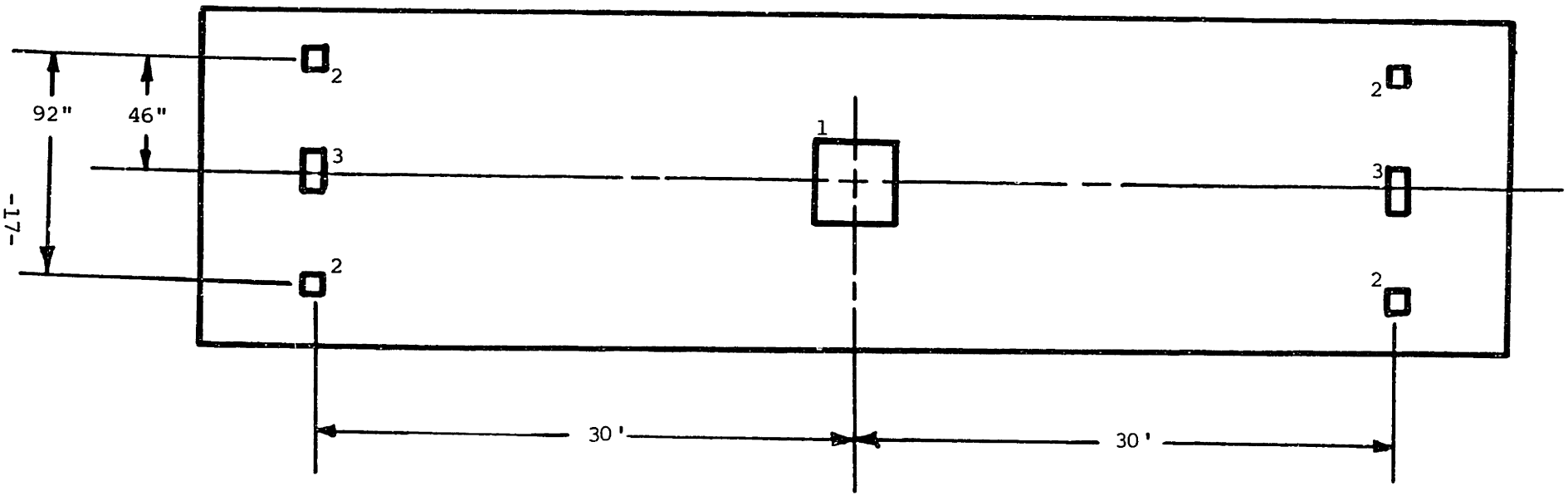

1. 3-Axis Accelerometer Package
2. Vertical Accelerometers
3. Horizontal Accelerometers

FIGURE 2.2.2: ACCELEROMETER LOCATIONS

TABLE 2.2.1: MAJOR EQUIPMENT USED IN RIDE QUALITY TESTS

TRANSDUCERS

6 individual accelerometers (TSC equipment)

3-axis accelerometer package (TSC)

4 string pots, displacement measurement (AMTRAK)

British Rail "Ridemeter" (Amtrak)

Slip ring velocity indicator (Amtrak)

Wheel/Rail Profilometer (MIT)

SIGNAL CONDITIONING

Analog filters, low pass (TSC & MIT)

Signal conditioning amplifiers (MIT)

Operational Amplifiers (MIT)

RECORDING

14-channel F.M. tape recorder (Amtrak)

6-channel strip chart recorder (Amtrak)

the car. Accelerometer signals were filtered before being recorded on a 14-channel F.M. Honeywell tape recorder, as shown in the Data Acquisition Plan (Figure 2.2.3).

The relative motion of the truck and carbody was measured with string pots (displacement transducers) located between the bolster and brackets welded to the carbody (Figure 2.2.4). No filtering was required for these signals, although a signal conditioner was used to attenuate the signal level before recording.

Also recorded was the forward velocity, as measured by an axle slip ring. Calibration was checked against mile markers while in-route.

A strip chart recorder was used to monitor the equipment while testing (Figure 2.2.5). Tape footage and time were marked on the strip chart and also on the voice track of the tape recorder to aid later in processing the data. Also recorded on the strip chart, for reference purposes, was the output of a British Ridemeter. This instrument matches a ride index to frequency weighted acceleration measurements.

Other than the speed signal and the British Ridemeter Output, the strip chart levels were uncalibrated and used only to monitor relative values. After changing tapes, for example, the recording head was left out. This was noticed only since no signals appeared on the strip chart recorder. The failure of a string pot was noticed shortly afterward when the strip chart output went to zero for that channel.

Once back at M.I.T., the hard copy output was used to locate long

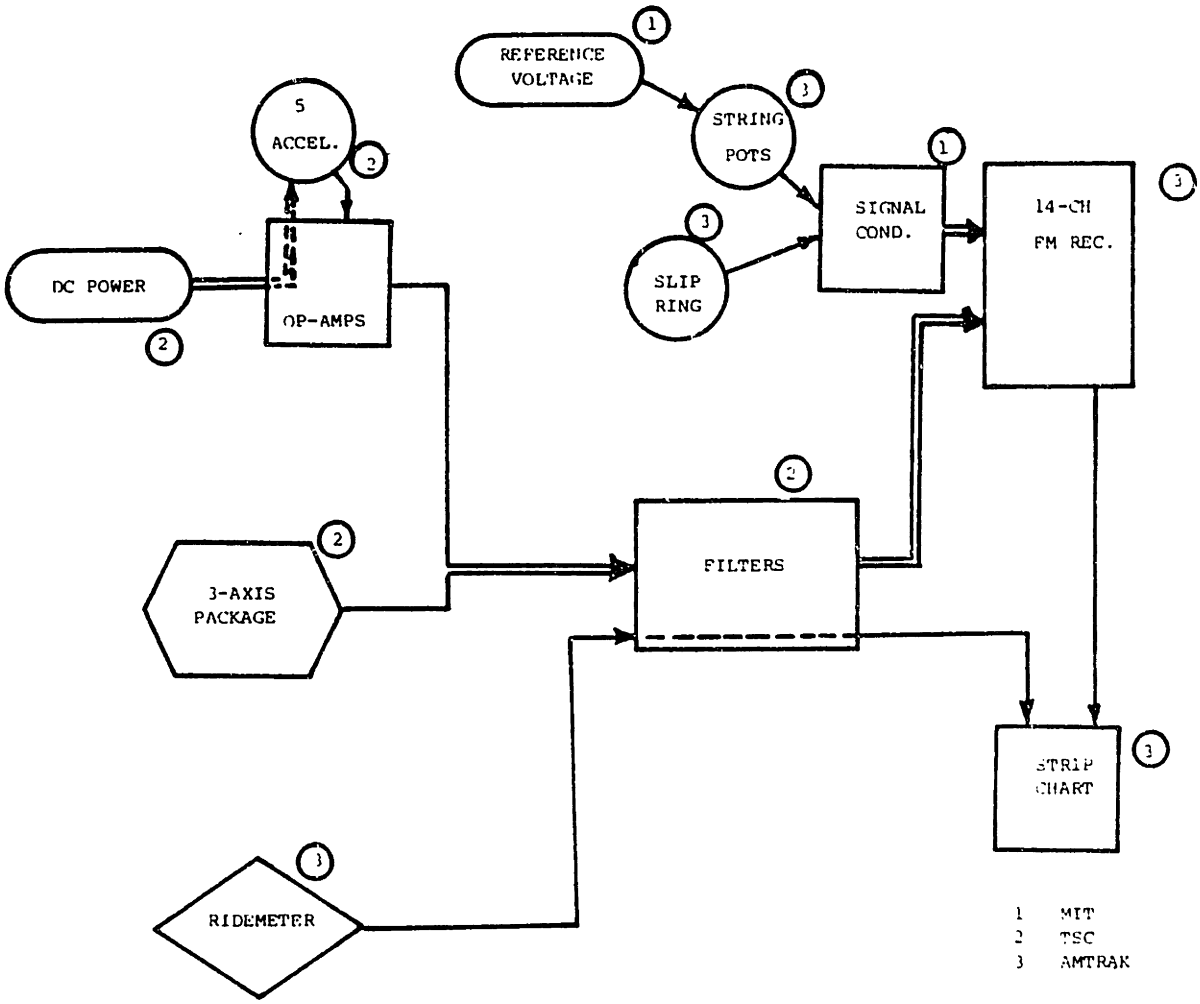

FIGURE 2.2.3: DATA ACQUISITION PLAN

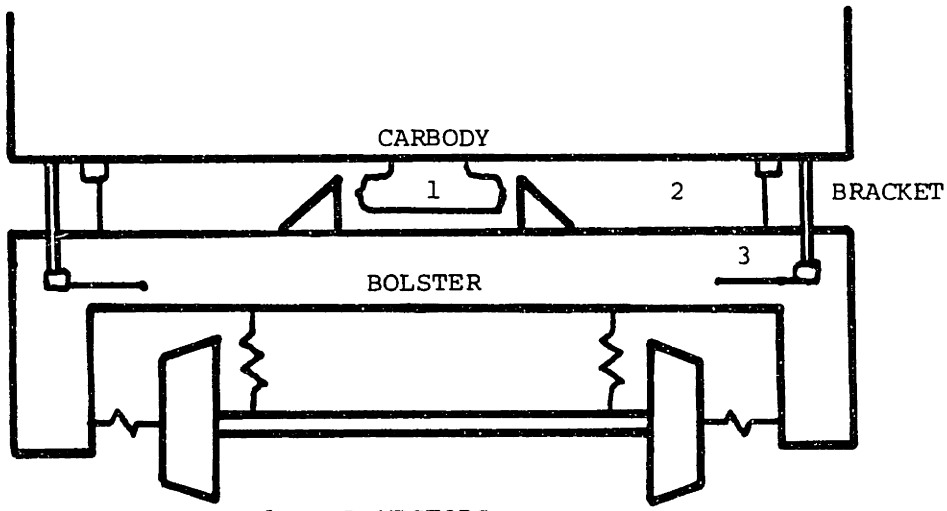

1. BUMPSTOPS
2. VERTICAL STRING POT
3. LATERAL STRING POT

FIGURE 2.2.4: STRING POT LOCATIONS

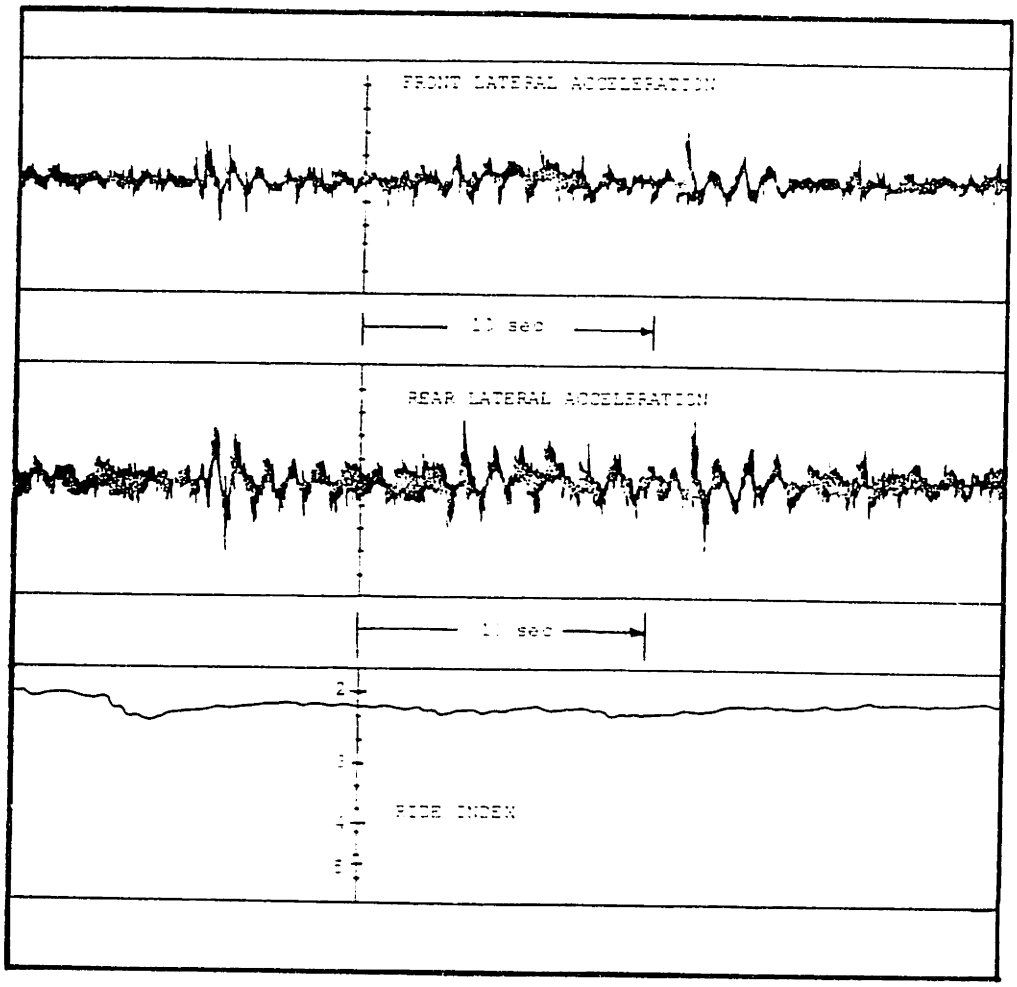

FRONT LATERAL ACCELEROMETER
REAR LATERAL ACCELEROMETER
BRITISH RIDEMETER

FIGURE 2.2.5: SAMPLE STRIP CHART RECORDER OUTPUT
(a) Accelerometers and Ridemeter

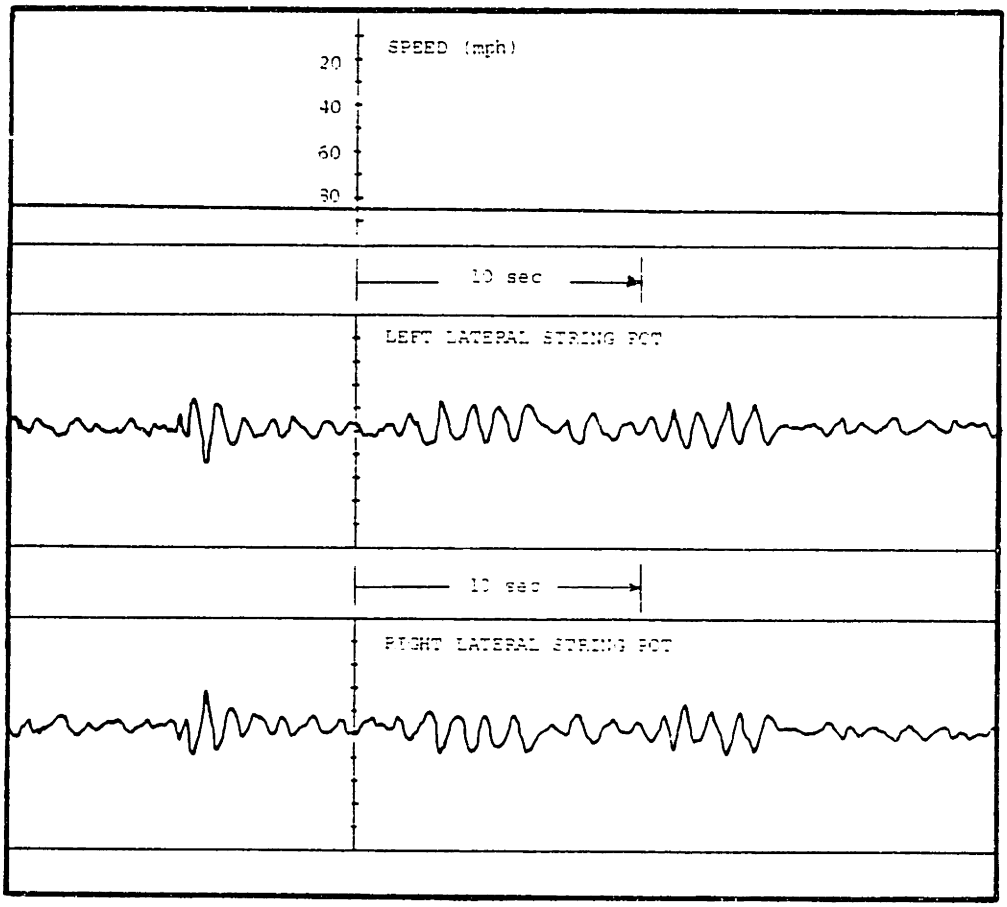

SPEED (64 mph)

LEFT LATERAL STRING POT

RIGHT LATERAL STRING POT

FIGURE 2.2.5 (cont.): SAMPLE STRIP CHART RECORDER OUTPUT
(b) Speed and String Pots

periods of stationary, random vibrations by visual inspection.

Figure 2.2.6 shows the placement of the equipment at the center of the car. Several rows of seats where removed to make room for the equipment, and plywood sheets were placed on tope of seats to create work tables.

Vertical and horizontal accelerometers are shown mounted on steel plates in Figures 2.2.7(a) and (b), respectively. Figures 2.2.8(a) and (b) show how the vertical and lateral string pots were mounted.

After the test run the car was moved to the South Boston Maintenance Facility. Equipment was removed from the car the following day and measurements were taken of the string pot placement. Wheel and rail profiles were recorded using a profilometer built at M.I.T. (Figure 2.2.9).

2.3 Experimental Results

The experimental data collected during the trip was processed later at M.I.T. The wheel profiles were taken on the Amcoach in the tests, the rail profile used is representative of a new rail head. The measured wheel-rail profiles were used to generate rolling radius and contact angle plots. Both are shown in Figures 2.3.1 and 2.3.2 as a function of wheelset displacement (y_w). The accelerations and string pot measurements were digitized and analyzed for frequency content on a Hewlett-Packard Structural Dynamics Analyzer.

Figure 2.3.1 shows the variation of the left and right rolling radii with the lateral wheelset excursion. In the tread region the

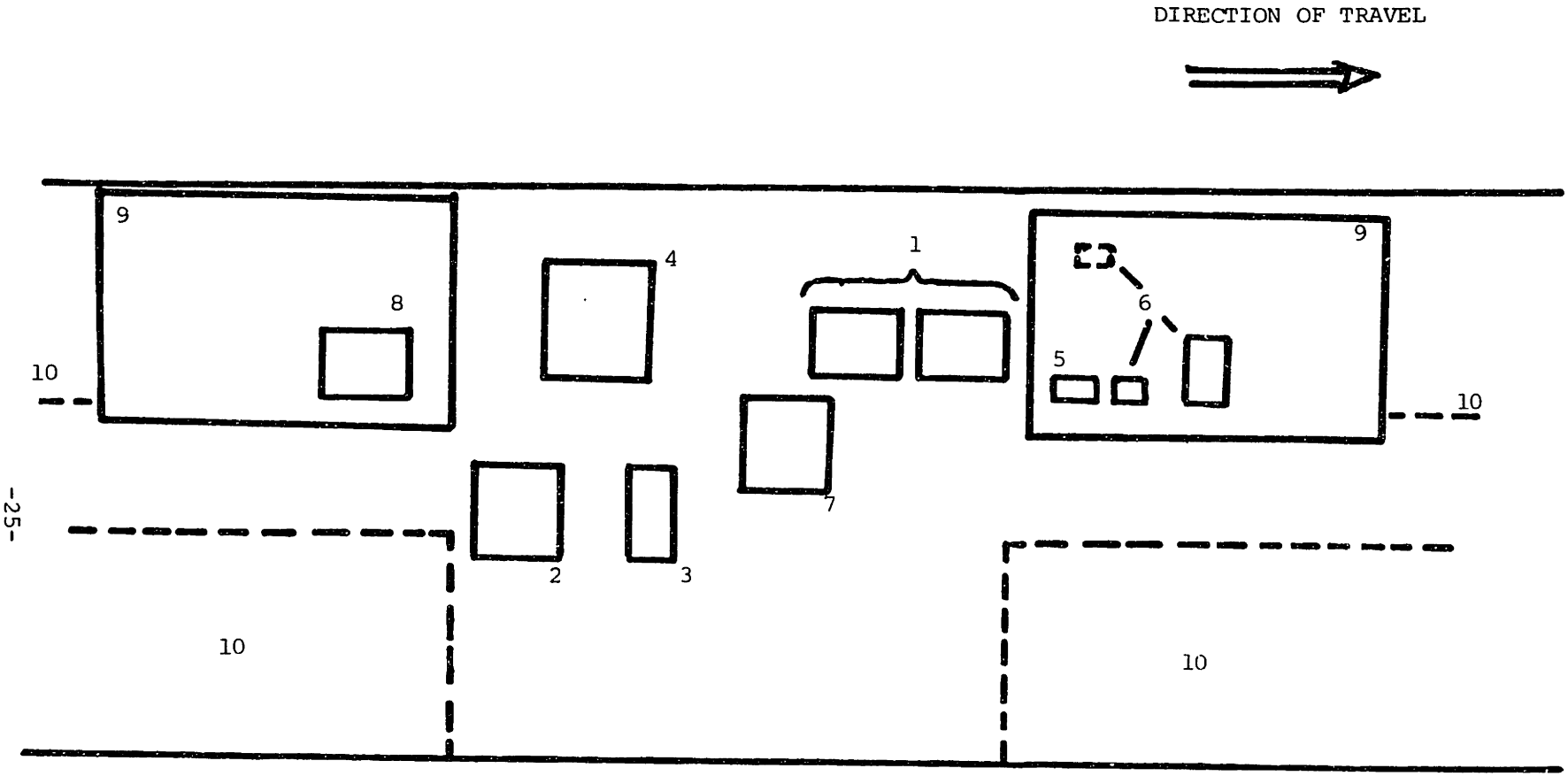

1. Filters
2. 3-Axis Package
3. British Ridemeter
4. Signal Conditioner
5. Operational Amplifiers
6. Power Supplies
7. FM Recorder
8. Strip Chart
9. Work Tables
10. Seats

FIGURE 2.2.6: EQUIPMENT LOCATION

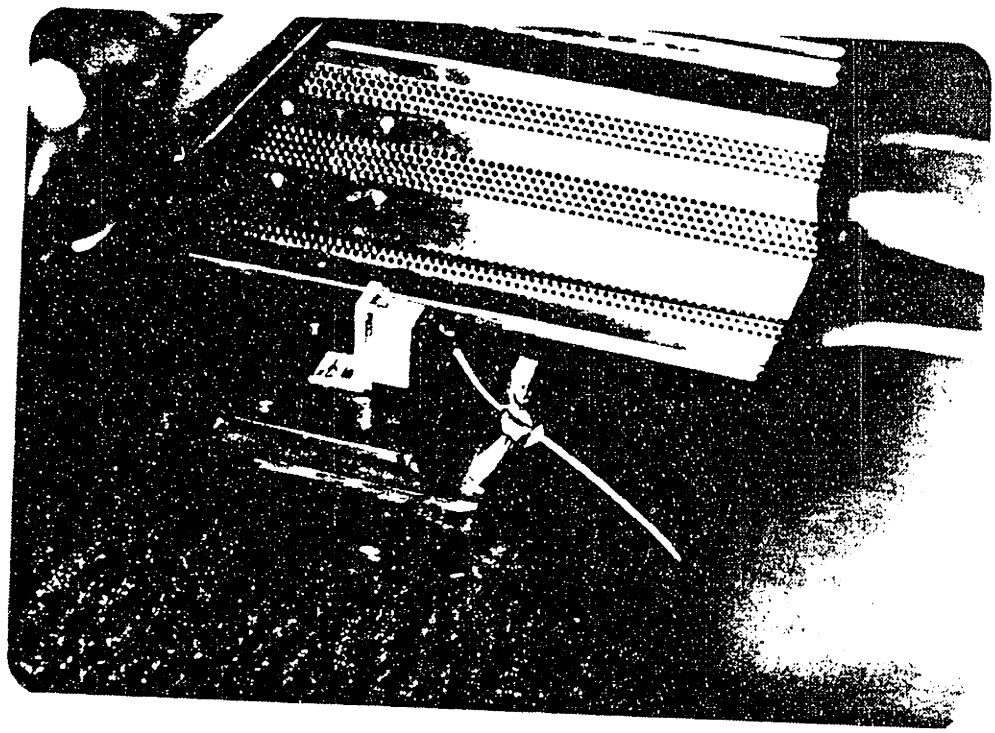

(a) Vertical

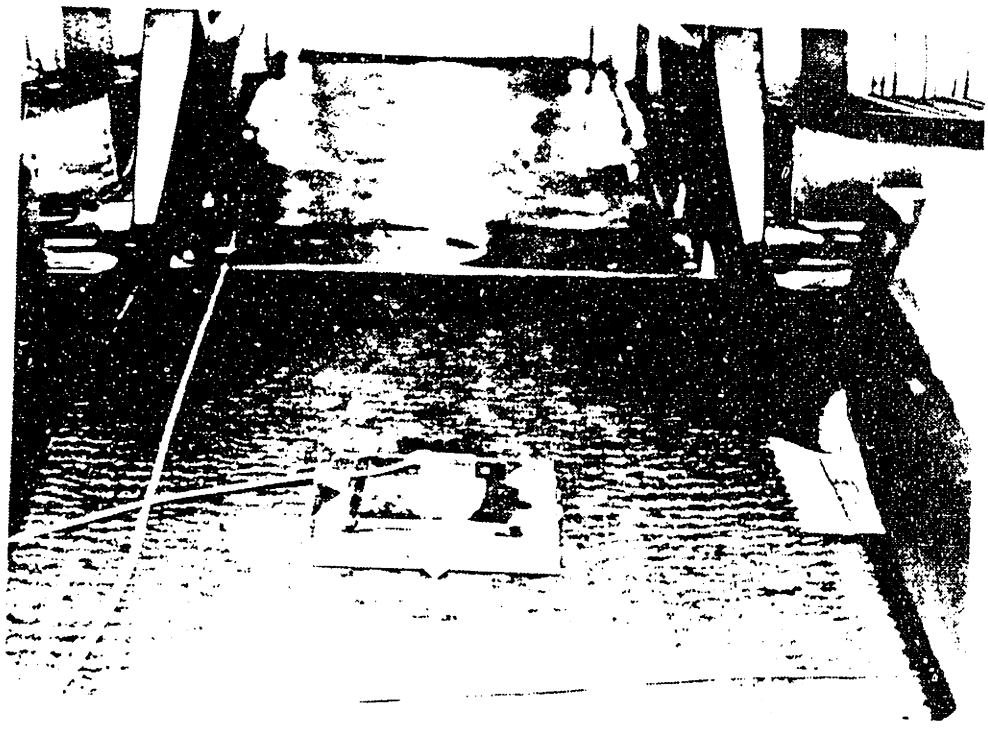

(b) Lateral

FIGURE 2.2.7: ACCELEROMETER MOUNTINGS OVER TRUCKS

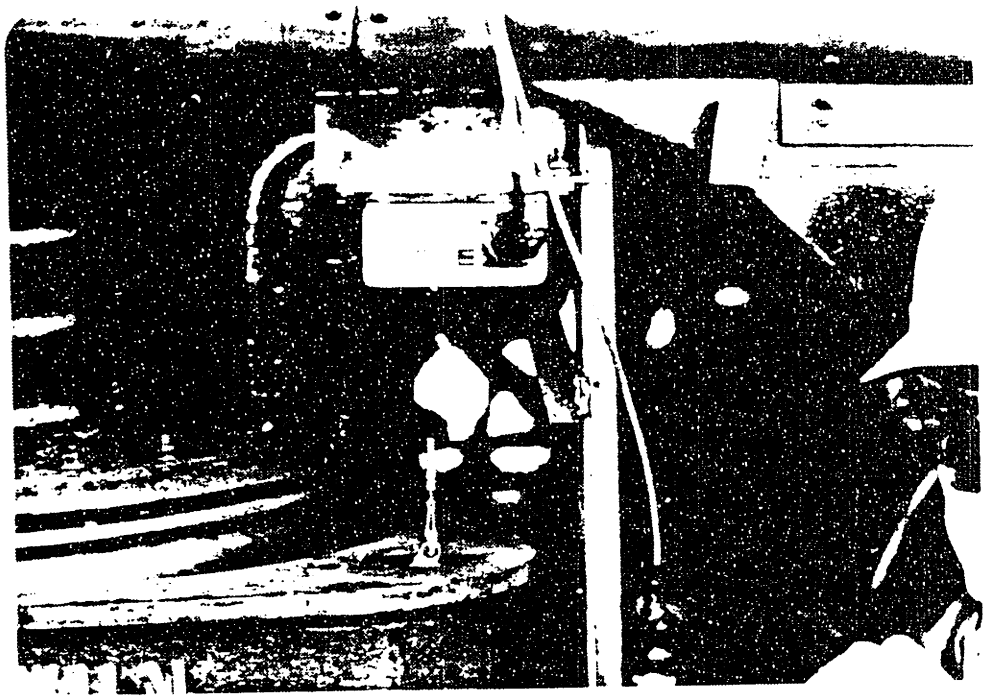

(a) Vertical

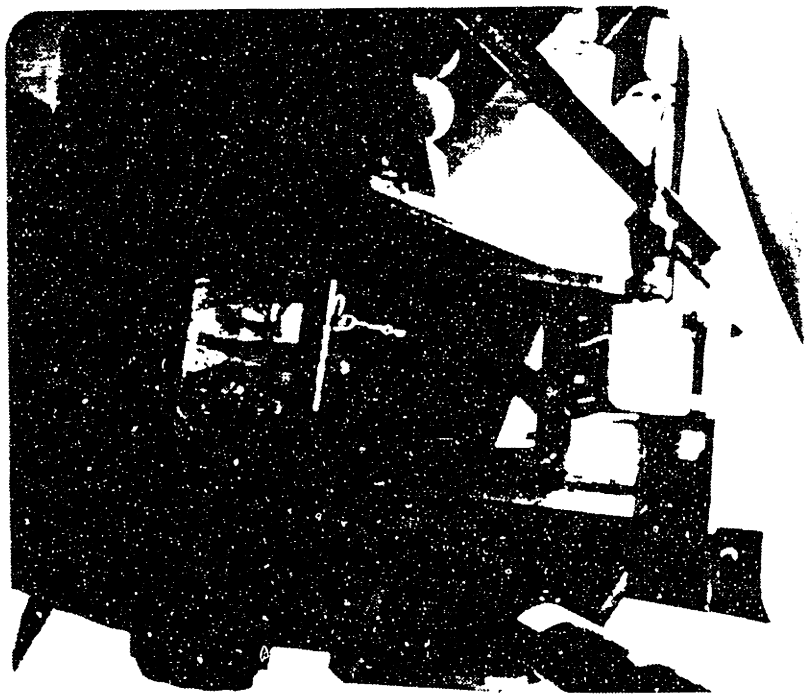

(b) Lateral

FIGURE 2.2.8: STRING POT MOUNTINGS

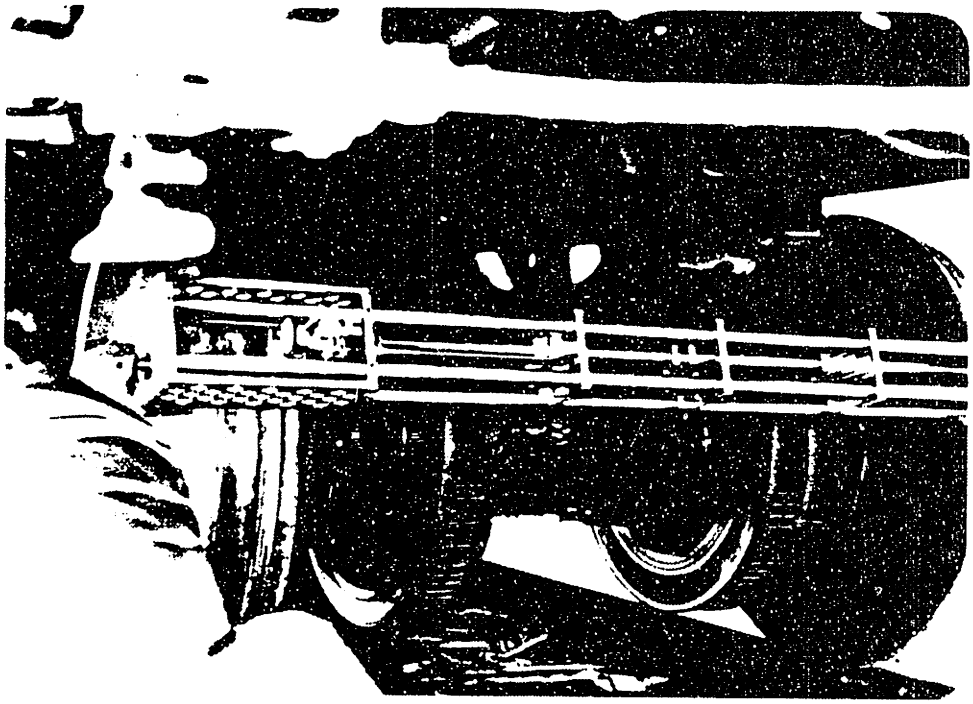

FIGURE 2.2.9: MIT WHEEL/RAIL PROFILOMETER

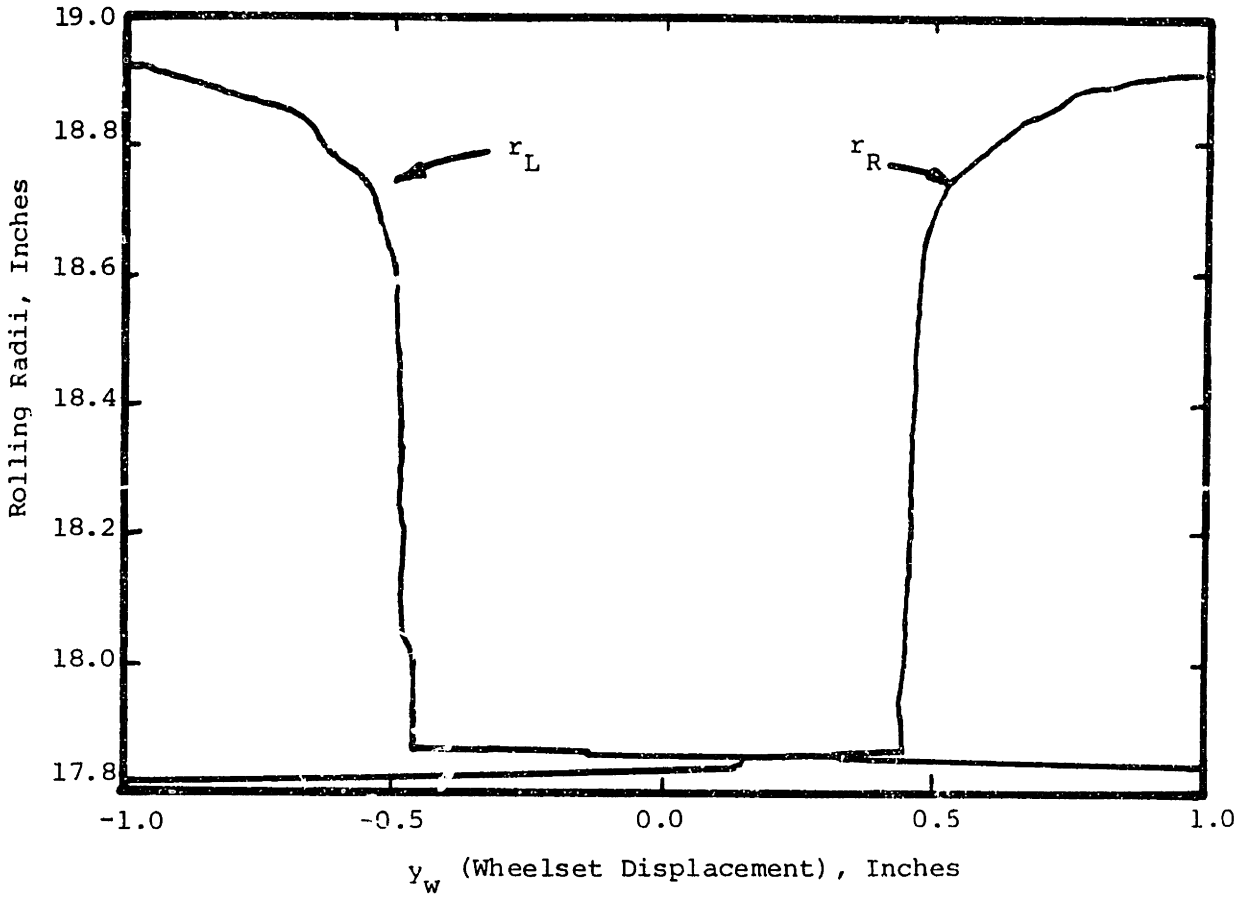

FIGURE 2.3.1: ROLLING RADII VS. WHEELSET DISPLACEMENT

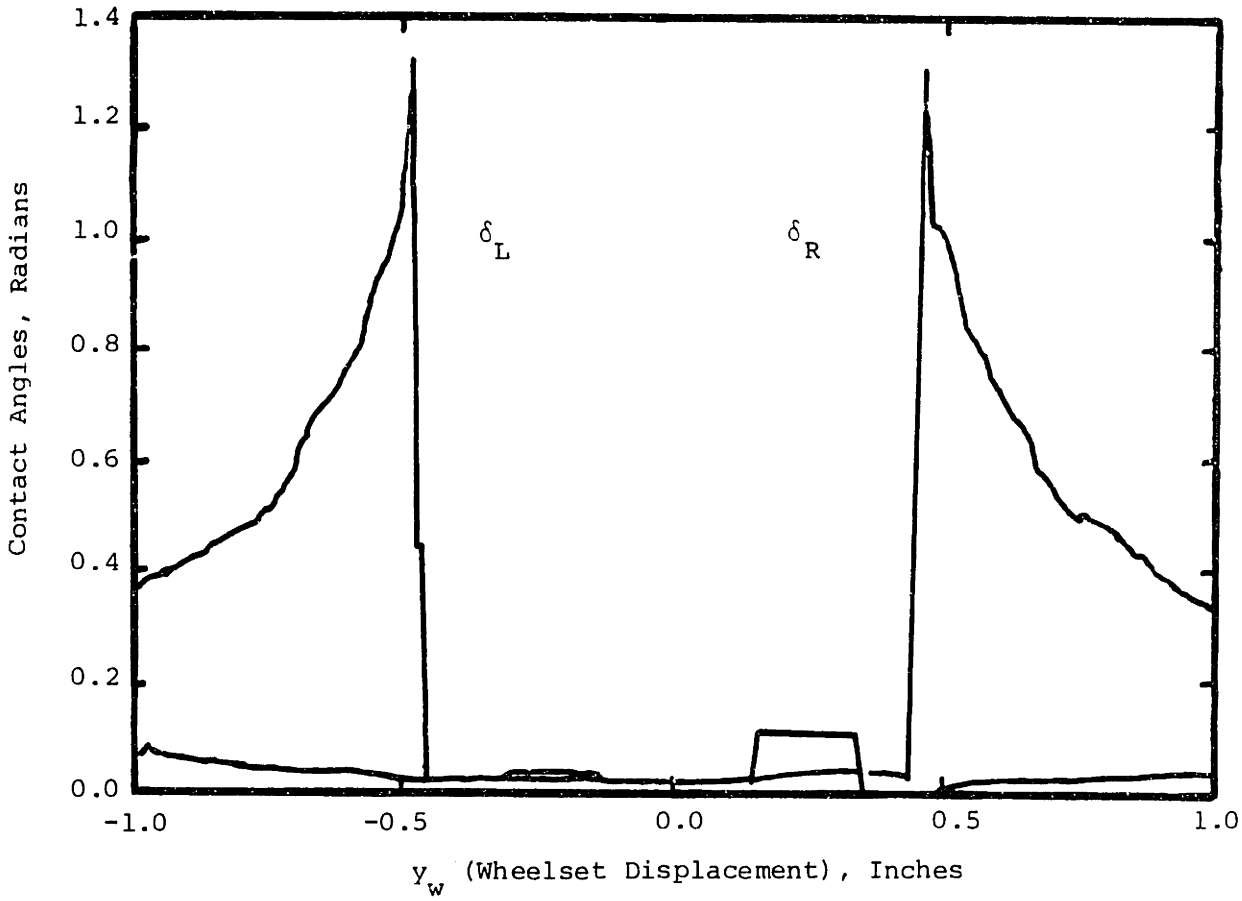

FIGURE 2.3.2: CONTACT ANGLE VS WHEELSET DISPLACEMENT

radii change linearly when the wheelset is displaced. The conicity, λ, for the tread region can be calculated using the relationship [2],

$$\lambda = \frac{r_L - r_R}{2y_w} . \qquad (2.3.1)$$

Averaging the values of λ calculated for each of the two extremes of the tread, an average λ of .025 was found. However, if the wheelset ventures more than about 0.46 inches the effective conicity will increase drastically.

The contact angle linearization constant, Δ_1, is defined as

$$\Delta_1 = \frac{\delta_L - \delta_R}{2y_w} a. \qquad (2.3.2)$$

Figure 2.3.2 shows the variation of contact angles with wheelset excursion. In the tread region one can see that, although an accurate estimation of Δ_1 is difficult, the difference between the two contact angles is consistently small. Thus, Δ_1 is effectively zero in the linear mathematical model used.

The Power Spectral Densities presented were processed from two sections of data: one strip at 80 miles per hour, recorded between Baltimore, MD and Wilmington, DL and the other at 60 mph, recorded between New Haven, CT and Boston, MA. Plots are presented in both linear scale and log-log formats. The PSD's are the result of averaging 20 statistically-independent samples with a resolution of 0.20 Hz.

Figure 2.3.3 shows the PSD for the rear lateral acceleration at 80 mph. Note that most of the power (the area under a linear scale psd)

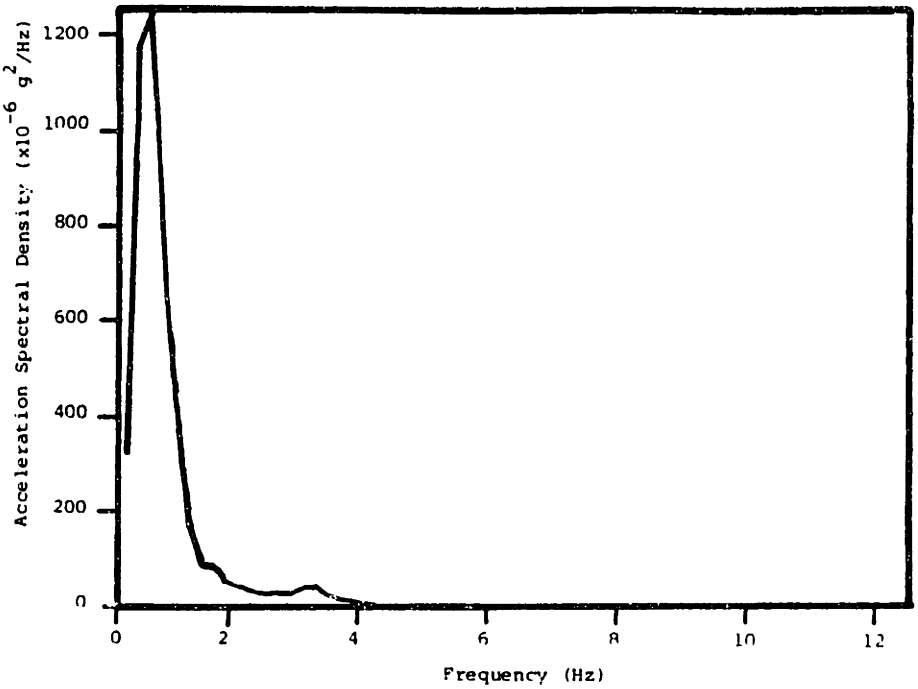

FIGURE 2.3.3: REAR LATERAL ACCELERATION SPECTRAL DENSITY (80 mph; linear scales)

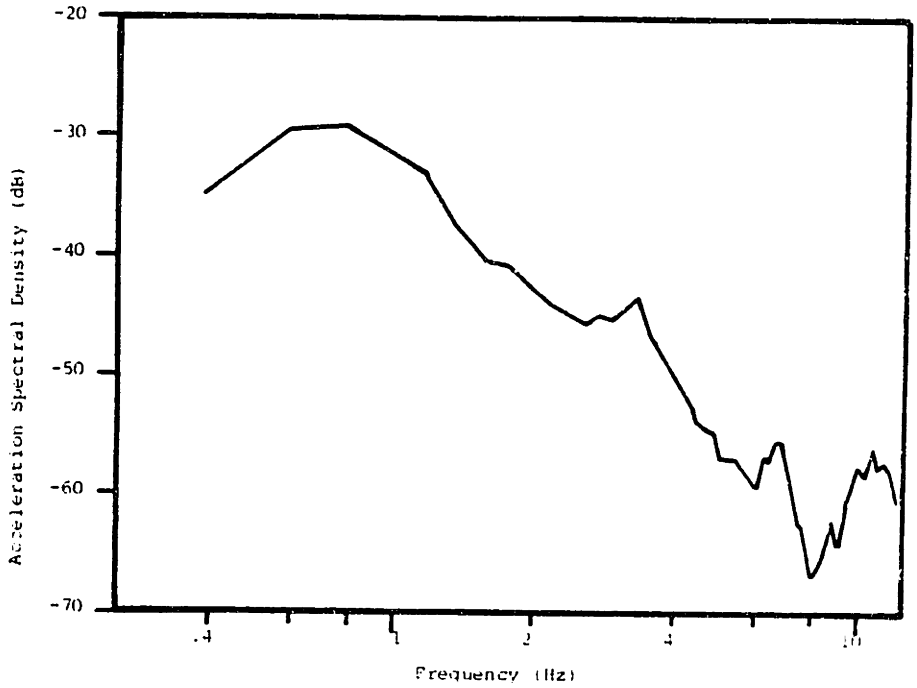

FIGURE 2.3.4: REAR LATERAL ACCELERATION SPECTRAL DENSITY (80 mph; log-log scales)

is concentrated near 1 Hz. The only other significant peak on the linear plot is at 3.2 Hz. A logarithmic scale (Figure 2.3.4) reveals other peaks, but these are all at least 20 decibels below the 1 Hz peak. Clearly, here the lateral ride quality is affected predominantly by the 1 Hz motion. RMS lateral acceleration values for the front and rear were 0.028 and 0.036 g's respectively. Figure 2.3.5 shows a linear plot of the right lateral string pot displacement spectral density. The string pot's reading is strongly coupled into the vertical motion such that the string pot does not purely measure the lateral stroke. The spectrum shows that the motion between the truck and the carbody is also predominantly a 1 Hz phenomenon.

Spectral analysis of the 60 mph section yields two major peaks (Figure 2.3.6): one occurring at 1 Hz, as also observed at 80 mph and the other at 2.4 Hz. Comparing the 60 mph and 80 mph PSD's shows speed-dependent frequency shifting of the higher-frequency peak. The peak's magnitude at 60 mph, however, is considerably larger than that at 80 mph suggesting the possibility of a track-induced response. The log-log plot (Figure 2.3.7) again shows higher-frequency vibrations to be insignificant.

2.4 Analytical Model Comparisons

The analytical rail vehicle model used is a linear 15 degrees-of-freedom lateral dynamics model documented in reference [2].

Seven mass elements are considered in this model: four wheelsets, two trucks, and a rigid carbody. States are restricted to those that contribute to lateral accelerations within the passenger compartment.

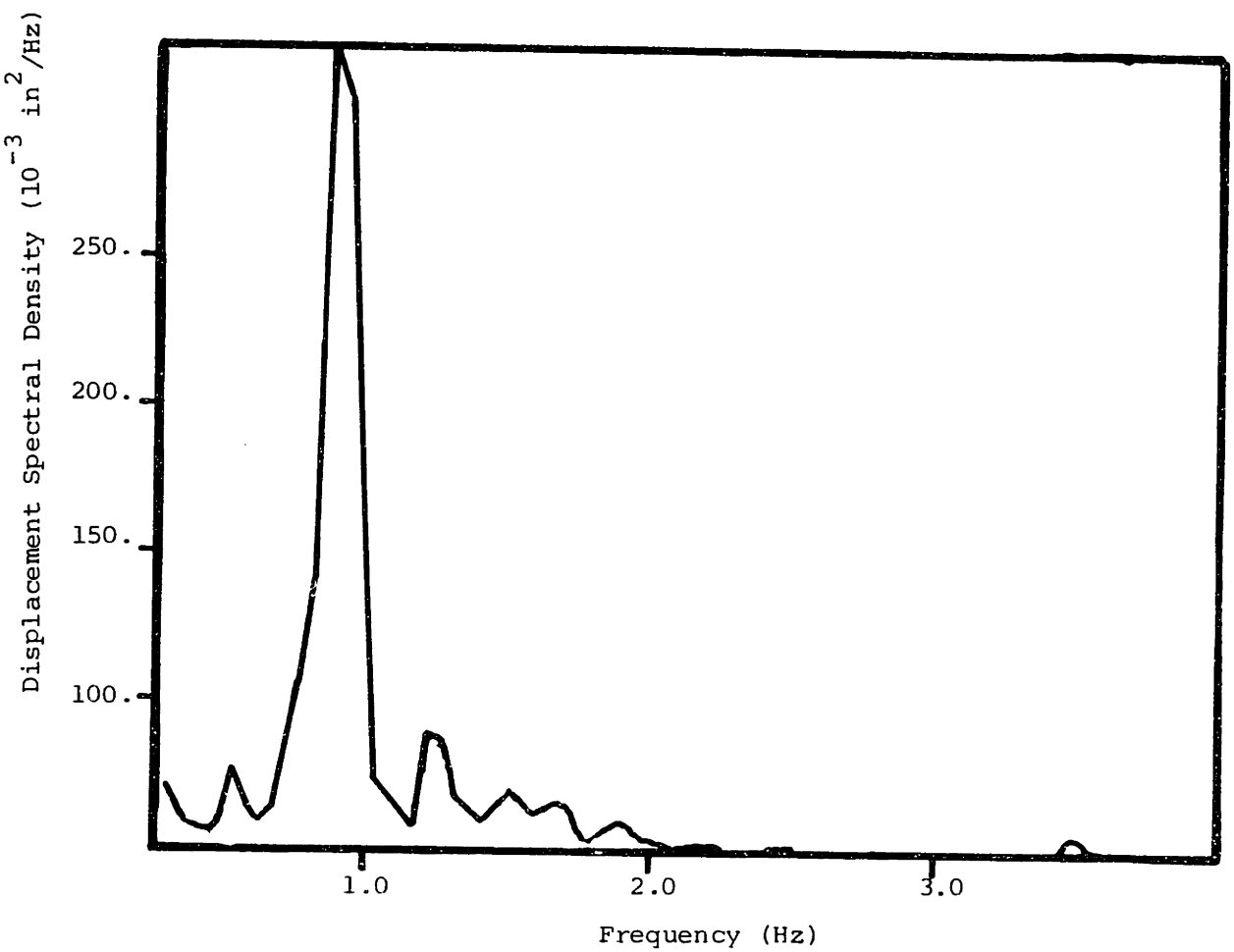

FIGURE 2.3.5: RIGHT LATERAL STRING POT DISPLACEMENT SPECTRAL DENSITY (80 mph; linear scales)

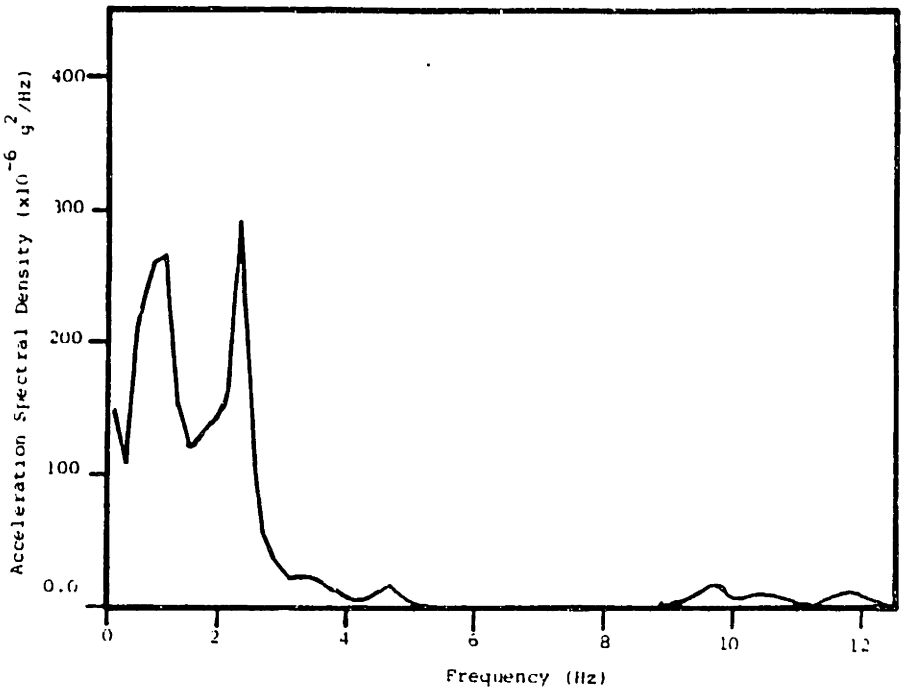

FIGURE 2.3.6: FRONT LATERAL ACCELERATION SPECTRAL DENSITY (60 mph; linear scales)

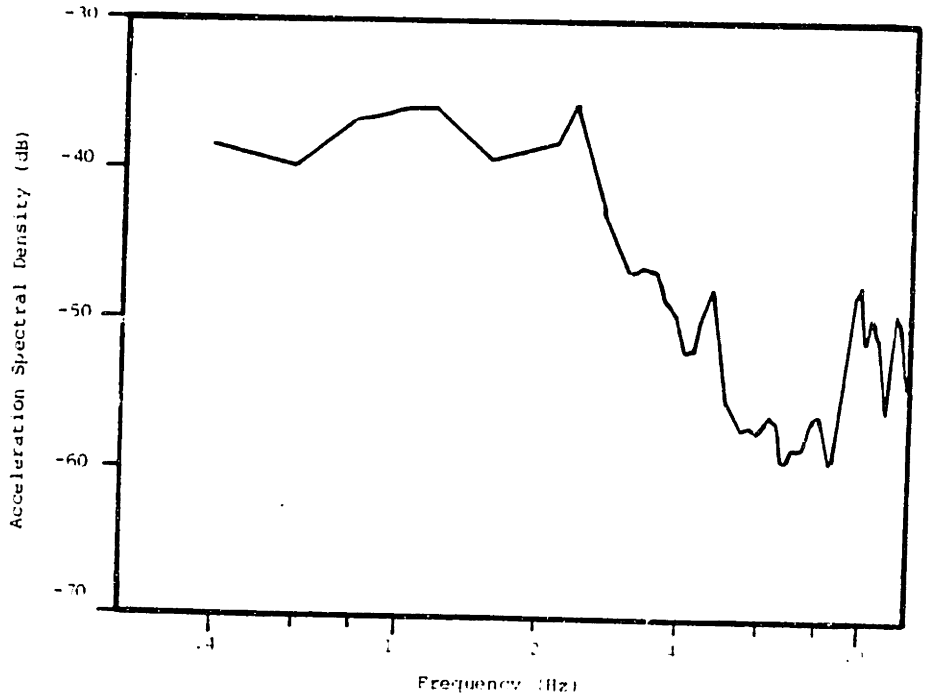

FIGURE 2.3.7: FRONT LATERAL ACCELERATION SPECTRAL DENSITY (60 mph; log-log scales)

Thus, carbody lateral displacement, yaw, and roll are used, as well as truck and wheelset yaw, and lateral displacement. Truck roll is considered to be the average of the two connected wheelsets' roll angles; wheelset roll, for small yaw angles is considered to vary linearly with wheelset excursion.

The suspension elements are modeled as linear springs and dashpots located as shown in Figure 2.4.1. Parameters, chosen to match those on the tested vehicle, were obtained from field measurements and AMTRAK drawings, as well as from references [2, 3 ,12]. These values are listed in Table 2.4.1.

Friction or "creep" forces between the wheels and the rails are calculated by Kalker's Linear Creep Theory. For comparison to the test results, one half of Kalker's linear creep coefficient values were used, because of less than perfect adhesion conditions. In the designs presented later in this report full Kalker values are used as a conservative design measure. Use of reduced Kalker values in design can lead to over-estimated critical speeds.

Figures 2.4.2a and b show the modal plots for the analytical model with the chosen parameters at both 60 and 80 mph. Only vibration modes below ten hertz are shown. These include secondary suspension vibrations and truck-wheelset hunting (kinematic) modes. Mode damping ratio is plotted versus frequency. The critical speed of the baseline vehicle is 310 mph.

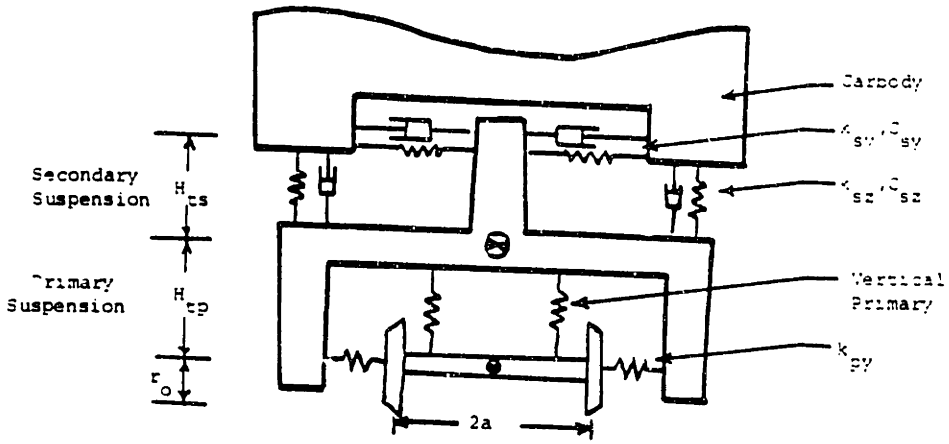

(a) Modeling of vertical suspension

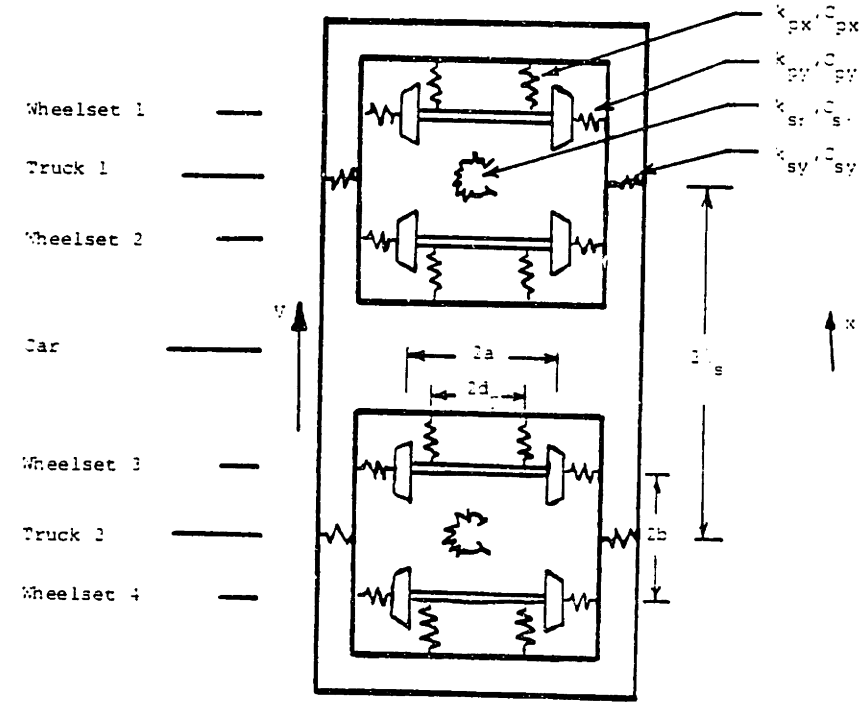

b) Modeling of Lateral and Longitudinal Suspension

FIGURE 2.4.1: VEHICLE MODEL

TABLE 2.4.1: BASELINE VEHICLE PARAMETERS

WHEEL RAIL PARAMETERS		
a_{11}	wheelset roll coefficient	0.025
δ_o	centered contact angle	0.025
Δ	contact angle difference	0.000
f_{11}	lateral creep force coefficient	1.0×10^6 lb
f_{12}	lateral/spin creep coefficient	8500 ft-lb
f_{22}	spin creep coefficient	80 ft^2-lb
f_{33}	longitudinal creep force coefficient	8.0×10^6 lb
WHEEL PARAMETERS		
a	half of track gauge	2.35 ft
N	load per wheelset	26100 lbs
λ	wheel conicity	0.025
Mw	wheelset mass	106.8 slugs
I_{wx}	wheelset roll moment of inertia	500 slugs-ft^2
I_{wy}	wheelset pitch moment of inertia	100 slugs-ft^2
I_{wz}	wheelset yaw moment of inertia	500 slugs-ft^2
Ro	centered wheel rolling radius	1.5 ft
TRUCK PARAMETERS		
dp	1/2 of primary springs lateral spacing	1.9 ft
b	1/2 of wheelbase	4.25 ft
h_{tp}	vertical distance from truck c.g. to primary lateral springs	0.35 ft
h_{ts}	vertical distance from truck c.g. to secondary lateral springs	1.33 ft

TRUCK PARAMETERS

I_{tz}	truck frame yaw moment of inertia	2108 slug-ft^2
M_t	truck frame mass	212 slugs

CARBODY PARAMETERS

d_s	1/2 of secondary spring lateral spacing	3.75 ft
h_{cs}	vertical distance from carbody c.g. to secondary lateral springs	3.1 ft
ℓ_s	1/2 of truck center pin spacing	30 ft
w	weight of carbody	77433 lbs
I_{cz}	carbody yaw moment of inertia	1.483×10^6 slugs-ft^2
I_{cx}	carbody roll moment of inertia	64193 slugs-ft^2
M_c	carbody mass	2405 slugs

PRIMARY SUSPENSION PARAMETERS

k_{py}	primary lateral stiffness (4 per truck)	480,000 lb/ft
k_{px}	primary longitudinal stiffness (4 per truck)	960,000 lb/ft
c_{py}	primary lateral damping ($k_{py}/250$)	2020 $\frac{\text{lb}}{\text{ft/sec}}$
c_{px}	primary longitudinal damping ($k_{px}/250$)	2850 $\frac{\text{lb}}{\text{ft/sec}}$

SECONDARY SUSPENSION PARAMETERS

k_{sy}	secondary lateral stiffness (2 per truck)	24000 lb/ft
k_z	secondary vertical stiffness (2 per truck)	22200 lb/ft
k_{spsi}	secondary yaw stiffness (1 per truck)	1×10^6 ft-lb/rad

SECONDARY SUSPENSION PARAMETERS

c_{sy}	secondary lateral damping (2 per truck)	1200 $\frac{lb}{ft/sec}$
c_{sz}	secondary vertical damping (2 per truck)	2000 $\frac{lb}{ft/sec}$
c_{spsi}	secondary yaw damping (1 per truck)	4000 $\frac{lb}{ft/sec}$

PASSENGER LOCATIONS FOR RIDE QUALITY

Front distance from carbody c.g.	x = 30 ft	z = -1.7 ft
Rear	x =-30 ft	z = -1.7 ft

PERFORMANCE CAPABILITIES OF BASELINE VEHICLE

Critical Speed	310 mph

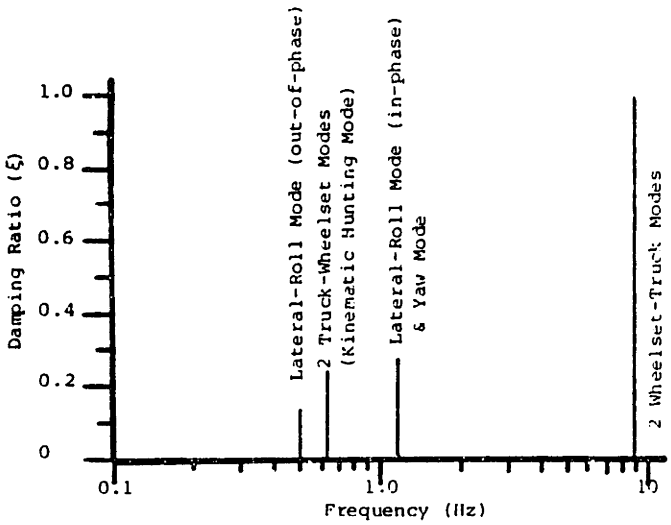

FIGURE 2.4.2: MODAL PLOT FOR TEST VEHICLE MODEL (a) (60 mph)

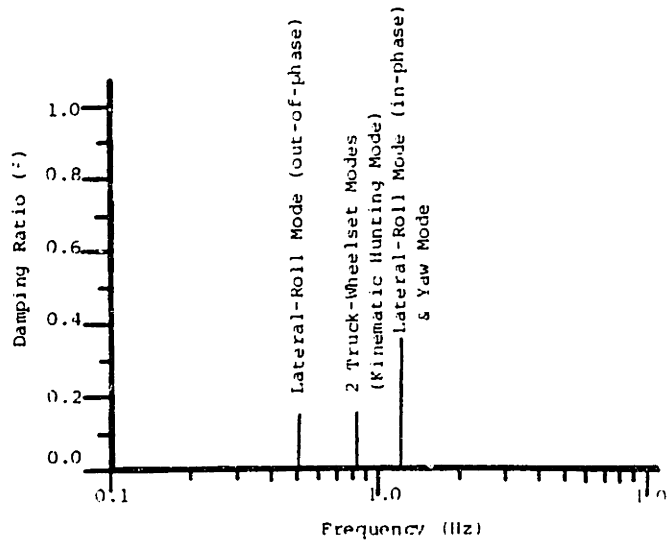

FIGURE 2.4.2: MODAL PLOT FOR TEST VEHICLE MODEL (b) (80 mph)

Two track models have been used as inputs to the vehicle model, both involving alignment and crosslevel components. The first is an analytical model for class-6 track [2]. Figure 2.4.3 shows this model for a forward v ..ity of 80 mph. The second model, shown in Figure 2.4.4, is based on information received from ENSCO, Inc. These PSD's were generated on a 5-mile section of track considered typical of the Northeast Corridor.

Comparing the acceleration PSD's in Figures 2.3.3 through 2.3.7 to the modal plots in Figure 2.4.2, the consistent 1 Hz resonance resulting from the lateral secondary suspension vibration modes can be seen.

The peaks at 3.2 Hz in the 80 mph experimental data and at 2.4 Hz at 60 mph move in proportion to forward velocity. Therefore, this vibration must be related to either kinematic motion of the trucks or to the input spectrum.

The modal plots (Figure 2.4.2) show that for a conicity of 0.025, as measured in the tread region, the kinematic hunting frequencies are much too low to cause the velocity-dependent resonance observed in the test data. Excursions beyond the tread, though, can cause an effective increase in the conicity resulting in a higher hunting frequency. For example, a conicity of 0.01 would move the kinematic frequency for 80 mph to 2.3 Hz. A softer primary suspension ($k_{py} = k_{px} = 170000$ lb/ft, $C_{px} = C_{py} = 800$ lb/ft/sec) than estimated would further increase the kinematic frequency to 3.0 Hz, very close to the observed vibration.

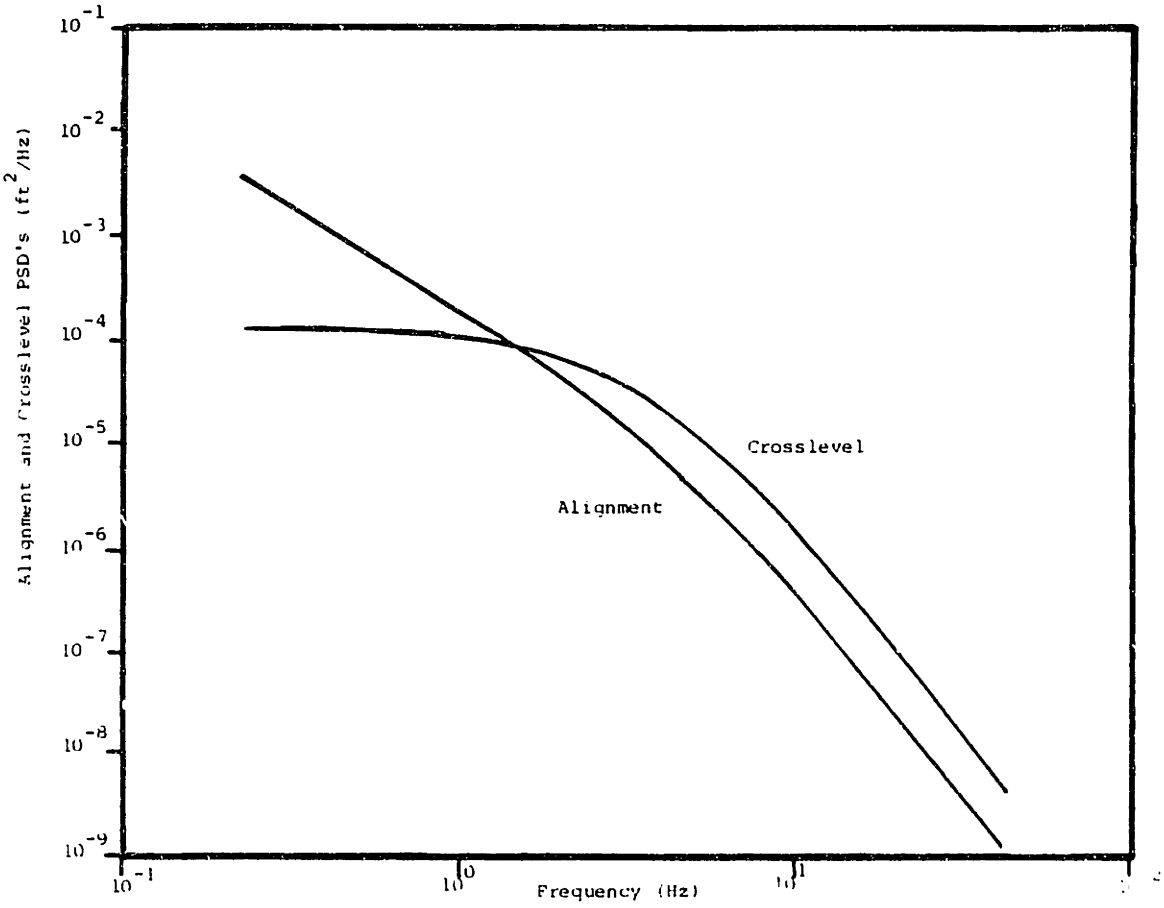

FIGURE 2.4.3: ANALYTICAL TRACK INPUT PSD-CLASS 6 (80 mph)

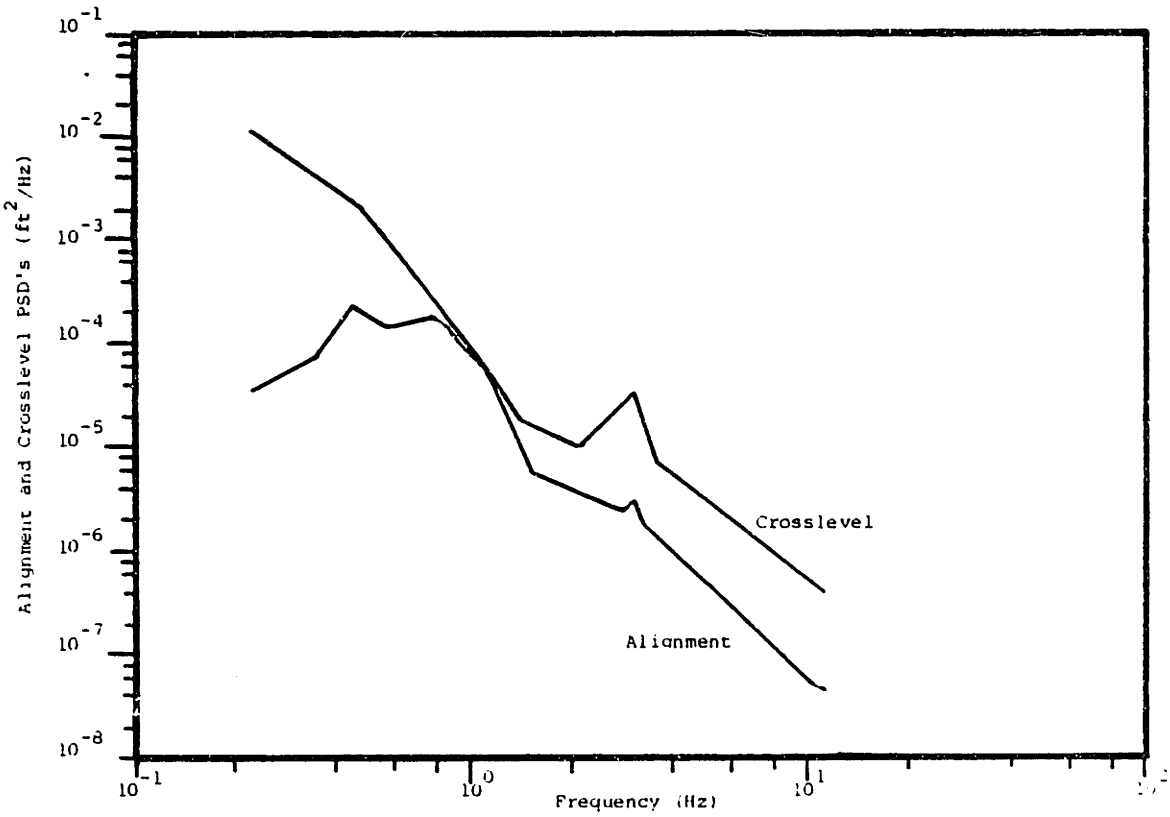

FIGURE 2.4.4: TRACK INPUT PSD FROM DATA TAKEN ON THE NORTHEAST CORRIDOR BY ENSCO (80 mph)

Figure 2.4.4 shows that both the crosslevel and alignment PSD's produced by ENSCO from Northeast Corridor track exhibit local peaks at a wavelength of 40 feet. At 60 mph this corresponds to frequency of 2.2 Hz, while at 80 mph the effective frequency is 2.9 Hz. Thus, there is strong evidence to suggest that the experimental peaks are track induced.

2.5 Conclusion

Analysis of the test data shows the Amcoach ride at a speed of 80 mph in the Northeast Corridor to be dominated by 0.5 to 1 Hz vibration. This motion is identified by the linear model as a lateral secondary suspension vibration. At lower speeds another vibration whose frequency varies with velocity is also significant. This motion has a 2.4 Hz frequency at 60 mph and varies directly with forward speed (3.2 Hz at 80 mph). This motion is probably due to 35 to 40-foot-wavelength track irregularities.

Track quality for high speed travel (110 mph) is expected to compare with that of track currently traversed at 80 mph. Thus, the vibration problem centers around the secondary suspension at 1.0 Hz as seen in the 80 mph data.

CHAPTER 3

ACTIVE SUSPENSION ANALYSIS

3.1 Introduction

Having identified the ride quality problem of the Amcoach Vehicle as a one hertz phenomenon attributed primarily to the secondary suspension vibrations, the task presented is to design a suspension to reduce these motions.

M.A. Partridge showed in ref. [5] that passive suspensions can be used to reduce r.m.s. accelerations, but with limited success.

Passive suspensions are limited by the restriction that forces can only be created from local, relative motion and energy can only be dissipated or stored and used later.

Active suspensions, however, are not held by either of these restrictions. Forces created by actuators can be related to any state, or combinations of states, that one is able to measure. External power is used to supply the energy added to the system. In ref. [4], G. Celniker presented active suspension control schemes for ride quality improvement, as well as increased stability. This chapter presents an application of Celniker's simplest and most efficient ride quality control law to a vehicle in parallel with a well designed passive suspension system. Feedback gains were picked assuming ideal actuators were available to supply exactly the desired active forces with no delay or attenuation. Then the model was augmented to incorporate a more realistic actuator model. This model allowed for "limited bandwidth" actuators and was used to

determine the actuator response speed needed for the controller to be effective.

Potential actuator systems are considered in Section 3.5. Advantages and disadvantages of hydraulic, pneumatic, and electro-magnetic systems are discussed.

3.2 Control Law

The active suspension designed in this paper utilizes a feedback algorithm referred to in reference [4] as a "local ride controller". Celniker showed that the kinematic motion of the trucks and the lateral vibration of the carbody can be controlled independently.

The truck motion is very sensitive to torques and can be effectively controlled by applying torque between the carbody and truck. The carbody, however, is relatively insensitive to this action. The long distance between trucks provides a large enough lever arm that only small lateral forces need to be generated on the carbody for the couple to counter the active torque [4].

Carbody motion, though, is extremely sensitive to lateral forces. Lateral actuators placed between the carbody and trucks would exert forces below the center of gravity and at the ends of the carbody. In this way, carbody roll and yaw modes can be excited, or controlled, as well as lateral carbody motion. Lateral force, though, Celniker showed to have little effect on the truck motion [4]. If the kinematic truck motion is such that no stability problem exists, then Celniker showed that it is possible to improve the vehicle's ride

quality with only lateral actuators placed in parallel with the passive lateral secondary suspension. This condition exists at speeds well below the vehicle's critical speed (the speed at which the vehicle becomes unstable).

At higher speeds the kinematic "hunting" motion of the trucks becomes so large that the ride is seriously impaired by it. Operation at higher speeds, therefore, requires torque actuators to control the truck motion, in addition to the lateral actuators for secondary vibration control. Both operations can be provided by a pair of linear force actuators on each truck (Figure 3.2.1). The pair supplies a force when operated in-phase and a torque when out-of-phase.

With the goal of improving the ride quality in the 100 to 110 mph range while requiring as little added expense as possible in equipment, operation, and maintenance, the lateral actuator carbody controller was chosen for this design. The control law used to drive the actuators required the use of only two accelerometers, one over each truck and attached to the carbody.

In this location, close to the actuators, the accelerometers give readings that reflect all three carbody motions involved in the lateral model: carbody lateral acceleration, roll acceleration, and yaw acceleration. The acceleration at the transducer is

$$\ddot{y}_{c\ell} = \ddot{y}_c - H_{c\ell}\ddot{\phi}_c \pm \ell_{c\ell}\ddot{\psi}_c$$

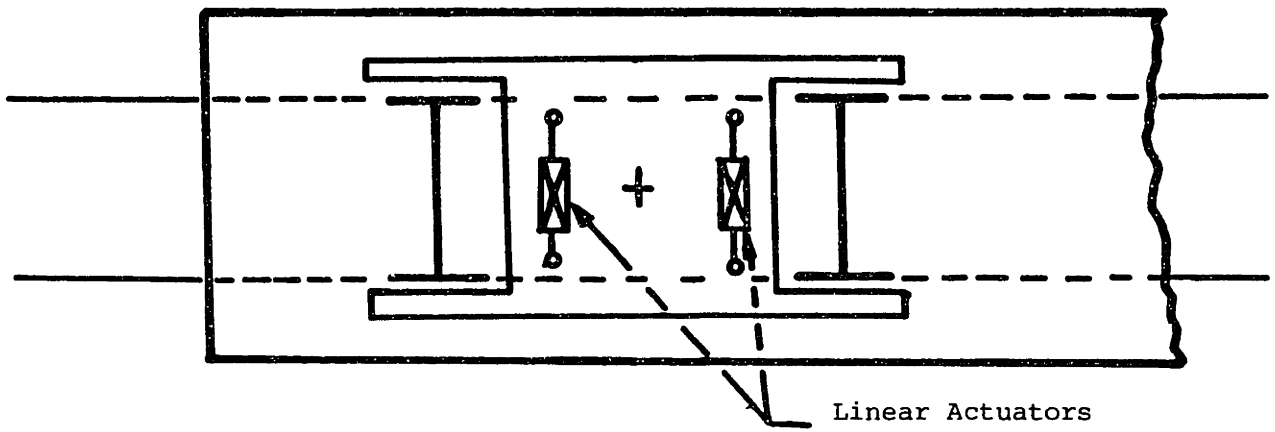

FIGURE 3.2.1: ACTUATOR POSITIONS ON TRUCK FOR TORQUE AND FORCE ACTUATION

where $\ddot{y}_{c\ell}$ refers to the "local" acceleration at the transducer, $H_{c\ell}$ is the vertical distance from the carbody center of gravity to the accelerometer, and $\ell_{c\ell}$ is the longitudinal distance between the cg and the accelerometer. The carbody lateral, roll, and yaw accelerations are given by $\ddot{y}_c$, $\ddot{\phi}_c$, and $\ddot{\psi}_c$, respectively. The plus sign is used for the leading truck accelerometer, the minus for the rear.

Although the location of the local accelerometers is arbitrary, this design placed them at secondary suspension level, above the centers of the trucks.

The command to the actuators is given by the following control law:

$$F_A = k_v \dot{y}_{c\ell} + k_A \ddot{y}_{c\ell}$$

where F_A is the total lateral force desired on the truck and that end of the carbody, and $\dot{y}_{c\ell}$ and $\ddot{y}_{c\ell}$ are the velocity and acceleration of the "local" accelerometer. No command is relayed from the accelerometer at the opposite end of the car; hence this controller is referred to as a "local" controller. Also note that F_A is the total linear actuator force desired if two actuators are used per truck, F_A is the algebraic sum of the two commands.

Celniker assumed ideal actuation was available [4]. Real actuators have a finite response time. Thus, F_A in the control law becomes the "desired" force, $F_{command}$, a signal to the actuator, and differs from the actual force, $F_{response}$. A model is needed for the actuator to relate the command and the response. The next section presents a linear means of modeling actuators to determine response

speed required. Generally, a quicker, more accurate system will cost more to build, operate, and maintain.

3.3 Bandwidth

An "ideal" actuator would immediately produce a force directly proportional to its electrical input signal. There would be no time delay nor attenuation of the desired force.

In a real system this is not possible. Inertia, friction, and system flexibility prevent a perfect response, causing time delay, and signal amplification or attenuation. For a sinusoidal command signal, this can be presented in terms of a magnitude change, or gain, and a phase change. In general, the bandwidth of an actuator is that frequency range over which the response-to-command ratio has a magnitude of approximately 1.

Figure 3.3.1 shows these two variables as a function of frequency for a first order dynamic model. This model is described analytically in the frequency domain by*

$$\frac{F_{response}}{F_{command}}(j\omega) = \frac{1}{1 + j\omega\tau},$$

where $\frac{F_{response}}{F_{command}}$ is the response force-to-command force ratio (a complex function) and τ is the system time constant. The break frequency, shown in Figure 3.3.1 as ω_b, is equal to $1/\tau$. It is also the frequency at which the magnitude of F_r/F_c drops below -3dB.

*j is the complex number ($\sqrt{-1}$)

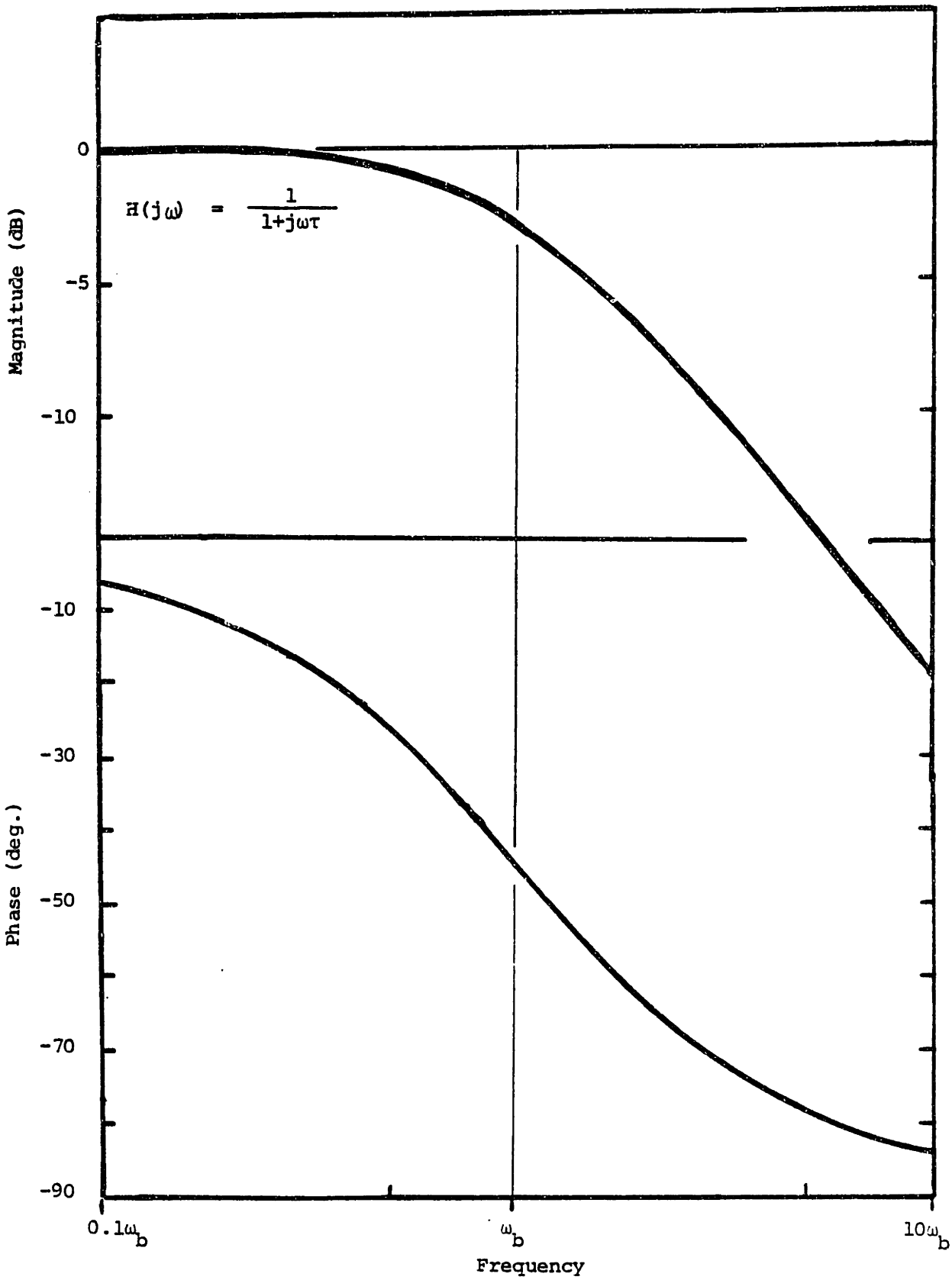

FIGURE 3.3.1: FREQUENCY RESPONSE: FIRST ORDER LAG

Therefore, ω_b marks the actuator's bandwidth.

For a second-order model, two parameters are required to describe the frequency response. Figure 3.3.2 shows this response, which is given by

$$\frac{F_{response}}{F_{command}}(j\omega) = \frac{\omega_n^2}{2j\omega\omega_n\xi + \omega_n^2 - \omega^2} .$$

Here the chosen parameters are ξ, the damping ratio, and ω_n, the undamped, natural frequency. For $\xi = 0.707$, no peak occurs, and ω_n marks the 3dB - down point. Thus, ω_n is a fairly good indicator of the second-order system's bandwidth.

Another perspective on system response comes from time domain analysis. Figure 3.3.3 shows the time responses of these $1^{\underline{st}}$ and $2^{\underline{nd}}$ order systems to a step input. Mathematically these are

$$\frac{F_{response}}{F_{command}}(t) = 1 - e^{-t/\tau} \qquad (1^{\underline{st}} \text{ order})$$

$$\frac{F_{response}}{F_{command}}(t) = (1 - e^{-t/\tau})\cos\omega_d t \quad (2^{\underline{nd}} \text{ order})$$

For the second order system the time constant, τ, is equal to $\xi\omega_n$ and ω_d is equal to $\omega_n\sqrt{1-\xi^2}$.

Note that for both systems the response reaches 95% of the command after three time constants and 98% after four.

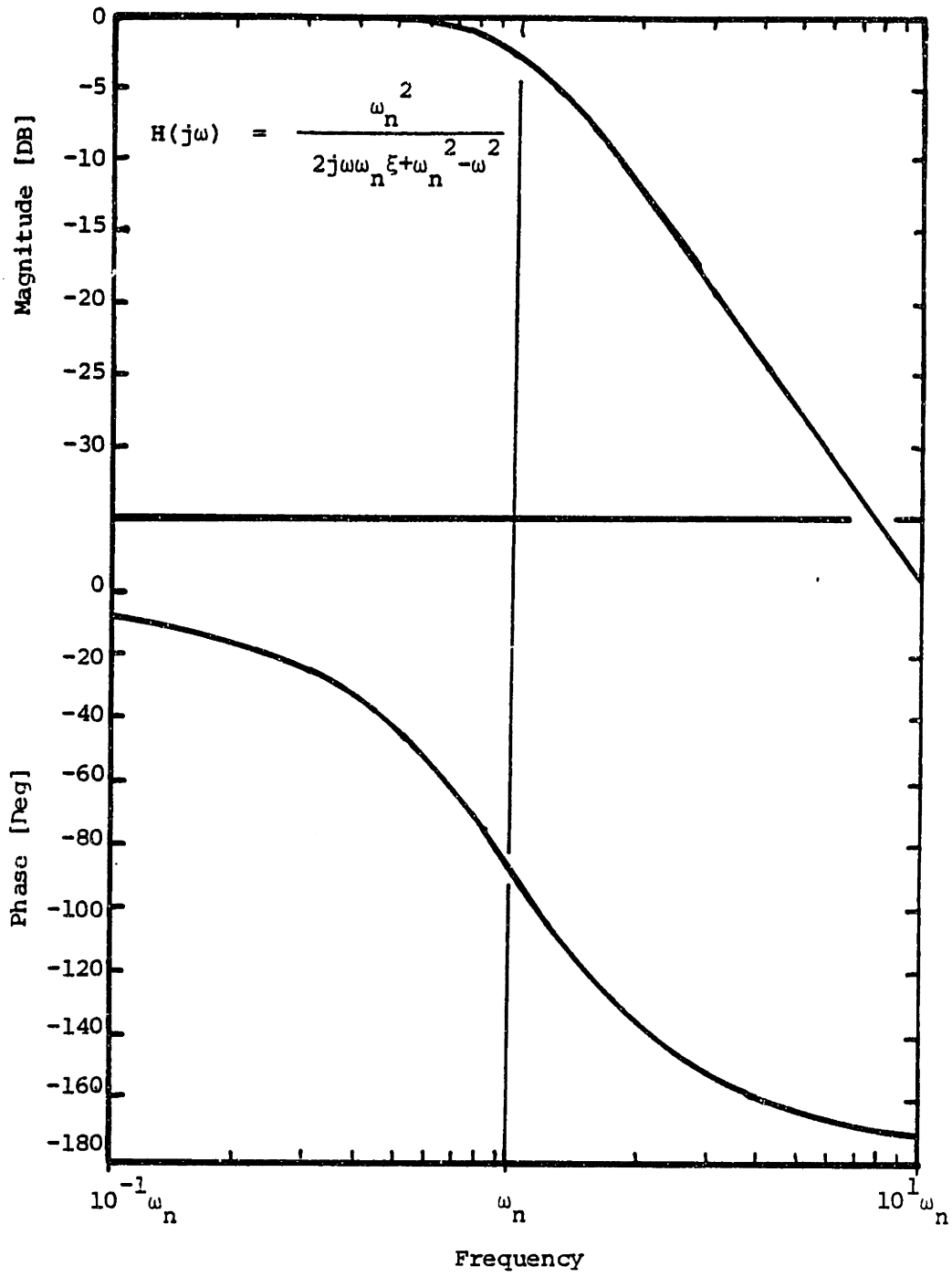

FIGURE 3.3.2: FREQUENCY RESPONSE: SECOND ORDER LAG

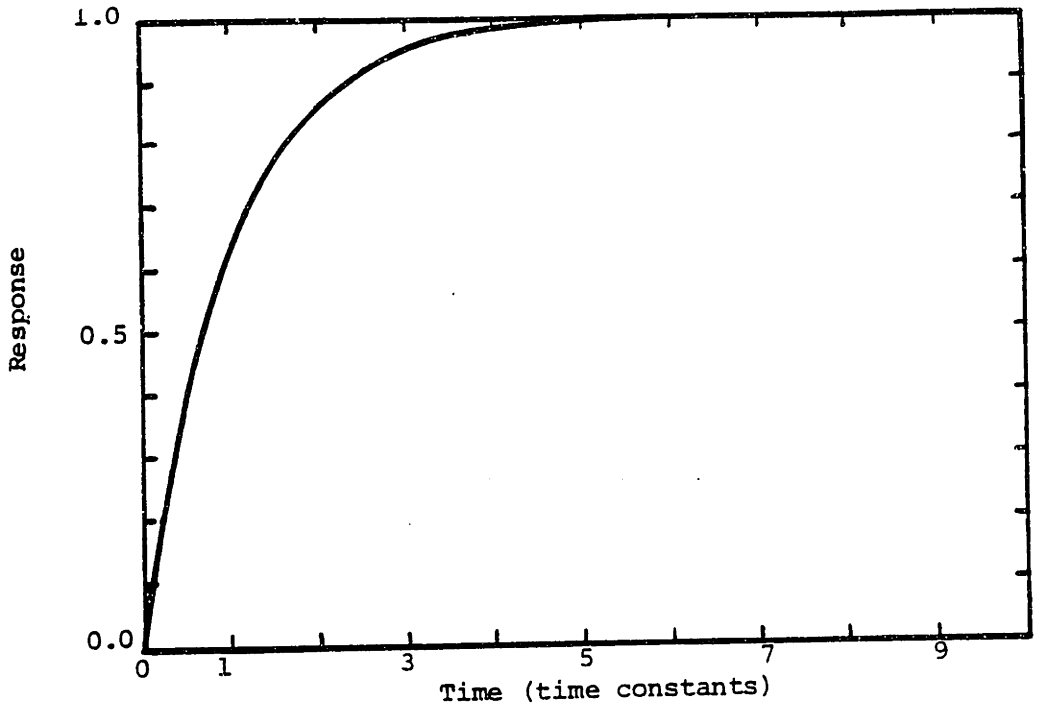

a. FIRST ORDER SYSTEM

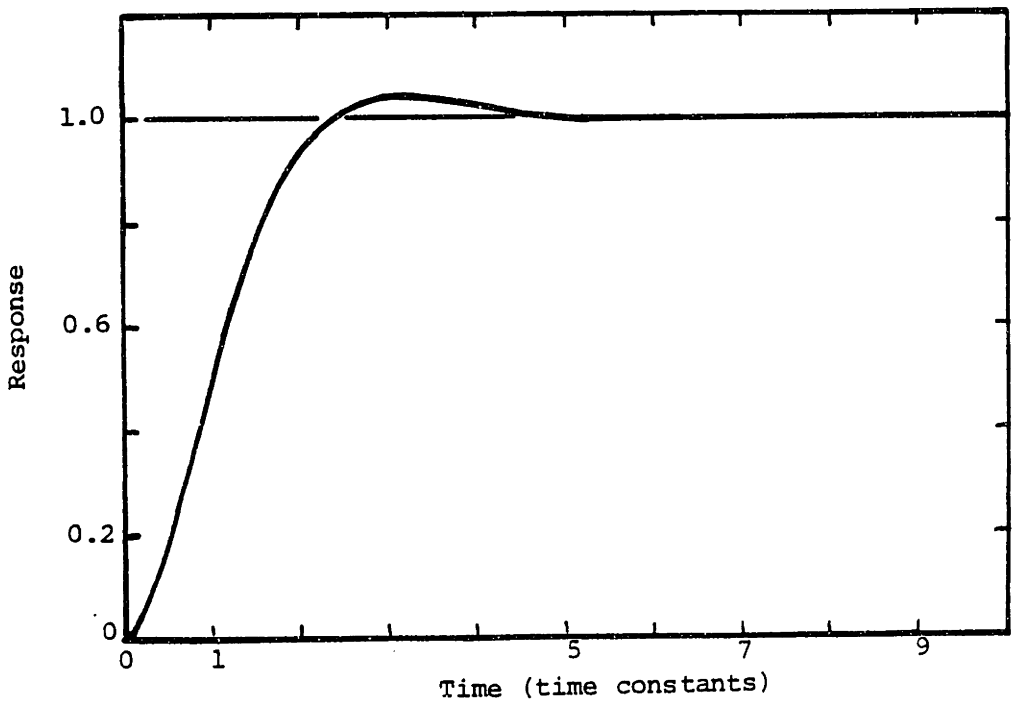

b. SECOND ORDER SYSTEM

FIGURE 3.3.3: TIME RESPONSE TO A UNIT STEP INPUT

Bandwidth and response time for higher-order models can be determined in a similar manner.

Beyond a system's bandwidth, the response will be lower in magnitude than desired and delayed by a significant phase lag. Therefore, the actuator system chosen should have a frequency response covering the entire spectrum of expected input commands.

3.4 Parametric Study - Band-Limited Active

Modeling the actuator dynamics as a first order lag, a frequency domain study was performed on an active vehicle model. The parameter varied in the study was the actuator's bandwidth.

3.4a Vehicle and Track Models

The vehicle model used is a revised version of the 15 degree-of-freedom lateral model presented in Chapter 2. Appendix A contains the equations of motion for the passive vehicle. Written in matrix form these equations can be expressed as:

$$\underline{\bar{M}}\,\underline{\ddot{x}} + \underline{\bar{C}}\,\underline{\dot{x}} + \underline{\bar{K}}\,\underline{x} = \underline{\bar{B}}\,\underline{y} \qquad (3.4.1)$$

where

$\underline{x}$ is the state vector

$\underline{M}$ is the mass matrix

$\underline{\bar{C}}$ is the damping matrix

$\underline{\bar{K}}$ is the stiffness matrix

$\underline{y}$ is the track input vector

$\underline{\bar{B}}$ is the input distribution matrix.

Including actuator dynamics in the model required a revision of the system equations. In matrix form these equations are:

$$\bar{\underline{M}}\,\ddot{\underline{x}} + \bar{\underline{C}}\,\dot{\underline{x}} + \bar{\underline{K}}\,\underline{x} = \bar{\underline{B}}\,\underline{y} + \bar{\underline{D}}\,\underline{f}_o . \qquad (3.4.2)$$

$\underline{f}_o$ is the actuator forces vector

$\bar{\underline{D}}$ is the active forces distribution matrix

The command to the actuator $\underline{f}_i$ is determined by

$$\underline{f}_i = \bar{\underline{K}}_m\,\ddot{\underline{x}} + \bar{\underline{K}}_c\,\dot{\underline{x}} + \bar{\underline{K}}_k\,\underline{x} \qquad (3.4.3)$$

where $\bar{\underline{K}}_m$, $\bar{\underline{K}}_c$, and $\bar{\underline{K}}_k$ are the active acceleration, velocity, and displacement feedback gain matrices, respectively. For the local controller in the bandwidth studies, $\bar{\underline{K}}_k$ is the null matrix, as only acceleration and velocity feedback are included in the control law.

Actuator dynamics relate the actuator force vector, $\underline{f}_o$, to the command, $\underline{f}_i$. Thus, the frequency domain,

$$\underline{f}_o(j\omega) = TF(j\omega) \cdot \underline{f}_i(j\omega) . \qquad (3.4.4)$$

The actuators' dynamics are assumed to be the same. So $TF(j\omega)$ is a complex scalar, rather than a matrix.

Reducing all these equations in the frequency domain, we derive

$$[\omega^2(TF \cdot \bar{\underline{D}}\cdot\bar{\underline{K}}_m - \bar{\underline{M}}) + (\bar{\underline{K}} - TF\cdot\bar{\underline{D}}\cdot\bar{\underline{K}}_k) + j\omega(\bar{\underline{C}}-TF\cdot\bar{\underline{D}}\cdot\bar{\underline{K}}_c)]\ \underline{x}(j\omega) = \bar{\underline{B}}\ \underline{y}(j\omega) \qquad (3.4.5)$$

This corresponds to the ideal actuator case if the actuator transfer function, TF, is set to 1. For the actuator bandwidth studies, $TF(j\omega)$ represented the actuator dynamics.

Appendix B shows the elements of matrices $\bar{\underline{K}}_c$, $\bar{\underline{K}}_m$ and $\bar{\underline{D}}$.

The track input to the vehicle model was represented by an analytical track PSD. Both alignment and crosslevel inputs were used. The two inputs are assumed to be uncorrelated.

For alignment

$$S_a(\Omega) = \frac{A_a\,\Omega_c^2}{\Omega^2(\Omega^2 + \Omega_c^2)} . \qquad (3.4.6)$$

For crosslevel

$$S_a(\Omega) = \frac{4A_c\,\Omega_c^2}{(\Omega^2 + \Omega_c^2)(\Omega^2 + \Omega_s^2)} . \qquad (3.4.7)$$

S_a and S_c are the track alignment and crosslevel spectral densities (in^2/rad/ft), Ω is the wavenumber (rad/ft), A_v and A_a are roughness parameters (in^2 - rad/ft), and Ω_c and Ω_s are break wavenumbers (rad/ft). Parameter values were chosen to match class-6 track. Their values are given by reference [2] to be

$$A_v = .00159 \quad in^2\text{-rad/ft}$$

$$A_a = .00159 \quad in^2\text{-rad/ft}$$

$$\Omega_s = .1335 \quad \text{rad/ft}$$

$$\Omega_c = 2\pi/25 \quad \text{rad/ft.}$$

Use of the PSD track input representation yields output PSD's for the state vector.

If equation (3.4.5) is written as

$$\bar{\underline{A}}(j\omega) \cdot \underline{x}(j\omega) = \bar{\underline{B}}\, \underline{y}(j\omega) \tag{3.4.8}$$

where $\bar{\underline{A}}(j\omega)$ represents the frequency dependent system dynamics matrix, one can see that solution for the matrix of transfer functions, $\bar{\underline{H}}(j\omega)$, between the track input and the desired outputs requires inversion of $\bar{\underline{A}}(j\omega)$ at each desired frequency:

$$\underline{x}(j\omega) = \underline{\bar{H}}(j\omega)\ \underline{y}(j\omega) \tag{3.4.9}$$

with

$$\underline{\bar{H}}(j\omega) = \underline{\bar{A}}(j\omega)^{-1}\ \underline{\bar{B}} \tag{3.4.10}$$

The transfer function matrix is a complex, 15x2 matrix, reflecting the output's dependence on both inputs. The total output PSD for a state is the sum of outputs propagated for each of the two uncorrelated inputs. The alignment and crosslevel input PSD's are multiplied by the squared magnitudes of their respective transfer functions, or

$$S_{xx}(\omega) = |H(j\omega)|^2_{al}\ S_{yy_{al}}(\omega) + |H(j\omega)|^2_{cr}\ S_{yy_{cr}}(\omega) \tag{3.4.11}$$

where

S_{xx} is the PSD of the desired output,

$S_{yy_{al}}$ is the alignment PSD,

$S_{yy_{cr}}$ is the crosslevel PSD,

$H(j\omega)_{al}$ is the alignment transfer function,

and $H(j\omega)_{cr}$ is the crosslevel transfer function.

3.4b Performance Indices

Although the "ride quality" of a rail vehicle is related primarily to the accelerations experienced by the passengers and cargo, other factors must be taken into account when rating the performance of a rail vehicle. Four indexes were instrumental in comparing the performances of different active suspensions: total rms acceleration, 1/3 octave rms acceleration, rms secondary lateral stroke, and average power usage.

Total rms acceleration was calculated for the lateral accelerations at the center of gravity and at the front and rear passenger points, and for the carbody yaw and roll angular accelerations. Calculations of the rms accelerations were made by taking the square roots of the integrals of the entire acceleration spectral densities.

Although total rms acceleration is convenient for comparing the ride quality of different suspensions, the frequency content of the acceleration is also important. The human body is more affected by vibrations at certain frequencies. Figure 3.4.1, from reference [1], shows lines of equal discomfort as determined for 1/3 octave frequency bandwidths by the International Organization for Standardization, I.S.O. Comparison to this standard required the determination of rms accelerations within 1/3 octave bands.

In passive suspension design a trade-off is often noted between acceleration reduction and secondary stroke reduction. Maintaining a moderately stiff secondary is necessary to support static loads in wind or curving. In order to assure that lateral clearances are

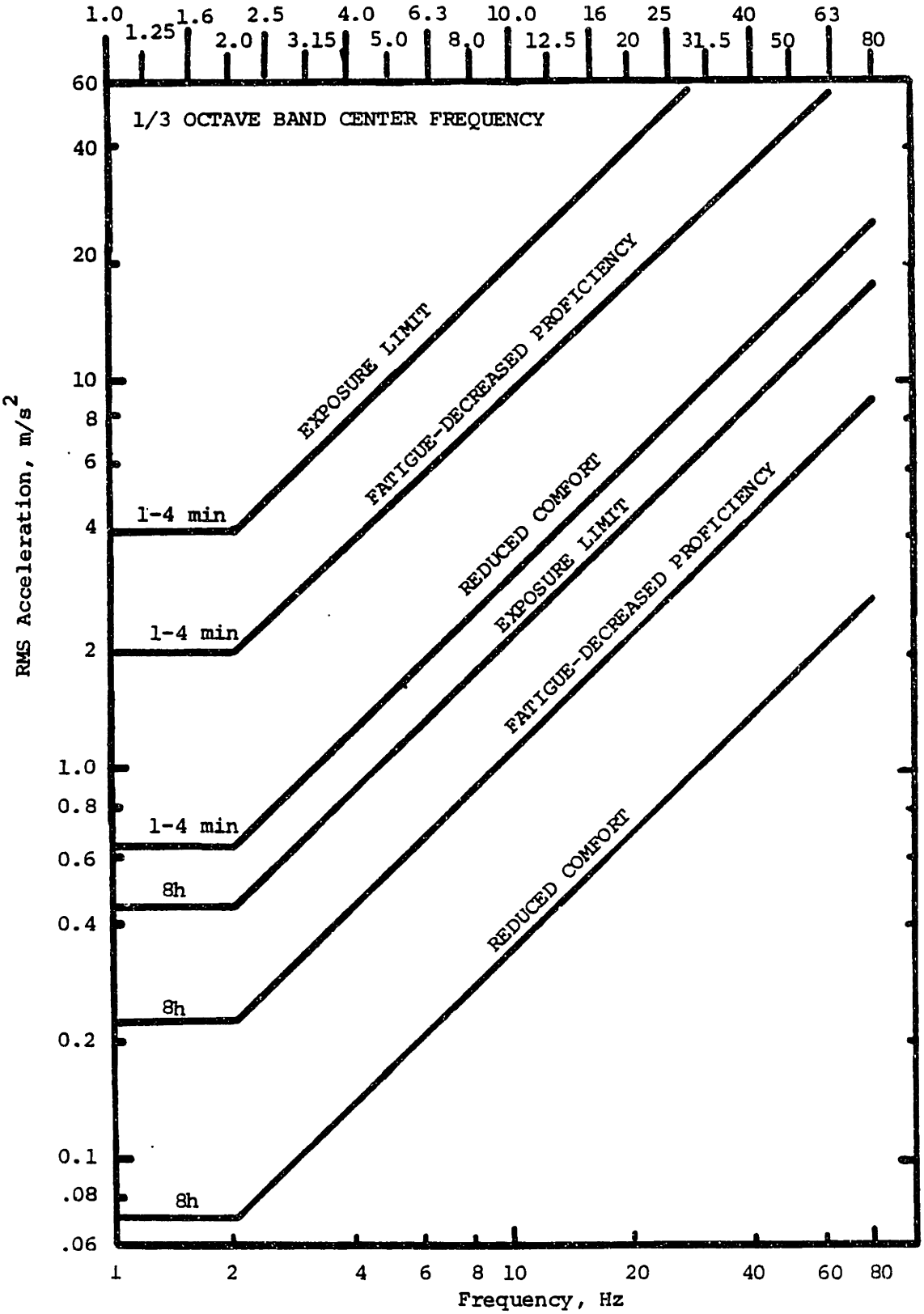

FIGURE 3.4.1: ISO ACCELERATION/FREQUENCY CURVES FOR LATERAL AND LONGITUDINAL AXES [1]

maintained, the Pioneer III trucks by the Budd Company have rubber "bumpstops" which are contacted when the lateral secondary stroke exceeds $\pm$ 1.5 inches. Figure 3.4.2 shows the bumpstops' locations between the bolster and carbody. With a stiffness tested in the lab to be about 88,800 lb/ft per bumpstop, contact can quadruple the lateral stiffness of the secondary suspension. For this reason it is desirable to maintain peak secondary strokes of 1.5 inches or less. Assuming a normal (Gaussian) random distribution with 3σ peaks, root mean squared strokes should have a maximum value of one half inch.

An important parameter for active systems is average power usage. For the comparison of different bandwidth systems presented here, a hydraulic actuator model was used to estimate power. Figure 3.4.3 shows a typical hydraulic, double acting actuator. In general,

$$\text{Power} = \text{Force} \times \text{Velocity}. \tag{3.4.12}$$

where the force is equal to the piston area times the pressure drop across the actuator. This yields

$$\text{Power} = \Delta P \cdot A_p \cdot V_p \tag{3.4.13}$$

where

ΔP is the actuator pressure differential,

A_p is the piston area, and

V_p is the piston velocity.

Note that the product of the piston's area and velocity is the volume flow rate, Q, needed to fill the expanding of the actuator.

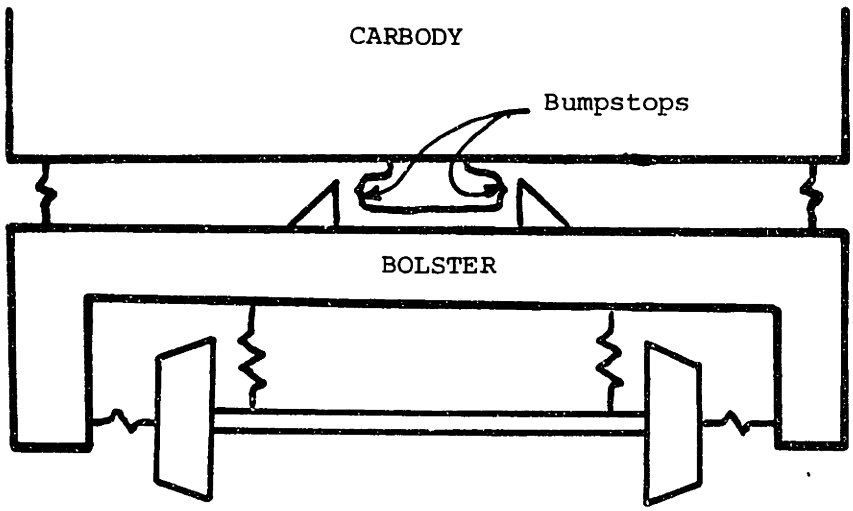

FIGURE 3.4.2: BUMPSTOP LOCATIONS

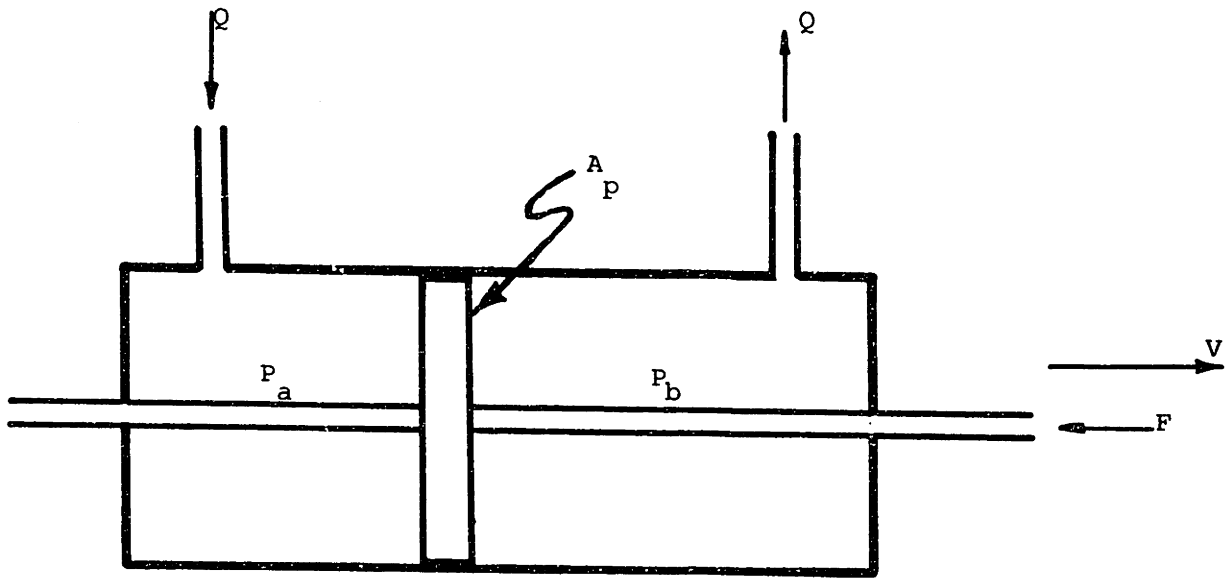

$$Q = V \cdot A_p$$

$$F = (P_a - P_b) \cdot A_p$$

FIGURE 3.4.3: DOUBLE ACTING HYDRAULIC ACTUATOR

$$\text{Power} = \Delta P \cdot Q \tag{3.4.14}$$

This flow into the actuator is provided by the supply. A reverse flow would require a pressure differential across the piston greater than P_s, reflecting an actuator force greater than the maximum design force. Since the supply pressure and piston area were designed to meet the maximum force, the reverse flow condition should occur infrequently.

The pump supplies the flow at P_s, the supply pressure. Therefore, the average power consumed by the hydraulic system is

$$\text{Ave.Power} = P_s \cdot Q_{ave}. \tag{3.4.15}$$

Since the average flow rate is equal to the average rectified velocity, $|V_p|_{ave.}$ times the piston area and the supply pressure times the piston area yields the peak force, F_{peak}, the average power can be calculated from

$$\text{Ave. Power} = F_{peak} \cdot |V_p|_{ave.} \tag{3.4.16}$$

In terms of root mean square values calculated from the PSDs:

$$\text{Average Power} = (3\sigma_f)\left(\sqrt{\frac{2}{\pi}}\,\sigma_v\right), \tag{3.4.17}$$

Since $F_{peak} = 3\sigma_f$ and

$$|V|_{ave.} = \sqrt{\frac{2}{\pi}}\,\sigma_v \tag{3.4.18}$$

for normally distributed, random forces and velocities. The rms force and rms lateral secondary velocity are given by σ_F and σ_v, respectively.

All four performance indices are input dependent. Hence, their absolute values are meaningful only as estimates of in-service performance. The indices are very useful, however, in showing improvements of one suspension over another.

3.4.c Band-Limited Actuator Study

This analysis studied the performance of an active vehicle for a variety of actuator bandwithds. The vehicle parameters were picked to simulate the structure of an Amcoach Passenger Car. An optimized passive suspension was designed to meet the following specifications:

1. Conicity of 0.05
2. Critical speed of 200 mph
3. Curving capability of 1 Degree-Curve (without flanging)
4. Dimensions to match an Amcoach

Design methods outlined in [3] were followed. Ride quality and secondary stroke were balanced with static considerations to set the secondary suspension parameters. Table 3.4.1 lists the parameters for the passive vehicle.

Optimization runs with ideal actuators (unity gain and no phase lag) yielded optimal feedback gains for the local controller. These values are 9000 lbs-sec/ft for the velocity feedback gain and 400 $lb \cdot sec^2/ft$ for the acceleration feedback gain. Table 3.4.2 shows the

TABLE 3.4.1: OPTIMIZED AMCOACH PASSIVE SUSPENSION

WHEEL RAIL PARAMETERS		
a_{11}	wheelset roll coefficient	0.05
δ_o	centered contact angle	0.05
Δ	contact angle difference	0.0
f_{11}	lateral creep force coefficient	2.12×10^6 lb
f_{12}	lateral/spin creep coefficient	17500 ft-lb
f_{22}	spin creep coefficient	160 ft^2-lb
f_{33}	longitudinal creep force coefficient	2.30×10^6 lb
WHEEL PARAMETERS		
a	half of track gauge	2.35 ft
N	load per wheelset	26100 lbs
λ	wheel conicity	0.05
Mw	wheelset mass	106.8 slugs
I_{wx}	wheelset roll moment of inertia	500 slugs-ft^2
I_{wy}	wheelset pitch moment of inertia	100 slugs-ft^2
I_{wz}	wheelset yaw moment of inertia	500 slugs-ft^2
Ro	centered wheel rolling radius	1.5 ft
TRUCK PARAMETERS		
dp	1/2 of primary springs lateral spacing	1.9 ft
b	1/2 of wheelbase	4.25 ft
h_{tp}	vertical distance from truck c.g. to primary lateral springs	0.35 ft
h_{ts}	vertical distance from truck c.g. to secondary lateral springs	1.33 ft

TRUCK PARAMETERS

I_{tz}	truck frame yaw moment of inertia	2108 slugs-ft^2
M_t	truck frame mass	212 slugs

CARBODY PARAMETERS

d_s	1/2 of secondary spring lateral spacing	3.75 ft
h_{cs}	vertical distance from carbody c.g. to secondary lateral springs	3.1 ft
ℓ_s	1/2 of truck center pin spacing	30 ft
w	weight of carbody	77433 lbs
I_{cz}	carbody yaw moment of inertia	1.483×10^6 slugs-ft^2
I_{cx}	carbody roll moment of inertia	64193 slugs-ft^2
M_c	carbody mass	2405 slugs

PRIMARY SUSPENSION PARAMETERS

k_{py}	primary longitudinal stiffness (4 per truck)	200,000 lb/ft
k_{px}	primary longitudinal stiffness (4 per truck)	380,000 lb/ft
c_{py}	primary lateral damping ($k_{py}/250$)	800 $\frac{\text{lb}}{\text{ft/sec}}$
c_{px}	primary longitudinal damping ($k_{px}/250$)	1520 $\frac{\text{lb}}{\text{ft/sec}}$

SECONDARY SUSPENSION PARAMETERS

k_{sy}	secondary lateral stiffness (2 per truck)	15000 lb/ft
k_z	secondary vertical stiffness (2 per truck)	19000 lb/ft
k_{spsi}	secondary yaw stiffness (1 per truck)	1×10^6 ft-lb/rad

SECONDARY SUSPENSION PARAMETERS

c_{sy}	secondary lateral damping (2 per truck)	1200 $\frac{lb}{ft/sec}$
c_{sz}	secondary vertical damping (2 per truck)	1700 $\frac{lb}{ft/sec}$
c_{spsi}	secondary yaw damping (1 per truck)	4000 $\frac{lb}{ft/sec}$

PASSENGER LOCATIONS FOR RIDE QUALITY

Front distance from carbody c.g.	x = 30 ft	z = 3.75 ft
Rear	x = -30 ft	z = 3.75 ft

PERFORMANCE CAPABILITIES OF BASELINE VEHICLE

Critical Speed	197 mph
Curving	1.0 degree curve at balance speed without flange contact

TABLE 3.4.2: RIDE QUALITY AND STROKE FOR ACTIVE RIDE CONTROLLER ON AMCOACH MODEL (100 mph)

	RMS Front Lateral Accel. (g's)	RMS Rear Lateral Stroke (in)	RMS Actuator Force (lbs)	Average Power/Car (kw)
Passive	.069	.56	0	0
Active	.035	.48	500	3.3
Reduction	50%	14%		

Active Gains -- Velocity Feedback - 9000 $\frac{\text{lb-sec}}{\text{ft}}$

Acceleration Feedback - 400 $\frac{\text{lb-sec}^2}{\text{ft}}$

rms accelerations and strokes for both the passive and ideal-actuator active vehicles. Further reduction in either acceleration or stroke is possible, but only at the expense of the other criterion. As shown in Figure 3.4.4, this feedback gain selection caused a significant reduction in carbody acceleration, especially around one hertz.

Both $1^{\underline{st}}$ and $2^{\underline{nd}}$ order actuator models were tested; however runs showed that differences between the models were negligible. Table 3.4.3 shows the results of two comparison runs. The $2^{\underline{nd}}$ order system had the same bandwidth as the $1^{\underline{st}}$ order system, and had an optimally flat damping ratio of 0.707. Differences in the results are 2% or less; therefore, the remainder of the tests incorporated the $1^{\underline{st}}$ order actuator model.

The parameter runs used actuator bandwidths of 1, 2, 3, 5, 10, and 20 Hz; numerical results are listed in Table 3.4.4.

Figure 3.4.5 shows the change in RMS stroke and acceleration versus actuator bandwidth. Note that increasing bandwidth continues to improve stroke toward its infinite bandwidth value. RMS acceleration, though, reaches and slightly surpasses its ideal actuator value with only a 3 Hz cutoff frequency.

Overall, 3 Hz bandwidth actuators can produce RMS lateral acceleration reductions at both front and rear passenger points of more than 50%; stroke reductions of 11% for the rear (the worst end for stroke) and 7% for the front can also be recognized. These stroke reductions represent about three-quarters of that possible with ideal actuators.

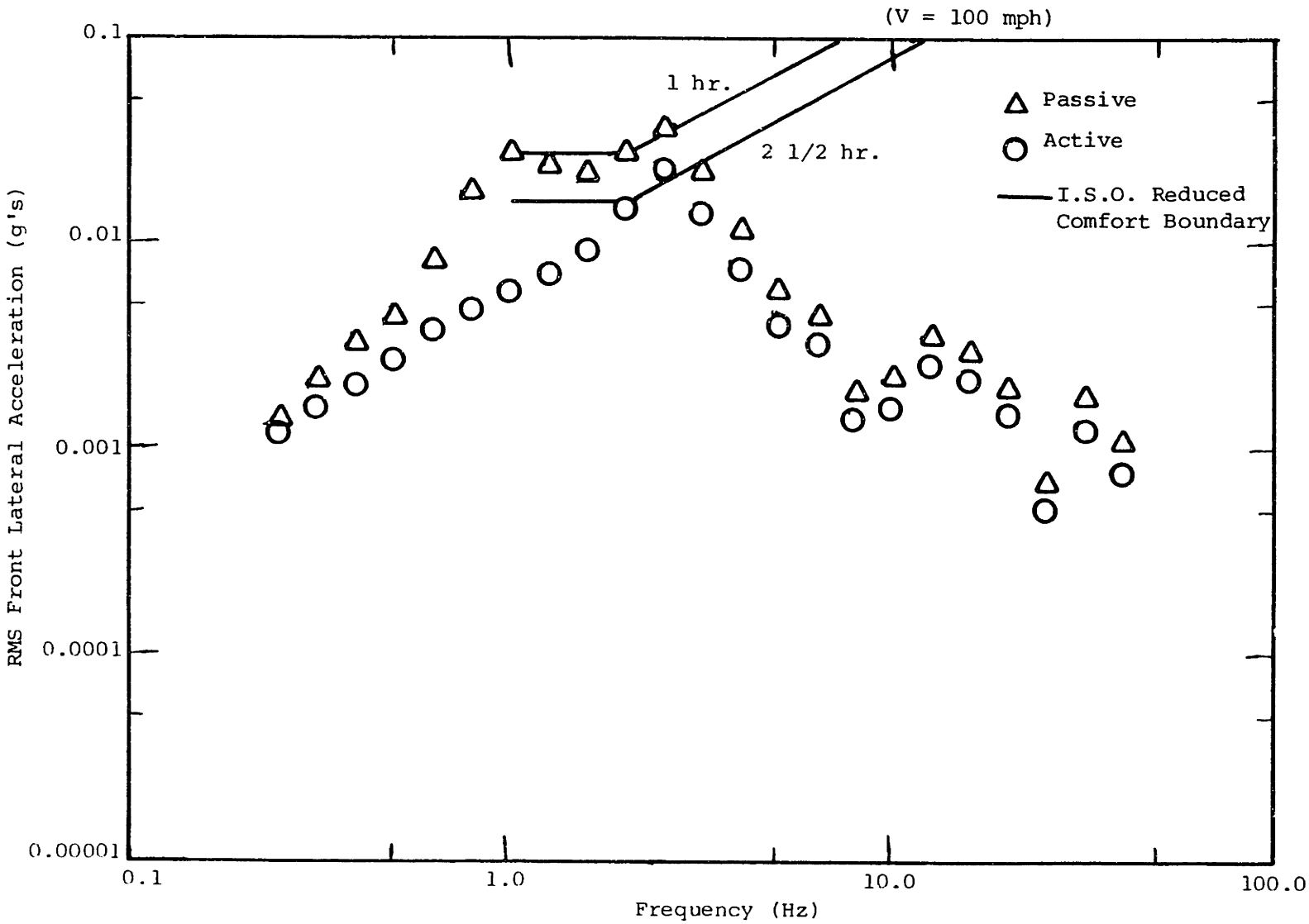

FIGURE 3.4.4: 1/3 OCTAVE BAND TOTAL RMS ACCELERATION FOR PASSIVE AND LOCAL-CONTROLLED AMCOACH

TABLE 3.4.3: COMPARISON OF 1st AND 2nd ORDER ACTUATOR MODELS (100 mph)

	RMS Front Acceleration (g's)	RMS Rear Stroke (in)	RMS Actuator Force (lb)	Average Power/Car (kw)
ACTUATOR MODEL				
Ideal	.0244	.505	566	3.97
1st Order	.0229	.514	502	3.49
2nd Order	.0224	.517	500	3.46
% Difference Between 1st and 2nd Order Models	2.0%	.6%	.4%	.8%

Break Frequency 5 Hz

2nd Order Damping 0.707

Active Feedback Gains

$k_3 = 12000 \frac{\text{lb-sec}}{\text{ft}}$

$k_4 = 1000 \frac{\text{lb-sec}^2}{\text{ft}}$

TABLE 3.4.4: VEHICLE PERFORMANCE WITH A BAND-LIMITED ACTIVE SECONDARY SUSPENSION (100 mph), LOCAL CONTROLLER

BREAK FREQUENCY	RMS FRONT ACCELERATION (g's)	RMS REAR STROKE (in.)	RMS ACTUATOR FORCE (lbs)	AVERAGE CAR POWER (kw)
∞ (Ideal)	.0346	.479	500	3.28
20 Hz	.0331	.482	485	3.16
10 Hz	.0323	.485	471	3.07
5 Hz	.0320	.491	448	2.94
3 Hz	.0333	.499	472	2.80
2 Hz	.0357	.509	408	2.69
1 Hz	.0424	.538	378	2.52
0 (Passive)	.0692	.559	0	0

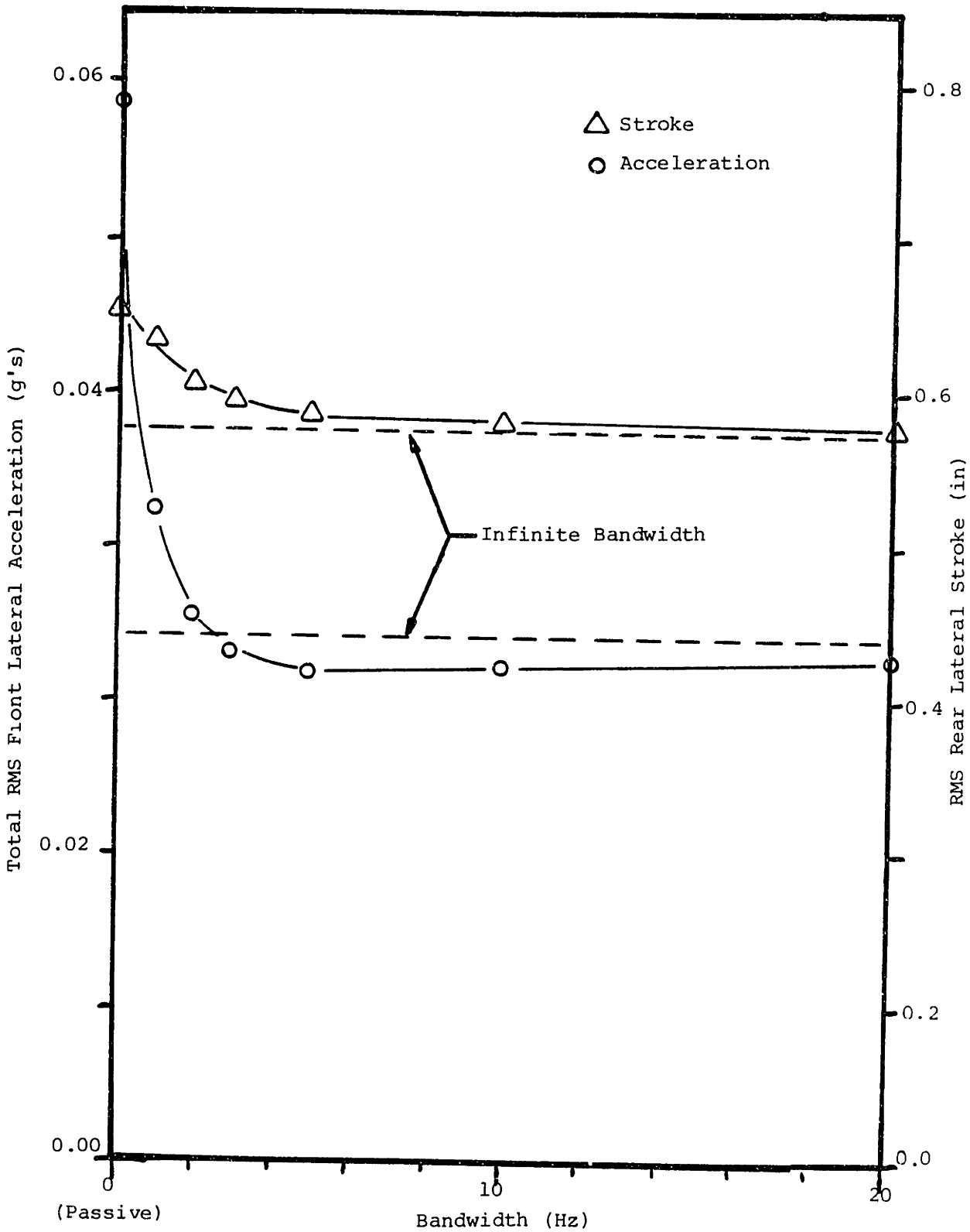

FIGURE 3.4.5: RMS VEHICLE PERFORMANCE VERSUS ACTUATOR BANDWIDTH

Average power consumption and RMS actuator force versus bandwidth are shown in Figures 3.4.6 and 3.4.7, respectively.

The ideal system demands 3.3 kw per car on the average. The lower bandwidths do not offer much of a savings; the 3 Hz actuators require 2.8 kw/car, or 85% as much power as the infinite bandwidth system.

RMS actuator force needed is similar. The 3 Hz actuators will produce 85% of the force predicted for ideal actuators. Thus, the system chosen should be capable of peak forces of 1500 lbs/actuator (2 actuators/truck) based on 3σ peak demands.

All systems must be able to respond with RMS velocities of .5 ft/sec.

A study of the active suspension design was also done at 110 mph. All other parameters were maintained. Results are presented in Table 3.4.5. At 110 mph the 3 Hz bandwidth active suspension reduced the RMS acceleration and stroke by 48% and 9%, respectively. Average power consumed was 3.4 kilowatts per car. Figure 3.4.8 shows the 1/3 octave RMS accelerations for the front lateral. The active suspension lowers the accelerations past the one hour reduced comfort limit and very close to the two and one-half hour limit. The most effective reduction is again below two hertz. Thus, significant performance improvements with reasonable power demands appear to be possible at up to 110 mph.

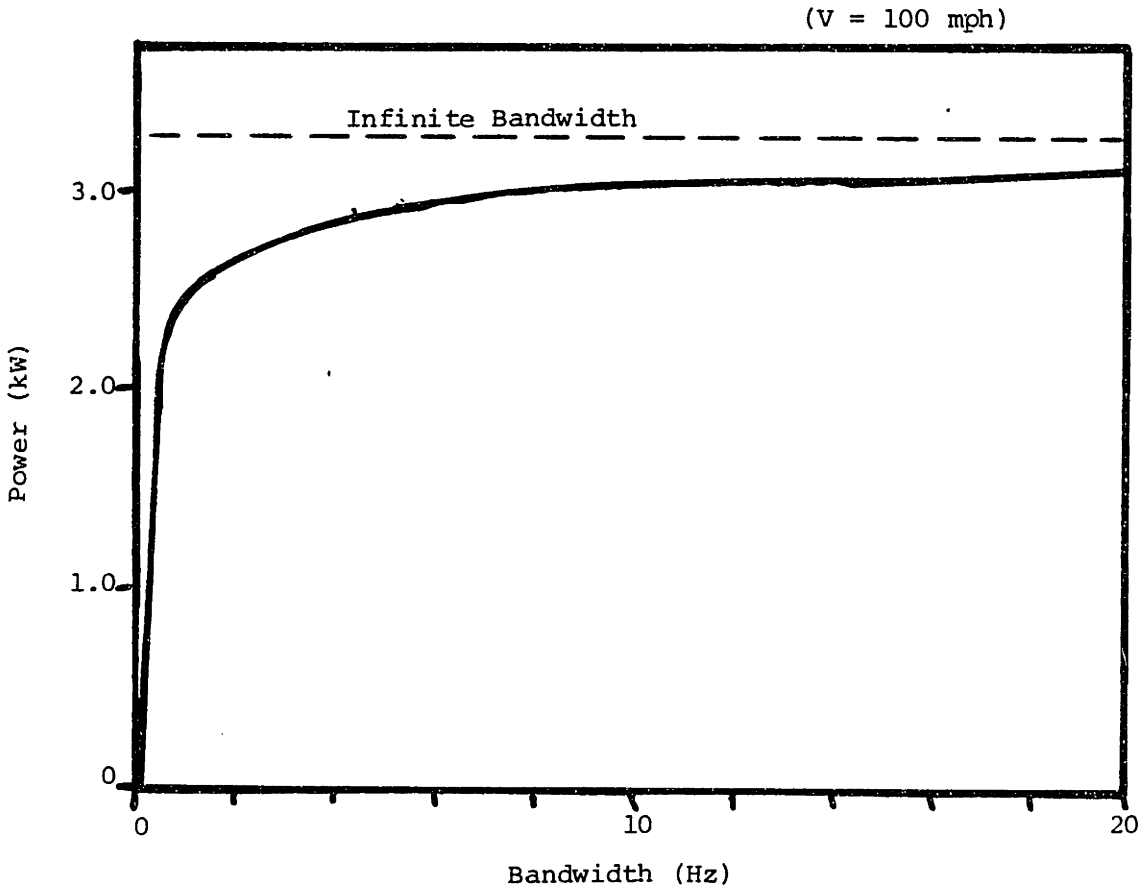

FIGURE 3.4.6: AVERAGE POWER CONSUMPTION VERSUS ACTUATOR BANDWIDTH

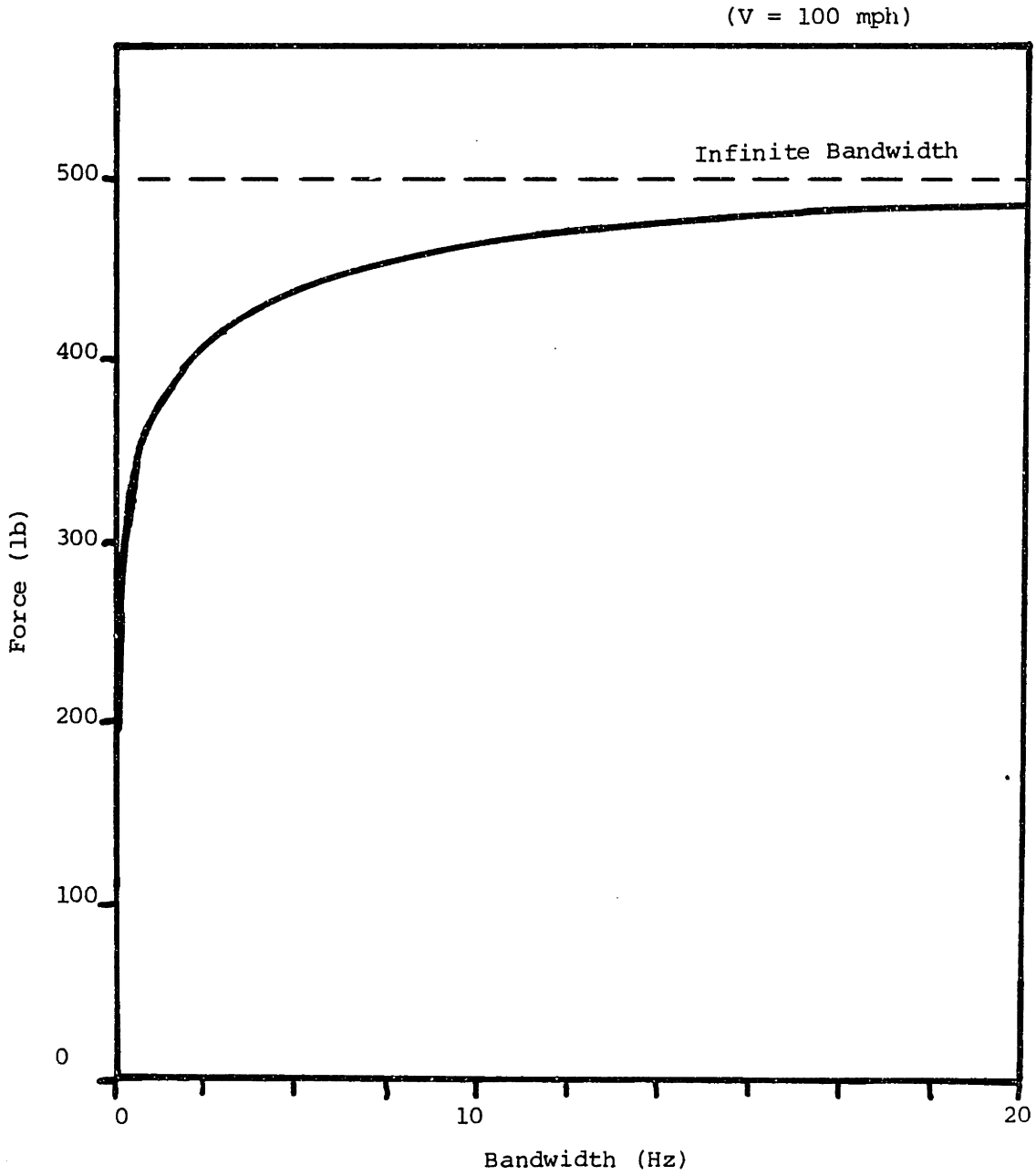

FIGURE 3.4.7: RMS ACTUATOR FORCE VERSUS ACTUATOR BANDWIDTH

TABLE 3.4.5: ACTIVE VEHICLE PERFORMANCE
(110 mph)

	RMS FRONT ACCELERATION (g's)	RMS REAR STROKE (in.)	RMS ACTUATOR FORCE (lbs.)	AVERAGE CAR POWER (kw)
Passive	.075	.58	0	0
Active	.039	.53	450	3.4

(3 Hz Bandwidth)

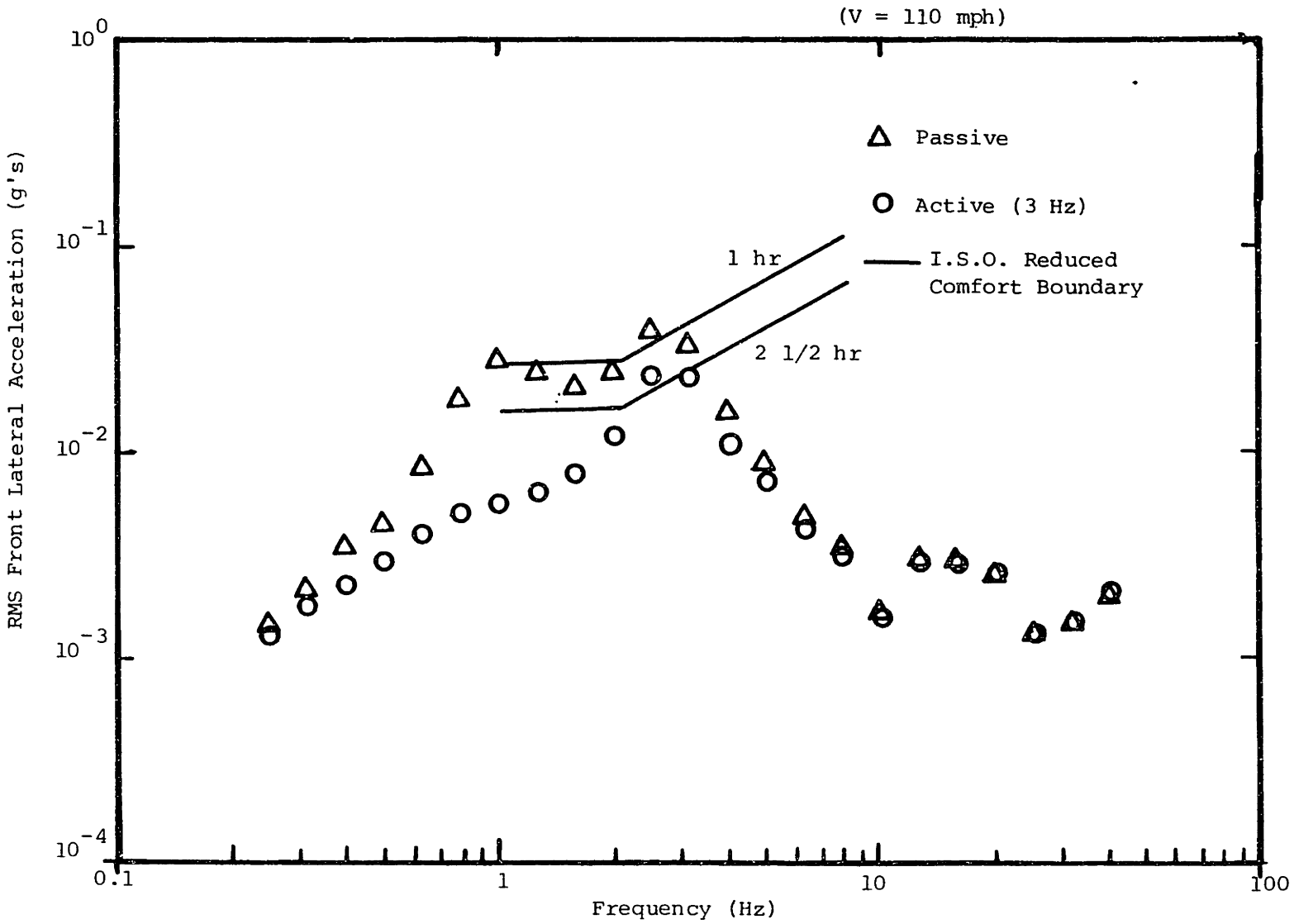

FIGURE 3.4.8: 1/3 OCTAVE BAND TOTAL RMS ACCELERATION FOR PASSIVE AND 3 HZ LIMITED BANDWIDTH ACTIVE AT 110 MPH

3.5 Equipment Considerations

The selection of active components is based on many factors:

1. Actuator performance
    i. peak force
    ii. peak velocity & stroke
    iii. frequency response
2. System Size
    i. actuator dimensions
    ii. power supply dimensions & weight
3. System Reliability, Maintenance

The performance requirements were determined in the bandwidth studies. Assuming 3σ peaks, the maximum values of force, velocity, and stroke required from an ideal actuator are 1500 lbs., 1.5 ft/sec, and 1.5 in., respectively. As shown previously, a bandwidth of at least 3 Hz is desired to get significant performance improvements.

In this section a critique of possible actuator systems is presented. The potential actuator types discussed are hydraulic, pneumatic, and electro-magnetic.

Hydraulic

Hydraulic actuation systems are noted for their ability to generate large forces, give large displacements, and provide high bandwidths. These systems are also rugged.

M.A.N. tested two hydraulic systems and found their response to be flat to at least 18 Hz [7]. British Rail Research has also tested hydraulic systems. Results of a servo-hydraulic powered, active lateral suspension indicate a 6 Hz bandwidth for the force control loop [13].

The major deterents to hydraulic power are the introduction of a new power source on board, the bulk of the system, and the added maintenance problems involved. Electric and pneumatic power are already used on AMTRAK vehicles. Hydraulic power would require new equipment and additional training for personnel not used to maintaining this type of system. Also, during failure hydraulic systems can become rigid (lock-up), causing severe vibrations.

Pneumatic

Pneumatic suspension systems also offer potential. Pneumatic brake systems and air bag secondaries are already in use; thus, pneumatic maintenance is practiced in the industry. However, the compressibility of air causes a lag in servo response.

Japanese National Railways and Hitachi Ltd. have designed pneumatic systems and tested them on a full-scale, single-degree-of-freedom model, and on a $\frac{1}{5}$ - scale model car [6]. The full-scale test used a supply of 50 N/cm (72.5 psi) and a 10 cm diameter cylinder (3.94 in). Stroke for the servo cylinders was $\pm$ 23 mm ($\pm$ .91 in). The servovalve had a 2.3 Hz break frequency. The $\frac{1}{5}$ - scale test incorporated a faster valve such that the unit provided a 3.2 Hz bandwidth to the point where the phase lag was 45°. Only 5 cm cylinders were used

for this test. Both tests yielded 50% reductions in vibration.

Based on a supply pressure of 250 psi, a piston area of 6 square inches would be required to meet the 1500 lb peak force requirements. Hence, the cylinder volume, V, and maximum flow, Q_{peak}, are 18 in^3 and 108 in^3/sec, respectively. The desired time constant corresponding to a 3 Hz break frequency is $\tau = 0.05$ sec. Thus, the system must allow

$$\tau = RC \tag{3.5.1}$$

$$C = V/\beta \tag{3.5.2}$$

where R is the valve resistance, C, the capacitance, and β is the bulk modulus (~60 psi). The maximum resistance yielded for the servo valve was calculated to be 0.17 $\frac{psi}{in^3/sec}$.

Calculations show the valve's resistance in ref. [6] to be about 0.20 $\frac{psi}{in^3/sec}$. The pneumatic systems should be investigated thoroughly as a possible source of actuation power. Pneumatics require no return lines and the compressibility offers compliance in case of failure. Power consumption levels must be studied.

Electro-Magnet

Electro-magnets can create large forces and have a high bandwidth [8]. Double acting electro-magnetic actuators operate in both attraction and repulsion. Limitations are based on the requirement to maintain a small air gap between surfaces.

3.6 Conclusion

This study of band-limited, actively-controlled lateral dynamics showed that a 3 Hz bandwidth actuation system can reduce RMS carbody accelerations significantly.

At 100 mph, the proposed vehicle is predicted to exhibit reductions in RMS accelerations of 50% over the passive vehicle. This is an equal reduction to that expected from a system with "ideal", or infinite bandwidth, actuators. Stroke reductions realized are about 75% of those predicted for an ideal system.

Due to the present practices of the rail industry, a pneumatic actuator system would be most satisfactory from implementation, maintenance, and failure standpoints.

Chapter 4 presents the designing, modeling and simulating of a pneumatic actuation system.

CHAPTER 4

PNEUMATIC ACTUATOR DESIGN

4.1 Introduction

Implementation of the control scheme presented in Chapter 3 requires the designing of an actuator system. Pneumatic power is used on Amtrak trains for brake lines and water pressure. Hence, it is available onboard in limited quantities, and maintenance of pneumatic systems is common practice for Amtrak personnel workers. This chapter pursues the design of a pneumatic actuator system, including system configuration, sizing requirements, analytical modeling, and digital simulation.

4.2 Actuator Requirements and System Configuration

The first step in designing the pneumatic system involved determining its performance requirements. These parameters were determined by the bandwidth parameter studies of Chapter 3 and set the basis for system sizing.

The bandwidth parameter studies used a linear, 15-DOF vehicle model (Appendix A) with a Class 6 track model as an input; the actuators were modeled as single-input, single-output, first order lags with the actuators' break frequency left adjustable. The vehicle's forward speed was 100 mph. Suspension performance was judged based on root mean square carbody accelerations and strokes, as well as comparison of 1/3-octave bandwidth rms lateral accelerations to the ISO 1/3-octave lateral ride quality standards.

The actuator performance demands are:

- Peak lateral force/truck $\pm$ 3000 lbs.
- Peak Velocity $\pm$ 1.5 ft/sec
- Peak Stroke $\pm$ 1.5 in
- Bandwidth $\geq$ 3 Hz

All states were considered to be Gaussianly distributed, zero mean variables, such that the peak values were assumed to be three times the rms values calculated in the frequency domain bandwidth studies of Chapter 3.

4.3 System Configuration

A pneumatic actuation system consists of many components. The major components are:

- actuator
- servovalve
- compressor
- accumulator

Figure 4.3.1 shows how the components are connected.

The accumulator, servovalve, and actuator are placed as close together as possible to reduce the pressure loss between components. The actuator is a transformer that converts the fluid pressure to force. Two typical actuator types are the pneumatic cylinder (Figure 4.3.1) and the airspring (Figure 4.3.2). In order to operate the airspring as a double-acting actuator, two airsprings must be used to back; this allows each airspring to maintain a preload. The pair

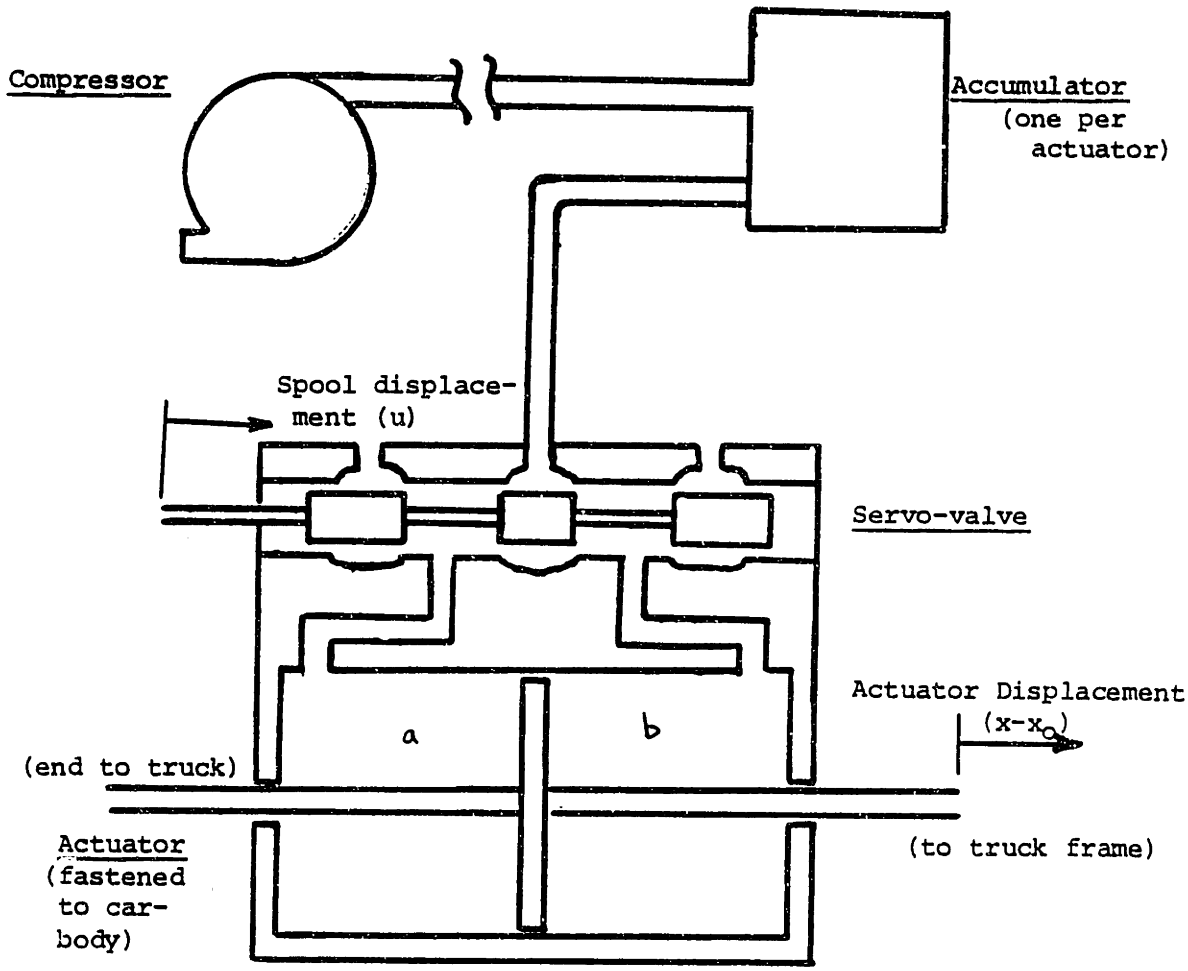

Active Equipment

FIGURE 4.3.1: ACTIVE SYSTEM COMPONENTS

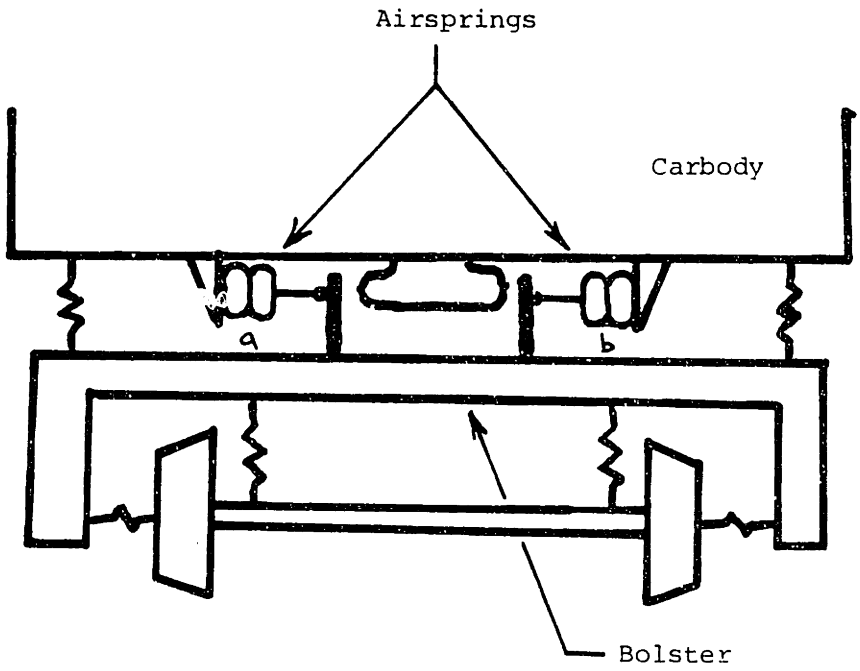

FIGURE 4.3.2: AIRSPRING PAIR AS A DOUBLE-ACTING ACTUATOR

can then create forces in both directions and functions the same way a pneumatic cylinder does. The force generated is given by

$$F = P_a \cdot A_{pa} - P_b \cdot A_{pb} \qquad (4.3.1)$$

where P_a and P_b are the internal pressures, and A_{pa} and A_{pb} are the piston areas for sides "a" and "b" of the actuator, respectively. For pneumatic cylinders the areas are constant and usually equal, in order to provide symmetric force characteristics. The effective piston areas for airsprings vary with the spring's compression or expansion. Compression causes the rubber sides to expand outward, increasing the effective piston area; expansion decreases the area.

The function of the servovalve is to direct airflow into and out of the actuator chambers such that the desired force is produced. Air into the actuator is supplied at high pressure by the compressor; air out of the actuator is vented to the atmosphere.

To even out the irregular demands of the servovalve an "accumulator" is placed between the compressor and the valve. A pneumatic accumulator is simply a large tank, filled with compressed air. It is filled at a constant rate by the compressor and discharged sporatically by the servovalve. The accumulator is designed to be large enough that it appears as a constant pressure source to the servovalve. The compressor provides the average flow, while the accumulator covers the peak flow demands.

Air compression can be provided by a single compressor or by multiple compressors spread among the consist.

Presently, an air compressor serving the brakes, the airbags, and the water tanks for the entire train is located in the locomotive. This compressor feeds two independent lines at about 130 psig. One line supplies the brakes; the second serves all other air needs (Figure 4.3.3). This second line could be tapped for active power. The compressors currently used onboard the Amtrak AEM-7 and F-40 locomotives have limited flow capacities of 135 and 254 ft^3/min, respectively.

Multiple compressor utilization requires the placement of electric compressors onboard the cars; either one per car, or a few cars per compressor. This configuration suffers less pressure loss between compressor and accumulator, but requires more individual pieces of equipment and demands more space per car. The individual cars' electrical needs would also increase.

Since the local controller being employed in the active suspension requires only that lateral forces are generated (no torques), a single actuator per truck is sufficient. Figure 4.3.4 is a schematic of the active component placement on the truck. Although future use of torque actuation is not possible with a one actuator design, the single lateral actuator located at the center of the truck cannot create any torques on the truck that might interfer with the curving dynamics of the vehicle.

The accumulator and the main body of the actuator are attached to the carbody for better isolation from vibrations. Components are placed in close proximity to allow short connection lines.

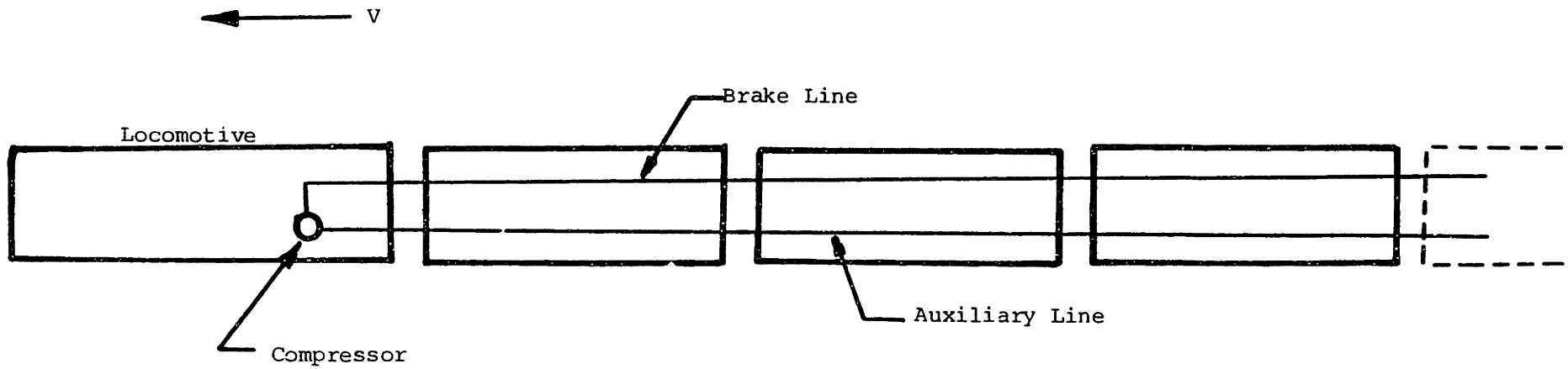

FIGURE 4.3.3: AMTRAK AIR SUPPLY

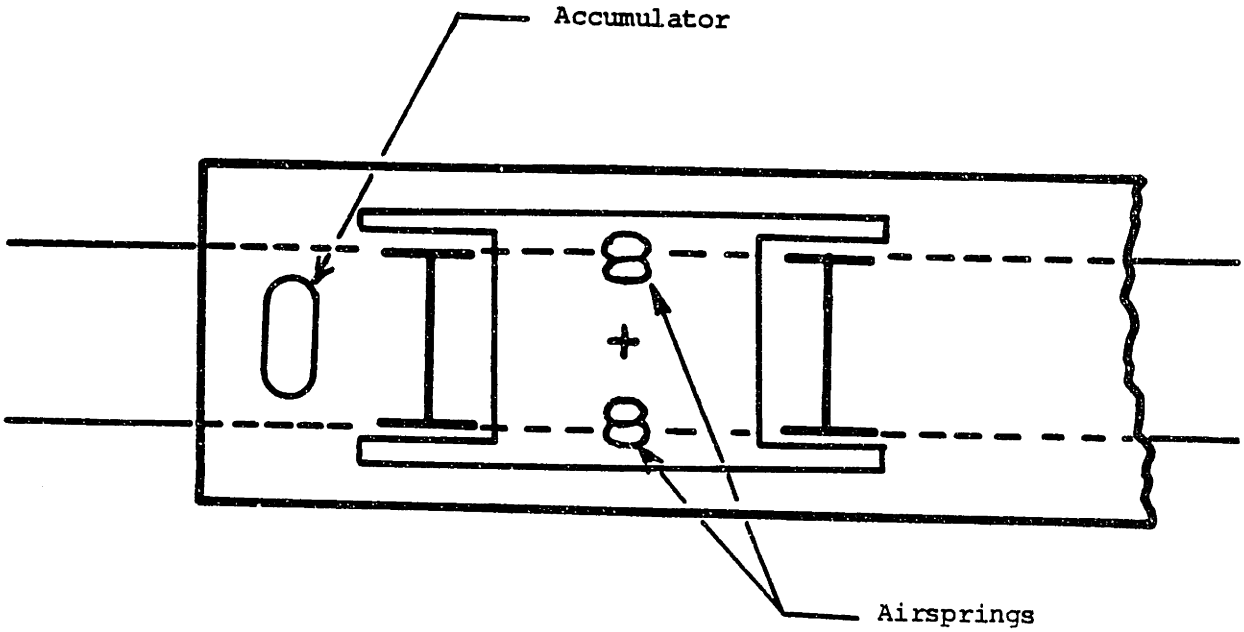

FIGURE 4.3.4: ACTIVE SYSTEM EQUIPMENT PLACEMENT ON TRUCK

4.4 Analytical Models

Design of the pneumatic actuator system required analytical modeling of each of the four major components; four separate models describe the four different functions served by the components. In addition, a force feedback loop is closed around the servovalve-actuator assembly to control the output force. This force feedback loop compares the actual and the desired forces, and drives the valve with a signal proportional to the force error, e. The closed loop, proportional controller increases the actuator system's bandwidth and its accuracy.

4.4a Actuator Dynamics

An actuator converts fluid power to mechanical power. The chambers in a pneumatic actuator function as variable-volume fluid capacitors due to the moving piston and the compressibility of the gas.

The transformer relation of the actuator is given algebraically by summing the forces on the piston for a pneumatic cylinder (Figure 4.4.1), or finding the difference of the two opposing forces for a double airspring actuator (Figure 4.4.2). In either case,

$$F = P_a \cdot A_{pa} - P_b \cdot A_{pb} \qquad (4.4.1)$$

where F is the resultant force, P denotes the chamber pressure, and A_p denotes the effective piston area (the transformer modulus). Subscripts "a" and "b" refer to the actuator chambers.

While the piston areas for a pneumatic cylinder are constant and

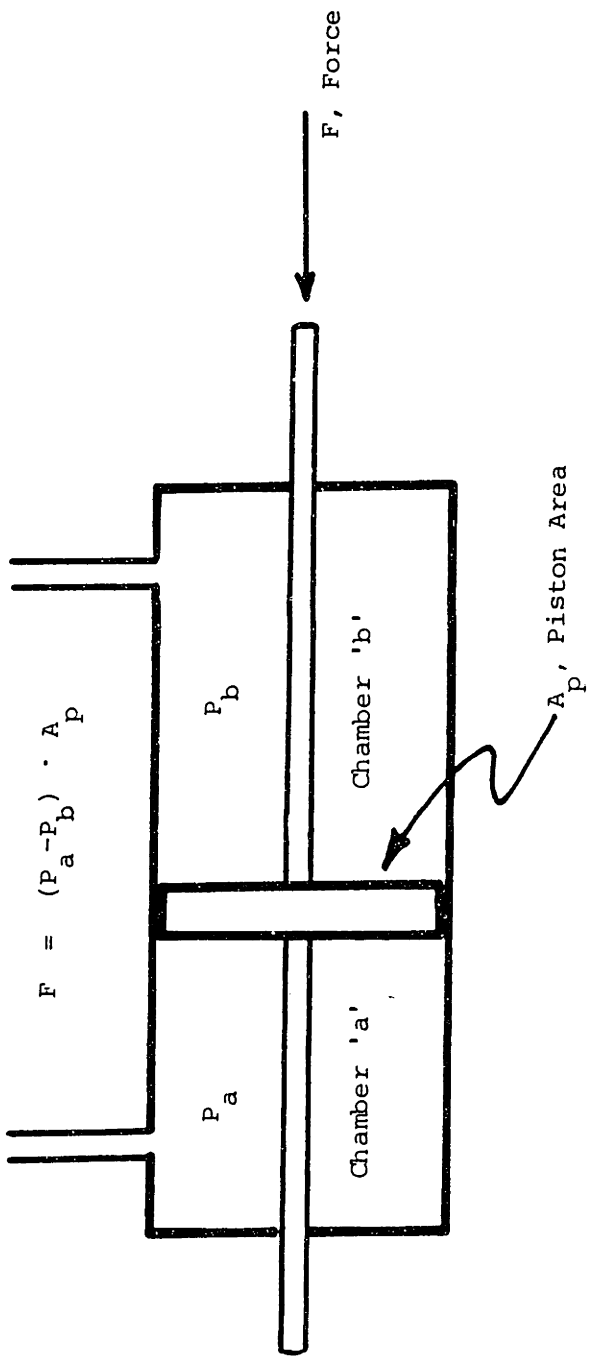

FIGURE 4.4.1: A PNEUMATIC CYLINDER AS A PRESSURE-FORCE TRANSFORMER

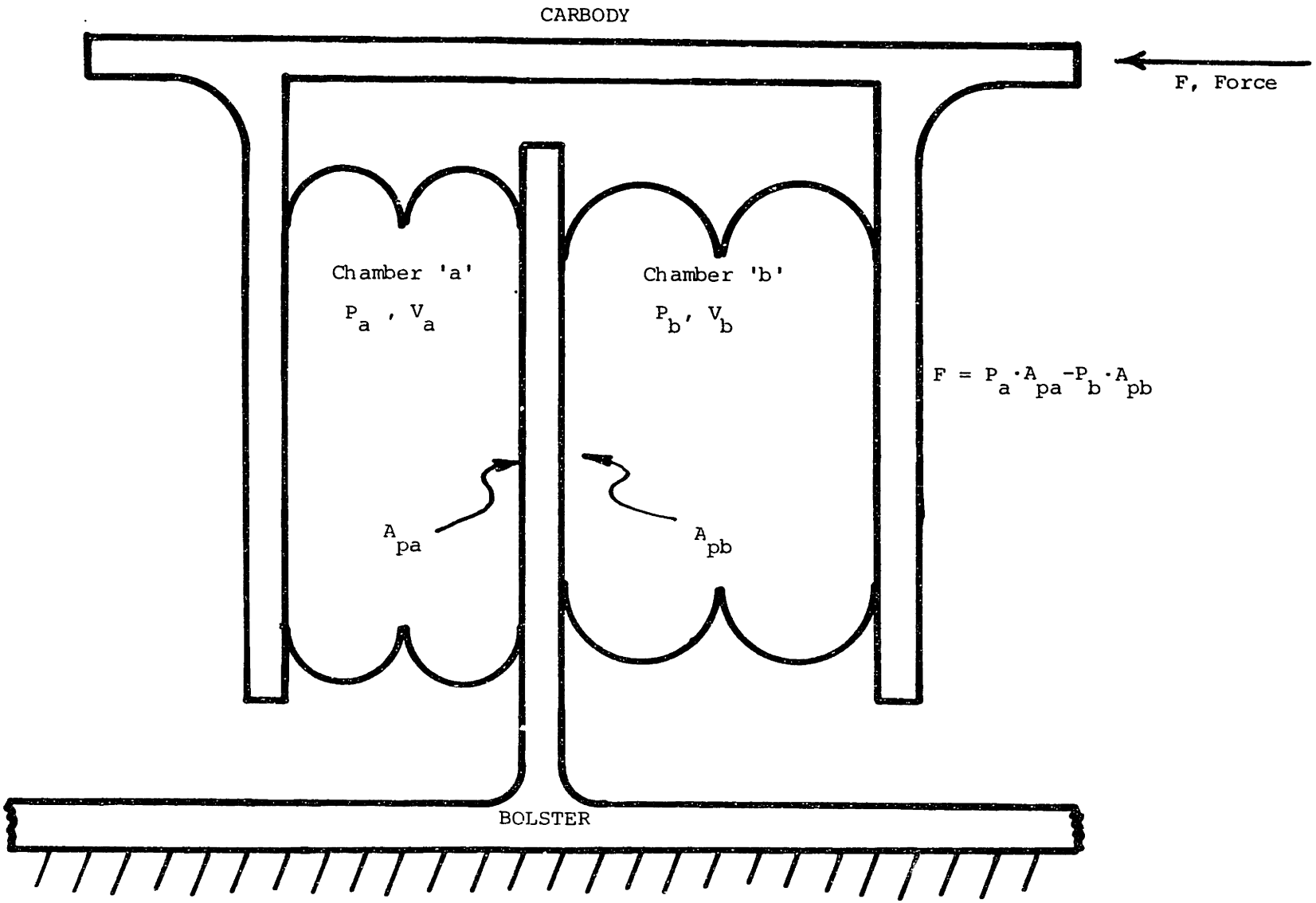

FIGURE 4.4.2: DOUBLE AIRSPRING ACTUATOR AS A PRESSURE-FORCE TRANSFORMER

often equal for both chambers, the effective area for an airspring varies due to the airspring extension. Figure 4.4.3, taken from reference [14], shows how the force varies with airspring compression for a constant pressure. The transformer modulus, A_p, at any airspring height is equal to the spring's force divided by the internal pressure.

Modeling the capacitance characteristic of an actuator chamber is more complex and results in a relationship between the chamber's pressure and volume, and the mass flow into the chamber (Figure 4.4.4).

The mass of air inside an actuator chamber is given by

$$m = \rho V \tag{4.4.2}$$

where ρ is the mass density, V is the chamber volume, and m is the mass of the air. The change of mass with time is equal to the rate of mass flow into the control volume (the chamber). Hence,

$$\dot{m} = \frac{dm}{dt} = \frac{d}{dt}(\rho V). \tag{4.4.3}$$

Assuming an ideal gas and substituting for ρ yields

$$m = \frac{d}{dt}\frac{PV}{RT} \tag{4.4.4}$$

where P and T are the pressure and temperature of the chamber air, respectively, and R is the universal gas constant. The process is assumed to be reversible, and in the extremes can take place isothermally or adiabatically.

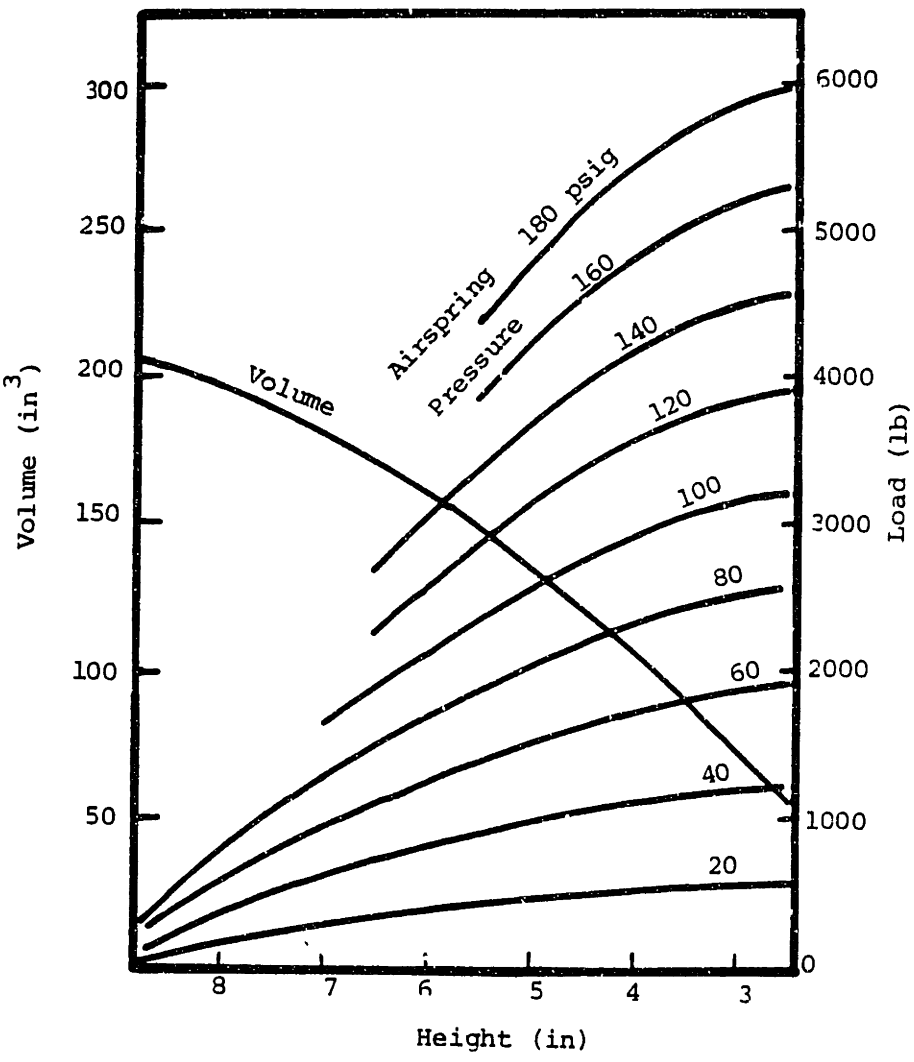

FIGURE 4.4.3: CHARACTERISTICS FOR FIRESTONE 224 AIRMOUNT ® AIRSTROKE ® AIRSPRING [14]

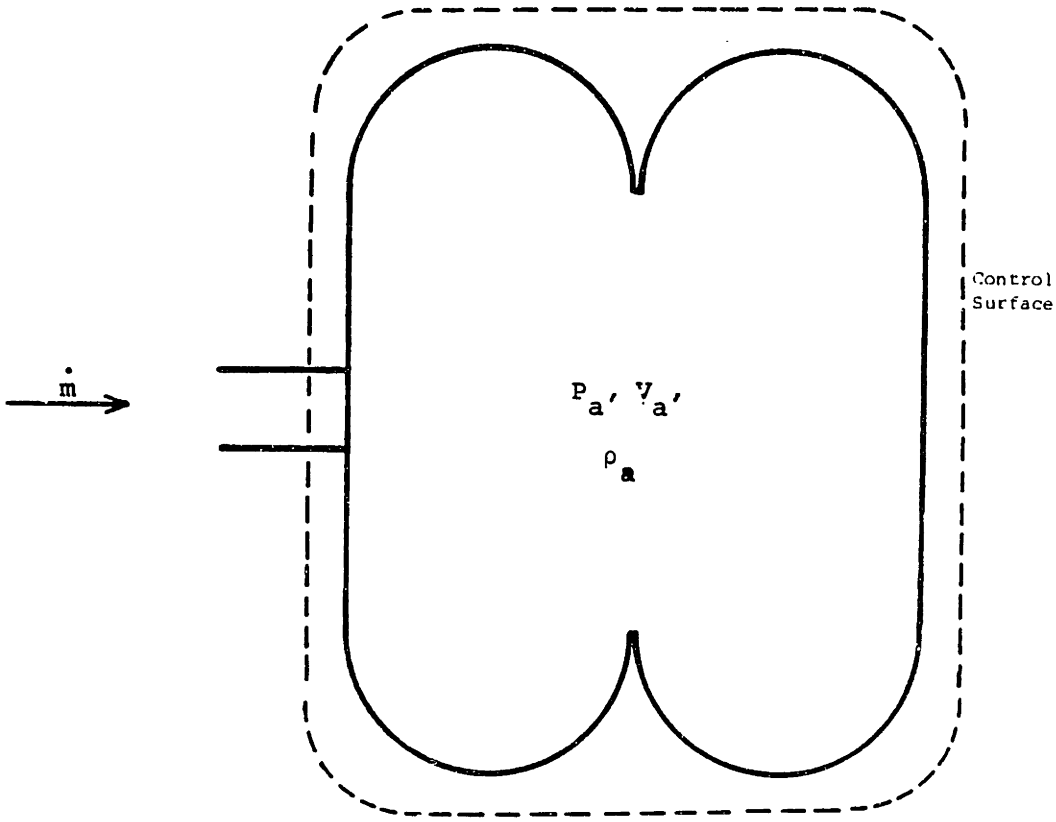

FIGURE 4.4.4: CONTROL SURFACE FOR AIRSPRING

An isothermal assumption implies a very slow process where the heat transfer is sufficient to maintain a constant gas temperature [15] with the temperature constant, equation (4.4.4) becomes

$$\dot{m} = \frac{V}{RT}\frac{dP}{dt} + \frac{P}{RT}\frac{dV}{dt}. \qquad (4.4.5)$$

If the system is cycling quickly, the heat transfer rate becomes negligible and the process can be considered adiabatic [15]. For an adiabatic process, reference [16] gives the relation

$$P\,\rho^{-k} = \text{constant}. \qquad (4.4.6)$$

The value of k for air is 1.4.

Solving this for ρ and substituting into equation (4.4.3) yields

$$m = \frac{1}{k}\,\frac{V}{RT}\,\frac{dP}{dt} + \frac{P}{RT}\frac{dV}{dt} \qquad (4.4.7)$$

when the differentiation is carried through.

Comparing equations (4.4.5) and (4.4.7) shows them to be identical except for the factor k in the denominator of the first term in equation (4.4.7).

Multiplying through the mass flow equations by the acceleration due to gravity, g, gives the weight flow rate, W. When using the actuator as a force source, the chamber pressure is the dependent, or state variable. Hence, the state equation form is

$$\frac{dP}{dt} = \frac{n}{V(h)}\left(\frac{RT}{g}\cdot W - p\,\frac{dV(h)}{dt}\right) \qquad (4.4.8)$$

where $1 \leq n \leq 1.4$. (4.4.9)

(isothermal) (adiabatic)

The actual process is neither isothermal nor adiabatic, but falls somewhere in between. These two ideal models demonstrate the conservative and liberal cases, respectively. Since the actuator is expected to cycle frequently the adiatatic assumption is closer to the actual process and was therefore used.

Thus, the actuator is modeled by equations (4.4.1) and (4.4.8). For an airspring the volume and effective piston area must also be known and are a function of the airspring compression.

4.4b Valve Dynamics

The purpose of the servovalve is to control the flow of fluid into and out of the actuator chambers such that the desired force is generated.

Figure 4.3.1 shows a four-way, spool valve. As the spool is moved to the right, it opens the ports connecting chamber "a" to the pressure source and exposes chamber "b" to atmospheric pressure. This increases pressure in chamber "a", while decreasing the pressure in chamber "b". The speed at which the pressure rise takes place is related to the size of the port openings exposed by the spool displacement.

The specification of "four-way" refers to the four ports on the valve which implies that both valves have the option of filling or exhausting. This function can be served identically by two synchro-

chronized three-way valves; Figure 4.4.5 shows both valve arrangements schematically. The valves shown here are three-position, solenoid valves. The orifice size in a solenoid valve is fixed and can only be fully open or closed. In the center position both actuator chambers are closed off. In the other positions one chamber fills, while the other exhausts. The spool valve has variable orifice areas; with the area linearly related to the spool displacement.

The flow rate through the valve is a function of the orifice area as well as the pressures on both sides of the orifice. This relation for compressible flow through an orifice is given in reference [15] as follows:

$$W = c_d A_o c_2 \frac{P_u}{\sqrt{T_u}} f_1\left(\frac{P_d}{P_u}\right) \qquad (4.4.10)$$

W = weight rate of flow, lb/sec

c_d = discharge coefficient of the orifice, dimensionless

A_o = orifice area, in^2

P_u = upstream stagnation pressure, psia

P_d = downstream pressure, psia

T_u = upstream stagnation temperature

c_2 = constant based on the gas properties

The function $f_1\left(\frac{P_d}{P_u}\right)$ is shown graphically for air in Figure 4.4.6. Analytically it is given by

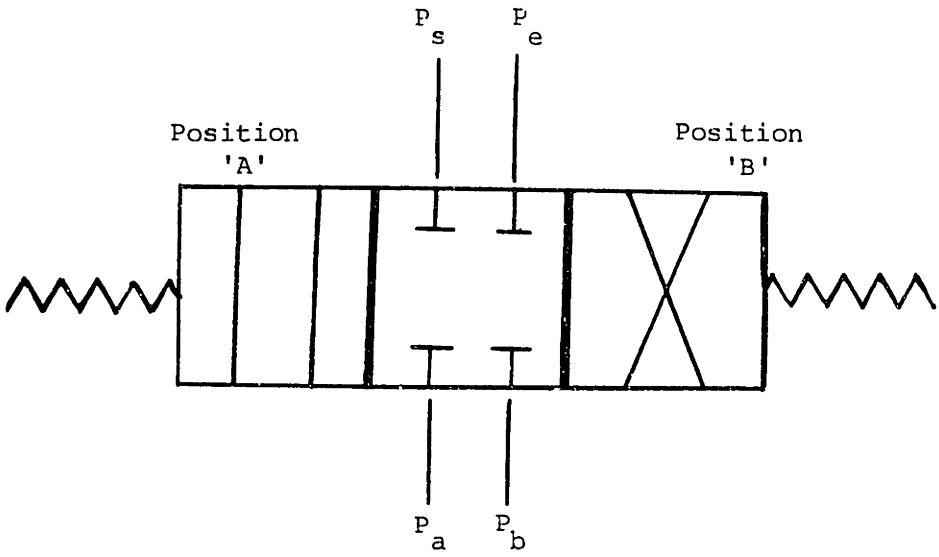

Four-Way Solenoid Valve

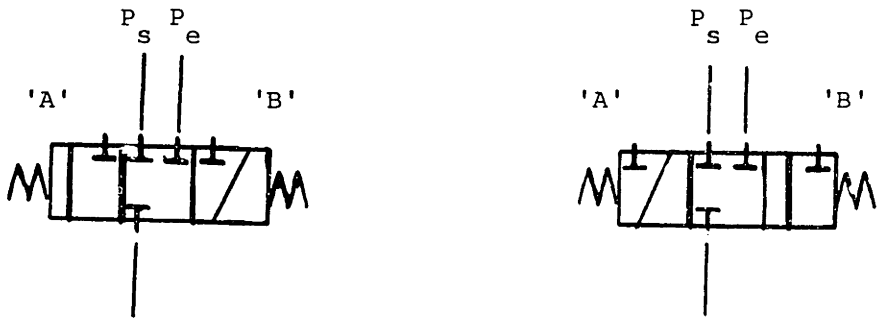

Two Synchronized Three-Way Solenoid Valves

FIGURE 4.4.5: SCHEMATIC OF FOUR-WAY SOLENOID VALVE VERSUS EQUIVALENT THREE-WAY VALVE PAIR

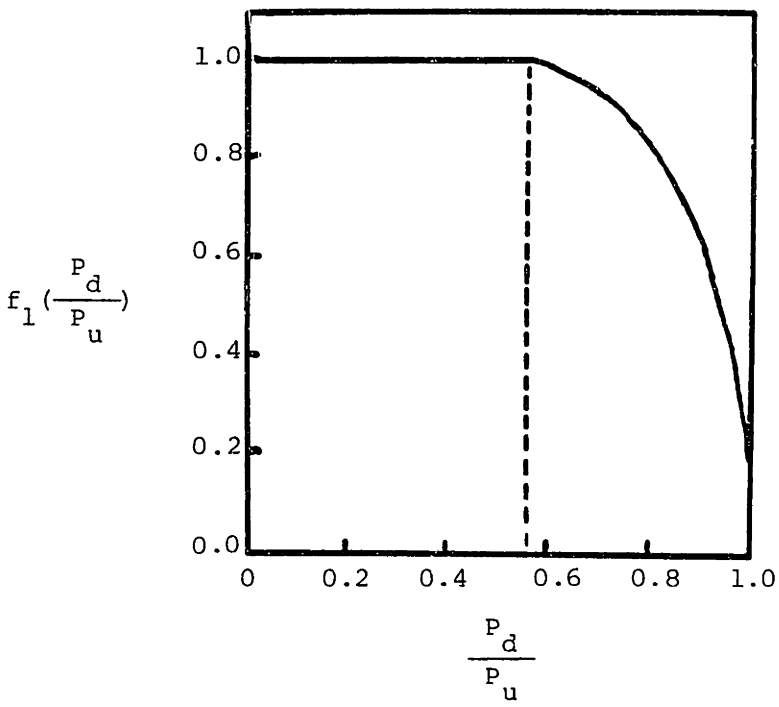

FIGURE 4.4.6: PLOT OF $f_1(P_d/P_u)$

$$f_1 = \frac{c_1}{c_2}\left(\frac{P_d}{P_u}\right)^{1/k}\left[1 - \left(\frac{P_d}{P_u}\right)^{(k-1)/k}\right] \quad \text{for } \left(\frac{P_d}{P_u}\right) > \left(\frac{P_d}{P_u}\right)_{crit}$$

(4.4.11)

$$\text{or} \qquad f_1 = 1 \qquad \text{for } \left(\frac{P_d}{P_u}\right) \leq \left(\frac{P_d}{P_u}\right)_{crit}$$

The constants c_1 and c_2 are given by

$$c_1 = g\sqrt{\frac{2k}{R(k-1)}}$$

(4.4.12)

$$c_2 = g\sqrt{\frac{k}{R\left(\frac{k+1}{2}\right)^{(k+1)/(k-1)}}}$$

with g = acceleration of gravity, 386 in/sec^2

k = ratio of specific heats for the gas

R = ideal gas constant.

For air, these values are

$k = 1.4$

$R = 2.47 \times 10^5$ in^2/sec^2 °R

$$c_1 = 2.06 \ \frac{\sqrt{°R}}{sec}$$

$$c_2 = 0.532 \frac{\sqrt{^\circ R}}{sec} .$$

When the flow being calculated is going into a chamber of the actuator from the supply, the upstream properties, denoted by the subscript "u", are those of the supply, the accumulator; the downstream properties, "d", are those of the chamber. For an exhausting chamber, the chamber properties serve as upstream properties, while the downstream properties are those of the atmosphere.

The critical pressure ratio, $(\frac{P_d}{P_u})_{crit.}$, is the ratio of pressures below which flow becomes "choked". Further decreasing the downstream pressure has no effect on the flow rate, because flow in the orifice is at the local speed of sound. The pressure information, or pressure wave, cannot travel upstream through the sonic flow; so, the flow rate remains constant even as P_d is decreased. For air, the critical pressure ratio is 0.528. Note that $f_1(\frac{P_d}{P_u})$, as shown in Figure 4.4.6, is constant below a 0.528 pressure ratio; thus equation 4.4.10 becomes independent of P_d for "choked" flow.

4.4c Accumulator

An accumulator is used in fluid systems to help isolate system components from one another's undesirable dynamics. The force demanded of the actuator is quite random in nature, and therefore the flows demanded by the servovalve will also be sporadic; while the pressure supplied to the valve, P_s, is preferred constant. The compression is best operated as under steady-state, steady flow conditions providing

the average flow needed at output pressure P_s.

The accumulator pressure should remain reasonably constant despite the loss of gas. Any flow demand greater than that supplied by the compressor must come from the air supply stored in the accumulator. Hence, the accumulator discharges to provide air during peak demands and recharges whenever demands are lower than that being supplied to it from the compressor.

The accumulator was sized to provide all the air for several full strokes of the actuator with only a small drop in pressure. Equating the mass flows out of the accumulator and into the actuator, and applying the ideal gas law to eliminate the density, the actutor volume is given by

$$V_{acc} = \frac{P_{mean}}{\Delta P_{acc}} \Delta V_{act}. \qquad (4.4.13)$$

Here

P_{mean} = mean chamber pressure

ΔP_{acc} = acceptable pressure change in the accumulator

ΔV_{act} = total volume of air displaced in the desired number of strokes.

4.4d Compressor Thermodynamics

Having provided sufficient capacitance in the accumulator, the pressure inside the accumulator remains fairly constant; allowing the compressor to maintain a steady flow rate. Thus, the compression is modeled as a steady-state, steady flow process (SSSF) and is assumed to be reversible.

Figure 4.4.7 shows the control surface used to analyze the compressor. The compressor takes air in from the atmosphere and compresses it to the supply pressure, P_s. Ideally this process could take place isothermally or adiabatically (or in some combination) depending on the amount of heat transfer that takes place. For any reversible, SSSF process with no change in kinetic or potential energy, the specific work is given in reference [16] to be

$$w = \int_i^e \frac{dP}{\rho} . \qquad (4.4.15)$$

This further reduces for the isothermal case where

$$\frac{P}{\rho} = \text{constant},$$

to yield,

$$w = RT_i \ \ell n \ \frac{P_e}{P_i} . \qquad (4.4.16)$$

For adiabatic compressions,

$$\frac{P^{1/k}}{\rho} = \text{constant},$$

yielding

$$W = \frac{k}{k-1} RT_i \left[\left(\frac{P_e}{P_i} \right)^{(k-1)/k} - 1 \right]. \qquad (4.4.17)$$

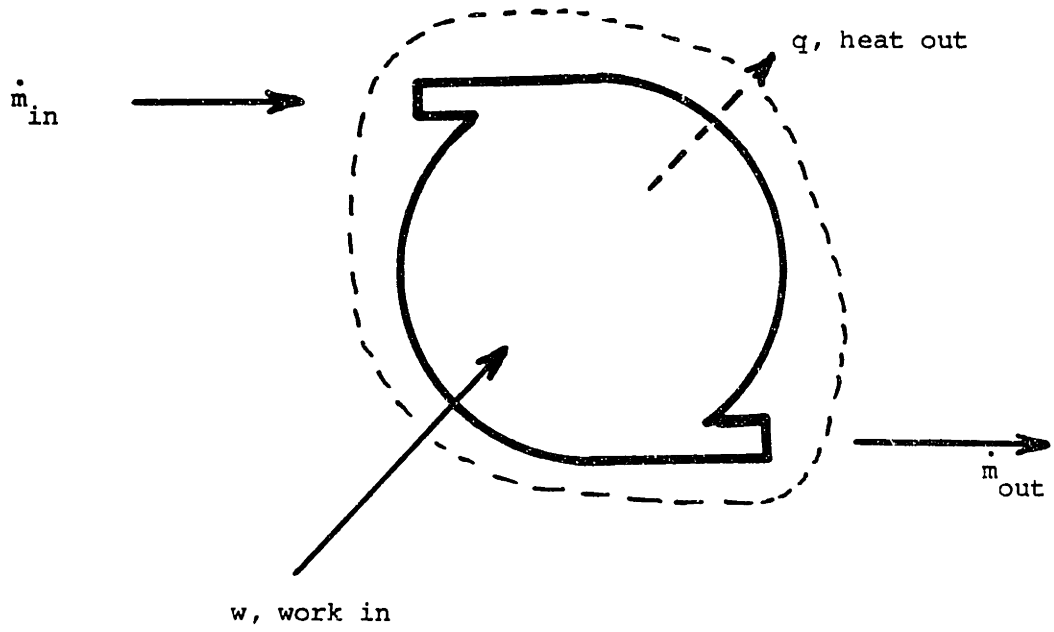

FIGURE 4.4.7: COMPRESSOR CONTROL SURFACE

The initial conditions are those of the surroundings and the exit pressure of the compressor, P_e, is equal to the supply pressure, P_s.

The actual process will take place with some heat transfer (not adiabatically) and some temperature rise (not isothermally), and therefore the specific work expended by the compression should lie between the predict values for these two ideal processes.

The power consumption rate is found by multiplying the specific work, w, times the mass flow rate, or

$$\text{Power} = \dot{m} \cdot w. \tag{4.4.18}$$

Note that once the supply pressure is picked, the specific work, w, can be found. Then, only the average flow required by the system, $\dot{m}$, is needed to find the power consumed by the active system.

If the fluid used is incompressible, such that the density, ρ, is a constant, equations 4.4.15 and 4.4.18 can be reduced to the power calculation shown in Chapter 3 for a hydraulic system. The specific work is given by reducing equation 4.4.15 for a constant density to

$$w = \frac{1}{\rho} (P_e - P_i) \tag{4.4.19}$$

where the exit pressure is P_s, the supply pressure, and the inlet pressure is the atmospheric pressure of 0_{psig}. Thus

$$w = \frac{1}{\rho} \cdot P_s \tag{4.4.20}$$

The mass flow rate is given by the density times the volume flow rate, Q, or

$$\dot{m} = \rho \cdot Q. \qquad (4.4.21)$$

Substituting equations 4.4.20 and 4.4.21 into equation 4.4.18 yields

$$\text{Power} = P_s \cdot Q \qquad (4.4.22)$$

for a hydraulic system, as was given in equation 3.4.15.

4.4.e Closed Loop Actuator Controller

The pneumatic servovalve-actuator pair modeled in this chapter cannot function effectively as an open-loop force generator. There are two reasons why this is so. Firstly, any displacement of the valve from its closed position causes air flows that stop only when the pressure drops across the orifices become zero. This means that the actuator force always rises to its maximum value, for any step valve displacement; only the rise time varies. Secondly, stroking of the actuator causes volume changes in the chambers which compress the gas and generate forces.

A closed-loop controller is used to remedy this problem. The actuator force is measured and the command to the valve is based on the error between the desired force, F_{des}, and the actual force, F_{act}. If the error is zero, the valve is shut off; but if the actual force is too large or too small the servovalve is opened in the

appropriate direction to increase or decrease the force.

4.5 System Sizing and Simulation

Using the analytical models developed in section 4.4, system components were sized; then the actuator system dynamics were simulated digitally to study the resulting dynamic response in order to make any necessary parameter adjustments.

The simulations use a linear spool valve model, where the orifice size of the valve varies linearly with the valve input command.

4.5a System Sizing

Initial sizing was based on meeting the design requirements presented in section 4.2. To preserve compatability with the present Amtrak pneumatic systems, a supply pressure of 130 psig was used in the design.

The piston area was sized to meet the maximum force requirement of the actuator. Assuming a 90% pressure drop across the valve, the required piston area is given by

$$A_p = \frac{F_{max}}{(90\%) \cdot P_s} . \qquad (4.5.1)$$

This showed the required area to be 25 square inches.

The nominal pressure for both chambers of the actuator was determined for a centered valve and an actuator with no load by assuming small leaks exist into and out of the valve. Applying the flow equation (4.4.10) to both inlet and outlet leaks, and equating the

weight flow rates yields

$$(c_d A_o)_e \, c_2 \frac{P_v}{\sqrt{T_v}} \, f_1\left(\frac{P_e}{P_v}\right) = (c_d A_o)_s \, c_2 \frac{P_s}{\sqrt{T_s}} \, f_1\left(\frac{P_v}{P_s}\right) \tag{4.5.2}$$

where the subscript "v" denotes the property inside the valve, "s" denotes inlet, or supply, properties, and "e" denotes exit, or exhaust, quantities. If the two leaks are assumed to be small and to have the same size areas, the equation reduces to

$$P_v f_1\left(\frac{P_e}{P_v}\right) = P_s f_1\left(\frac{P_v}{P_s}\right). \tag{4.5.3}$$

Recognizing that the exiting flow is choked ($f_1 = 1$), this further reduces to

$$\frac{P_v}{P_s} = f_1\left(\frac{P_v}{P_s}\right). \tag{4.5.4}$$

From Figure 4.4.6 this pressure ratio is seen to be 0.81, giving the nominal internal actuator pressure to be 102.5 psig. This pressure is an estimate of the average chamber pressures for the actuator.

The accumulator volume was calculated from equation 4.4.13, which is repeated here for reference:

$$V_{acc} = \frac{\Delta P_{mean}}{\Delta P_{acc}} \cdot \Delta V_{act}$$

The nominal internal pressure was used for P_{mean} and the acceptable pressure drop in the accumulator, ΔP_{acc}, was set at 10 psi. If the accumulator is sized to provide air for three full strokes of the actuator with only a 10 psi pressure drop, then

$$\Delta V_{act} = 3 \cdot A_p \cdot (2 \times \text{Peak Stroke}) \qquad (4.5.5)$$

$$= 450 \text{ in}^3.$$

Substituting these values into equation 4.4.13, shows that this requires an accumulator size of

$$V_{acc} = 3 \text{ cubic feet/truck.}$$

Having chosen the supply pressure, the specific work of the compressor can be calculated from equations 4.4.16 (isothermal compression) and 4.4.17 (adiabatic).

Assuming ambient conditions of 14.7 psia at 70°F, and using $R = 2.48 \times 10^5$ $in^2/sec^2 °R$ and $k = 1.4$ (values for air) the specific work of the compressor is estimated to be between 118 (isothermal) and 166 (adiabatic) $hp\text{-}sec/lb_m$. Complete compressor sizing required knowledge of the average mass flow rate, which was calculated in the digital simulations presented in the next section.

4.5b Digital Simulation

The equation describing the pneumatic flow through an orifice is highly nonlinear and non-nodal in form; exhaust flow is generally "choked", while flow from the supply is not (nonlinear), flow rates are not dependent on the pressure drops, but on the absolute pressures values (non-nodal). These factors make linearization difficult and limit usage of the resulting equations to very small perturbations from the origin.

For these reasons analysis of the valve response was done in the time domain rather than in the frequency domain. Three different digital simulations were used. Two of the simulations involved only the valve and actuator with the closed-loop, force feedback. The third simulation was a single degree of freedom mass model with active suspension control using a pneumatic actuator.

The core of the simulations was the DYSYS (DYnamic SYstem Simulation [17]) routine. The DYSYS program performs a fourth-order Runge-Kutta integration of first-order differential equations. These equations must be written by the user into a FORTRAN subroutine.

Two states are necessary to describe the actuator; the chamber pressures were used. Thus, the two valve simulations involved integration of two first-order equations. The active one-mass simulation required four states: the two chamber pressures, and the mass' velocity and displacement. The accumulator and pump were not modeled dynamically, but were assumed to be designed large enough to supply a steady pressure, P_s.

In the models the piston area, A_p, varies linearly with the chamber compression or extension. This permits a first order approximation of the change in effective piston area with extension observed in airsprings:

$$A_p \approx A_{po} + C_{ap} \cdot y_{ac} \tag{4.5.6}$$

where

$$C_{ap} = \frac{dA_p}{dy_{ac}} .$$

A_{po} gives the effective area for zero stroke (y_{ac}). The constant, C_{ap}, is zero for pneumatic cylinders and can be derived for airsprings from their force characteristics charts.

Since a positive stroke of the actuator compresses one airspring, while extending the other, the values of C_{ap} have equal magnitude, but opposite sign for the two airsprings in an actuator.

Chamber volume is also varied linearly with actuator stroke:

$$V \approx V_o + A_{vo} \cdot y_{ac} \tag{4.5.7}$$

where $A_{vo} = \frac{dV}{dy_{ac}}$.

For pneumatic cylinders this relation is exact, with A_{vo} equal to A_p, the actual piston area, on one side and equal to $-A_p$ on the other side. For airsprings this is only a first order approximation and A_{vo} is not generally equal to A_{po}.

The block diagram in Figure 4.5.1 demonstrates the dependence of the actuator's output force on two inputs: the input command (desired force) and the actuator stroke velocity (which defines the chamber volume rate of change). The success of the actuator design is based on the ability of the output force to follow the first input, while ignoring the second.

The two valve simulations addressed precisely these questions. The first program, VALVE.FOR (Appendix C), studies the response of the actuator force (output) to a step input in the desired force when no stroke is allowed. The second simulation, STROKE.FOR (Appendix D), shows the response of the actuator to a sinusoidal stroke of the actuator with $F_{desired} = 0$. The parameters used for the actuator were chosen to match Firestone Airmount® Airstroke® 224 airsprings mounted with nominal heights of five inches; these airsprings were chosen for their nominal piston areas and nominal volumes. The 224's characteristics are shown in Figure 4.4.3. Parameters used in the valve simulations are shown in Table 4.5.1.

Having prescribed the other parameters by actuator selection and supply pressure selection, only one parameter remained to vary the system response speed: the closed-loop force feedback gain, k_f.

It should be mentioned that the simulations dealt only with the effective orifice area, $A_{eff} = c_d \cdot A$.

The discharge coefficients, C_d, for valves generally range from 0.6 to 1.0, but should be determined experimentally for each valve [15].

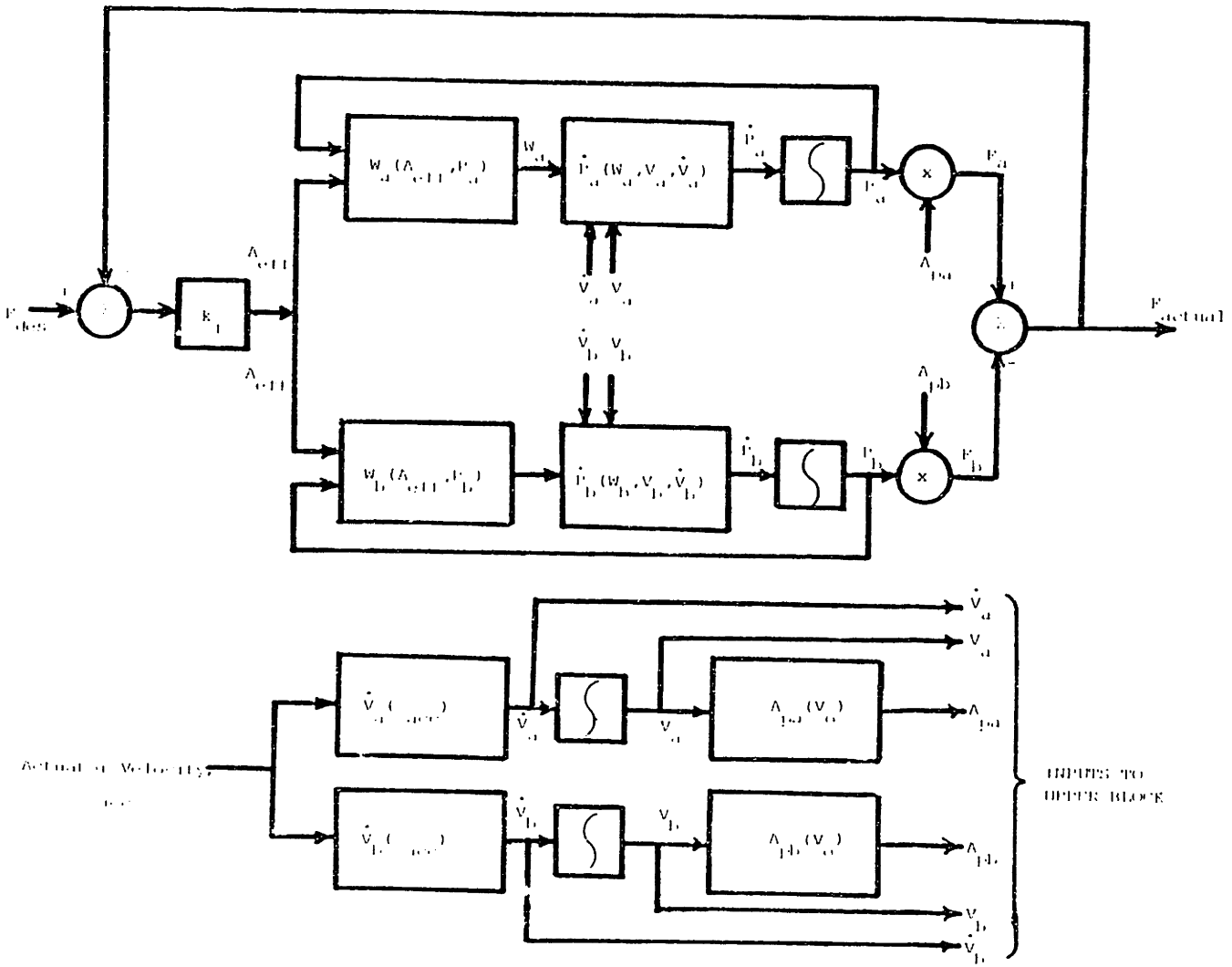

FIGURE 4.5.1: BLOCK DIAGRAM FOR ACTUATOR-VALVE DYANMICS

TABLE 4.5.1: ACTUATOR PARAMETERS USED IN DIGITAL SIMULATIONS

CONSTANTS		
k	Ratio of Specific Heats	1.4
R	Ideal Gas Constant for Air	2.4×10^5 $in^2/sec^2 °R$
T_s	Stagnation Temperature	530°R
g	Acceleration of Gravity	386 in/sec^2
P_e	Exhaust Pressure	14.7 psia
ACTUATOR PARAMETERS		
V_o	Nominal Chamber Volume	150 in^3
A_{vo}	Volume Change Linearization constant	27.3 in^3/in
A_{po}	Nominal Effective Piston Area	25.7 in^2
C_{ap}	Piston Area Linearization Constant	-3.9 in^2/in
P_s	Supply Pressure	144.7 psia
$P_{ai,bi}$	Initial Chamber Pressures	117.2 psia

Step Response

Using the step response program, VALVE.FOR, an initial value of k_f was chosen which set the rise time for the undisturbed actuator (no stroke velocity) based on the rise time for a 3 hertz bandwidth, first-order, linear model. As shown in section 3.3, the bandwidth is equal to $1/\tau$, where τ is the system time constant. The rise time to 95% of the final value is 3τ; therefore, the 95% response time needed is 0.16 seconds or shorter.

Figure 4.5.2a shows the step response to a 1414 pound step input for various k_f values. This magnitude corresponds to the peak value of a sine wave with a 1000 lb. root mean square value, which is the rms actuator force requirement predicted by the frequency domain study in Chapter III. A k_f value of 0.00003 in^2/lb gives a rise time of about 0.26 sec, equivalent to that of 1.8 Hz bandwidth linear system; a k_f of 0.00008 in^2/lb a 0.11 second rise (4.3 Hz), while a k_f of 0.0003 in^2/lb rises in 0.03 seconds (16 Hz).

For a larger step the rise times are greater, because of the nonlinear effects. Figure 4.5.2b shows the response to a 3000 lb step input. With the step equal to the peak random value expected in service, the 0.00008 in^2/lb gain takes about 0.27 seconds to rise (1.8 Hz) and 0.0003 in^2/lb gain takes 0.084 seconds (5.7 Hz). These results show a necessary force feedback loop gain between 0.00008 and 0.0003 in^2/lb for the expected operating range of the actuator.

The step response simulation required large valve openings (i.e. 0.9 in^2) and large flow rates (2.4 lbm/sec). However, a step input

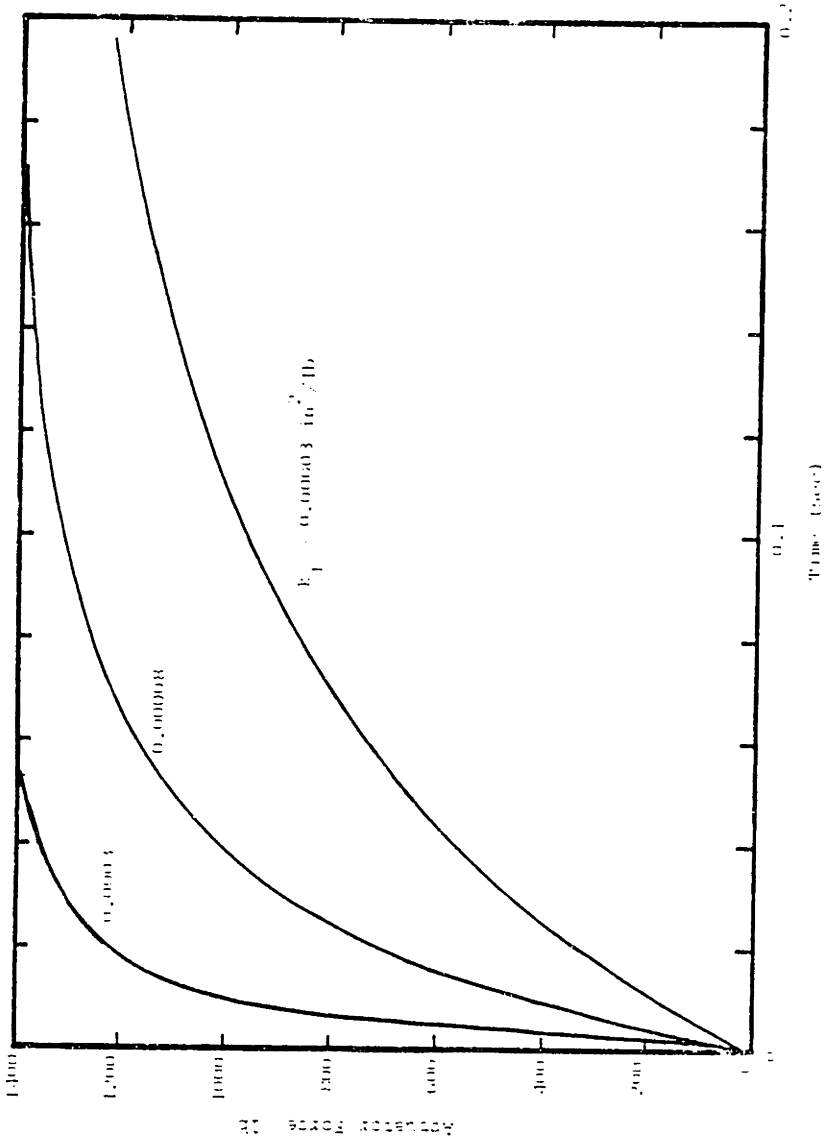

FIGURE 4.5.2a: VALVE-ACTUATOR STEP RESPONSE FOR DIFFERENT VALUES OF k_f; INPUT: 1414 lb STEP

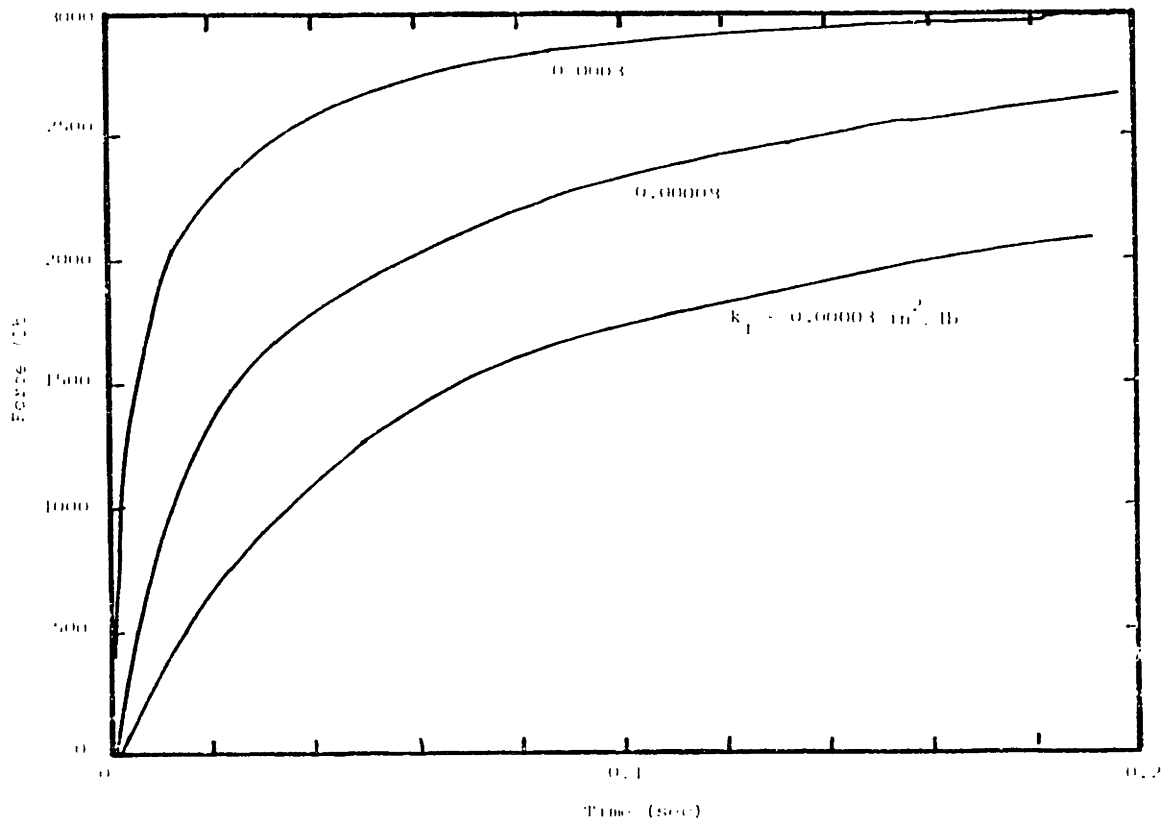

FIGURE 4.5.2b: VALVE-ACTUATOR STEP RESPONSE FOR DIFFERENT VALUES OF k_f; INPUT: 3000 lb STEP

has an infinitely high frequency content; in the rail vehicle application the input frequency content is bandlimited. For this reason the effect of orifice opening saturation was not studied here, but is taken up in Chapter V.

Disturbance Response

The response of the actuator was studied for sinusoidal stroke disturbances of different amplitudes and frequencies using STROKE.FOR. Table 4.5.2 shows the results of the simulations. The disturbance response has the characteristics of relative damping. The force varies almost proportionally to the velocity and was shown by the simulation to be 180° out-of-phase with it. Figure 4.5.3 shows the stroke and actuator force for a 0.707 inch peak, one hertz stroke disturbance. When the slope of the displacement (the velocity) is at its greatest positive value, the force is at its greatest negative value. These damping rates for k_f values of 0.00008 in^2/lb and 0.0003 in^2/lb are on the order of 1000 lb-sec/ft and 300 lb-sec/ft, respectively.

The passive secondary presented in Chapter III used dampers providing 2400 lb-sec/ft of lateral damping per truck. With one actuator added to each truck, the secondary vehicle damping would increase significantly. This damping effect was also noticed in the single degree of freedom mass model presented in the next section.

Other insights gained in these simulation related to the orifice size and flow rates required merely to try to maintain a zero force. A 0.50 inch rms stroke, the rms stroke expected onboard a train, re-

TABLE 4.5.2: VALVE-ACTUATOR ASSEMBLY: RESPONSE TO SINUSOIDAL STROKE DISTURBANCE

	STROKE			ACTUATOR
k_f (in^2/lb)	RMS Displacement (in)	RMS Velocity (in/sec)	FREQUENCY (Hz)	PEAK Force (lb)
.00008	.50	3.14	1	290
	.17	3.14	3	267
	.50	9.42	3	769
.0003	.50	3.14	1	81
	.17	3.14	3	80
	.50	9.42	3	238

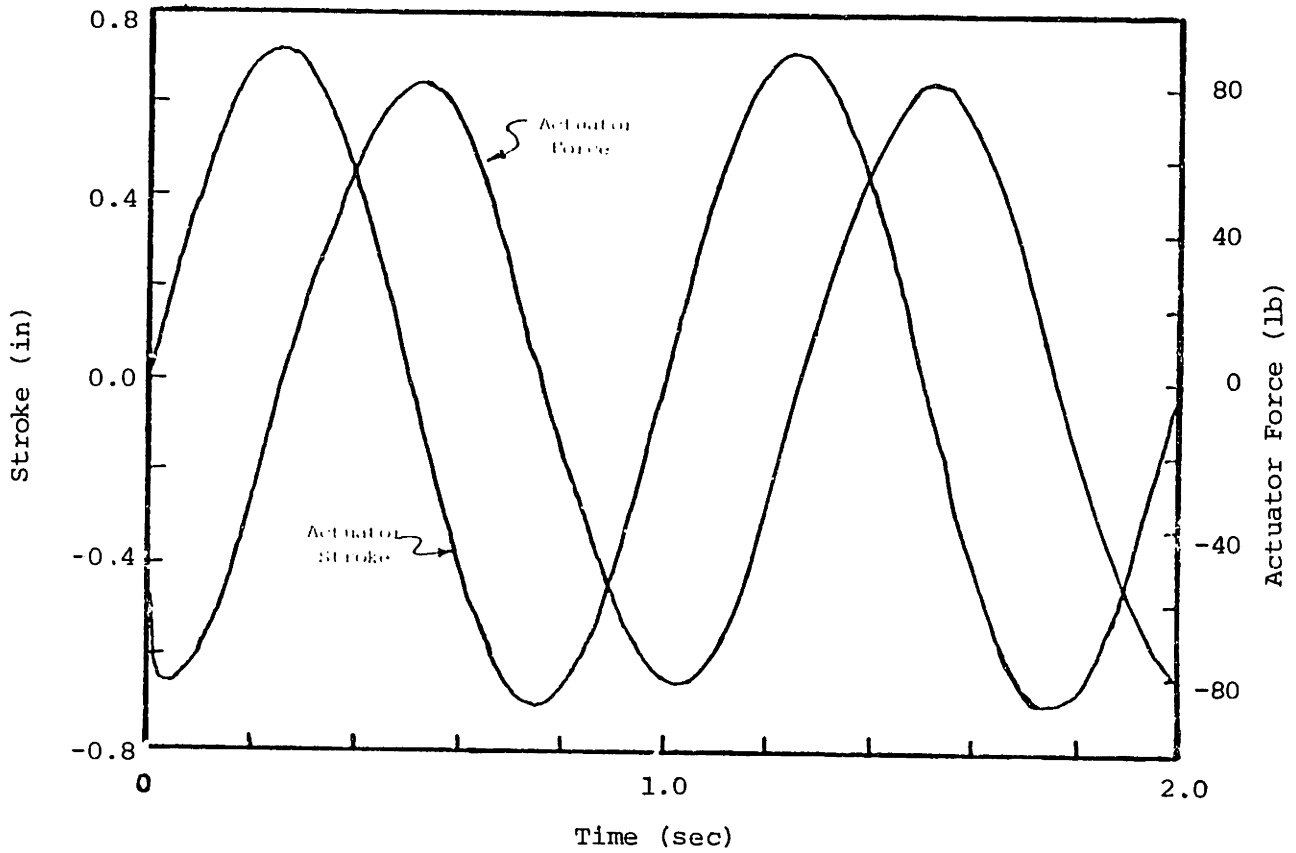

FIGURE 4.5.3: VALVE-ACTUATOR ASSEMBLY -- RESPONSE TO A SINUSOIDAL STROKE DISTURBANCE; k_f=0.0003 in^2/lb

quired a 0.07 in^2 effective orifice at 3 Hertz with k_f = 0.0003 and used peak flow rates of 0.19 lbm/sec. This effective area corresponds to a 0.3 inch diameter orifice (larger for $c_d < 1$). At 1 hertz the same magnitude stroke required a 0.024 in^2 effective orifice and 0.065 lbm/sec peak flow rates.

4.5c Single Degree of Freedom Model

A one mass, active suspension model was used to study the performance of the pneumatic valve and actuator in a suspension system. This simple time domain model made it possible to compare the nonlinear active suspension to both the passive and the ideal active suspensions. Appendix E lists the program, AIRMASS.FOR, used in the simulations.

This model was scaled to represent a half carbody with one linear degree of freedom (Figure 4.5.4). The passive parameter values match one half of the total lateral stiffness and damping of the full vehicle model used in Chapter III. Acceleration and velocity were fedback from the mass to the actuator system using the gains chosen for the bandwidth study. Vehicle parameter are shown in Table 4.5.3.

The input was designed to simulate the lateral truck motion. Six sine waves spanning six octaves were summed to simulate the frequency spectrum of the truck which was determined in the frequency domain study of Chapter III. Integrating the truck lateral spectral density over an octave gave the mean square value for the sine wave at the center frequency of that octave. The input frequencies were at 0.315, 0.630, 1.26, 2.52, 5.04, and 10.08 hertz; the corresponding peak magnitudes were 0.4182, 0.3146, 0.2911, 0.4355, 0.0791, and

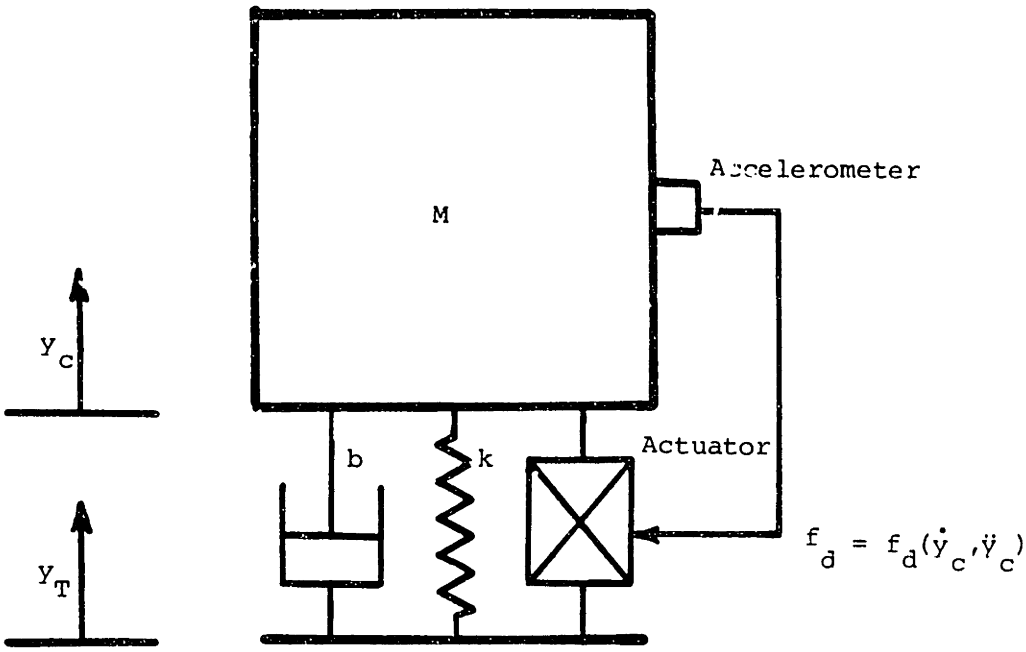

FIGURE 4.5.4: SINGLE MASS ACTIVE VEHICLE SUSPENSION MODEL FOR ACTUATOR DESIGN

TABLE 4.5.3: VEHICLE PARAMETERS FOR ONE MASS DIGITAL SIMULATIONS

PASSIVE PARAMETERS

M_c	Vehicle Mass	1200	slugs
k_{sy}	Passive Spring Stiffness	2500	lb/in
c_{sy}	Passive Damping Coefficient	200	

ACTIVE PARAMETERS

C_v	Velocity Feedback	-750	$\frac{\text{lb-sec}}{\text{in}}$
C_a	Acceleration Feedback	-33.3	$\frac{\text{lb-sec}^2}{\text{in}}$

0.0134 inches, respectively; the phase shifts were 1, 4, 3, 6, 2 and 0 radians. The resulting displacement input was periodic with a period matching the lowest frequency, 0.315 hertz (Figure 4.5.5).

The one mass simulation was run for 6.3 seconds, two cycles of the lowest frequency and an integer number of cycles for all input frequencies. This gave the input a zero mean and was long enough that the runs and mean values for the outputs showed negligible effect of the original transient. The passive simulation was permitted by zeroing the feedback gains, c_v and c_a, as well as actuator constants A_{vo}, A_{po}, and C_{ap}. This effectively removed the actuator model from the simulation.

The ideal actuator simulation required revision of the program AIRMASS.FOR to remove the actuator's dynamics, feeding back the desired force directly as the actual force.

Table 4.5.4 shows the variation in performance and system demands for the passive, ideal, and simulated "pneumatic powered active" vehicles.

As expected, the performance of the pneumatic system approached that of an ideal system as the error gain, k_f, increased. The ideal active suspension reduced rms accelerations by 41%, reduced the rms stroke by 11%, and lowered the rms mass displacement by 47% over the values for the passive vehicle simulation. The simulation of the pneumatic actuator system showed that for a high error gain (k_f = 0.003 in^2/lb) the ideal system's performance can be realized; for a lesser gain (0.0003 in^2/lb) the stroke and displacement rms

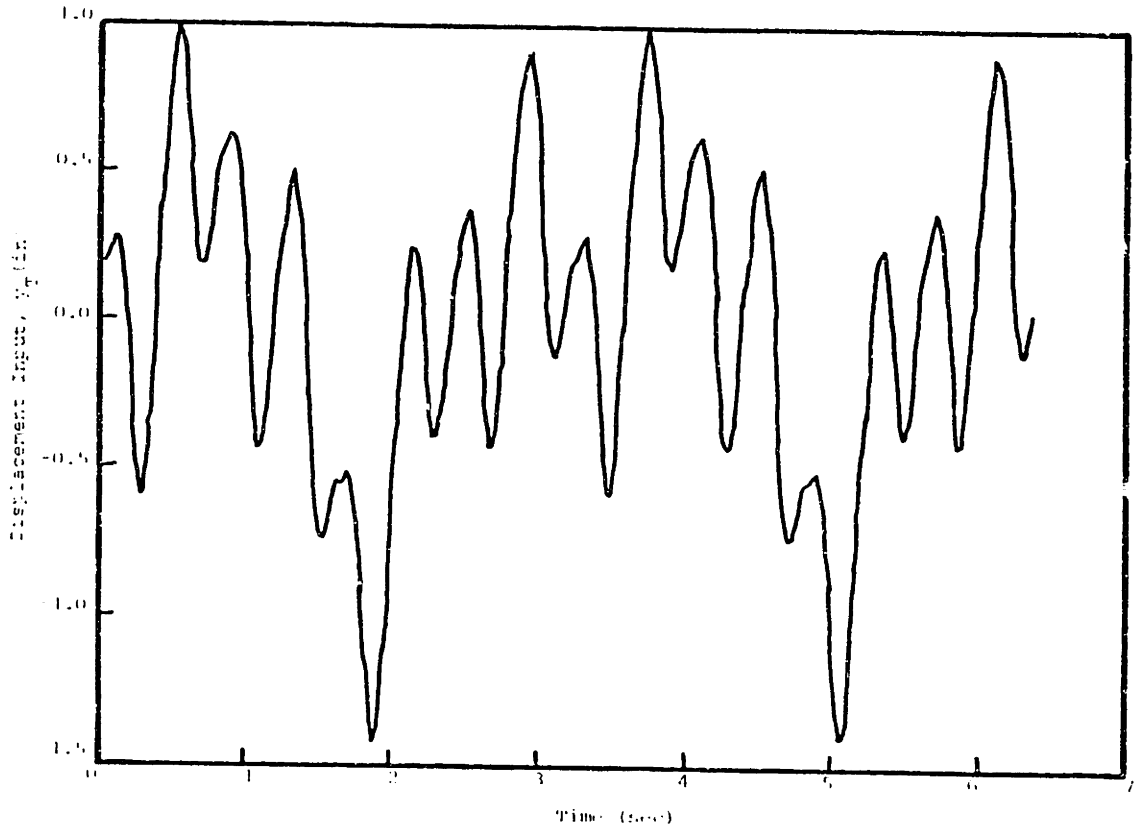

FIGURE 4.5.5: DISPLACEMENT INPUT FOR SINGLE MASS MODEL TIME DOMAIN SIMULATIONS

TABLE 4.5.4: ACTIVE SUSPENSION PERFORMANCE FROM ONE MASS SIMULATION

	Passive	k_f=0.00008 in^2/lb	k_f=0.0003 in^2/lb	k_f=0.0008 in^2/lb	k_f=0.003 in^2/lb	Ideal
RMS DISPLACEMENT (in)	.601	.3317	.323	.319	.319	.318
RMS STROKE (in)	.539	.454	.470	.475	.476	.479
RMS FORCE (lb)	—	899	899	907	913	914
RMS A_{eff} (in^2)	—	.0539	.0587	.0601	.0617	—
PEAK A_{eff} (in^2)	—	.113	.114	.150	.162	—
AVERAGE FLOW (lb/sec)	—	.112	.115	.114	.113	—
AVERAGE FLOW (ft^3/min)	—	180	185	183	181	—
RMS ACCEL. (g)	.0478	.0390	.0307	.0289	.0280	.0281

values can match the ideal system to 1.9% and 1.5%, respectively, although the acceleration reduces only within 9.3% of ideal.

The system demands, such as the rms flow rate and rms valve opening stopped increasing with rising k_f as the system speed became so much faster than the input signal that the actuator tracked the input essentially perfectly.

The minimum rms stroke values occur for the lower values of k_f. This resulted from the increased damping effect noticed before in the "stroke" simulations (STROKE.FOR). As the valve-actuator response speed increases, the valve becomes able to relieve pressure quickly and the disturbance from the stroke becomes negligible.

Although these results would tend to support use of larger and larger feedback gains, other factors limit the value of k_f. Large k_f values cause the actuator system to be sensitive to high frequency electronic noise.

The peak orifice required was shown by the simulations to be about 0.14 in^2, corresponding to a circular orifice diameter of 0.42 inches for an ideal orifice ($c_d = 1$).

The average flow rate varied very little with the error feedback gain and was essentially 0.115 lb/sec. Using the specific power values calculated for isothermal (118 hp-sec/lb) and adiabatic (166 hp-sec/lb) compressions yields a power consumption per car estimate of 27 to 38 horsepower for the pneumatic powered, actively controlled suspension.

This power consumption estimate is many times larger than the estimate in Chapter III; the power estimate used in the linear frequency domain study was based on a hydraulic actuator model which is inherently more efficient. Chapter V studies this power 'discrepancy' in more detail.

4.6 Conclusions

In this chapter a pneumatic actuator system was designed and its performance simulated. The system consists of four major parts: a compressor, an accumulator, a servovalve, and an actuator.

Sizing of the system was based on the performance requirements determined in Chapter III, modified for a one actuator/truck design. Simulations assumed the use of a spool-type, four-way servovalve. A supply pressure of 130 psig was assumed, the pressure currently used onboard Amcoaches.

The actuator parameters used in the simulations matched those for the Firestone 224 Airmount® Airstroke® airspring, which was chosen for its piston area (~25 in^2) and relatively small volume (150 in^3). Two airsprings are used, one on either side of the truck, to create a single double-acting pneumatic actuator.

Digital simulations showed that valve with a 0.14 square inch maximum, effective orifice and an average air flow rate of 0.115 lb/sec (92 ft^3/min at 14.7 psia) could produce rms acceleration and stroke reductions close to those expected from an ideal active suspension. This requires an error feedback gain to the servovalve orifice of 0.0003 in^2/lb, providing a frequency response bandwidth greater than 3 hertz. Power consumption for the pneumatic system is estimated to

be 26 to 37 horsepower per car. An accumulator capacity of 3 cubic feet/truck is needed.

These simulations allowed the servovalve to open linearly with the error signal command. Chapter V examines the system performance when valve saturation or complete system failure takes place.

CHAPTER 5

ACTIVE SUSPENSION IMPLEMENTATION CONCERNS

5.1 Introduction

The pneumatic system designed in Chapter 4 was developed to meet performance requirements. Parameters were changed and gains were increased until the performance was satisfactory. Little consideration was given to equipment limitations. This chapter looks at some of these equipment problems and the limitations of the active system's implementation, and the resulting effects on vehicle performance.

5.2 Valve Saturation

The orifice area of a spool valve is limited by the maximum possible spool stroke; when the command to the valve requires a larger stroke than is physically possible, the orifice remains in the fully open position until the command returns to the operable valve range. This relation is shown graphically for a linear spool valve in Figure 5.2.1 and is known as valve saturation.

The simulations in Chapter 4 demonstrated peak orifice openings of about $0.14\ in^2$. Table 5.2.1 shows the results of the one mass simulation for valves with maximum openings of 0.07, 0.09, and $0.11\ in^2$. The error gain, k_f, was $0.0003\ in^2/lb$ for all runs. It can be seen from these results that a valve of only half the desired size is highly unsatisfactory. The controller loses its ability to reduce rms accelerations as the valve starts to saturate. However, saturation at 64% to 80% of the desired peak orifice size has little effect on performance. Figure 5.2.2 shows the

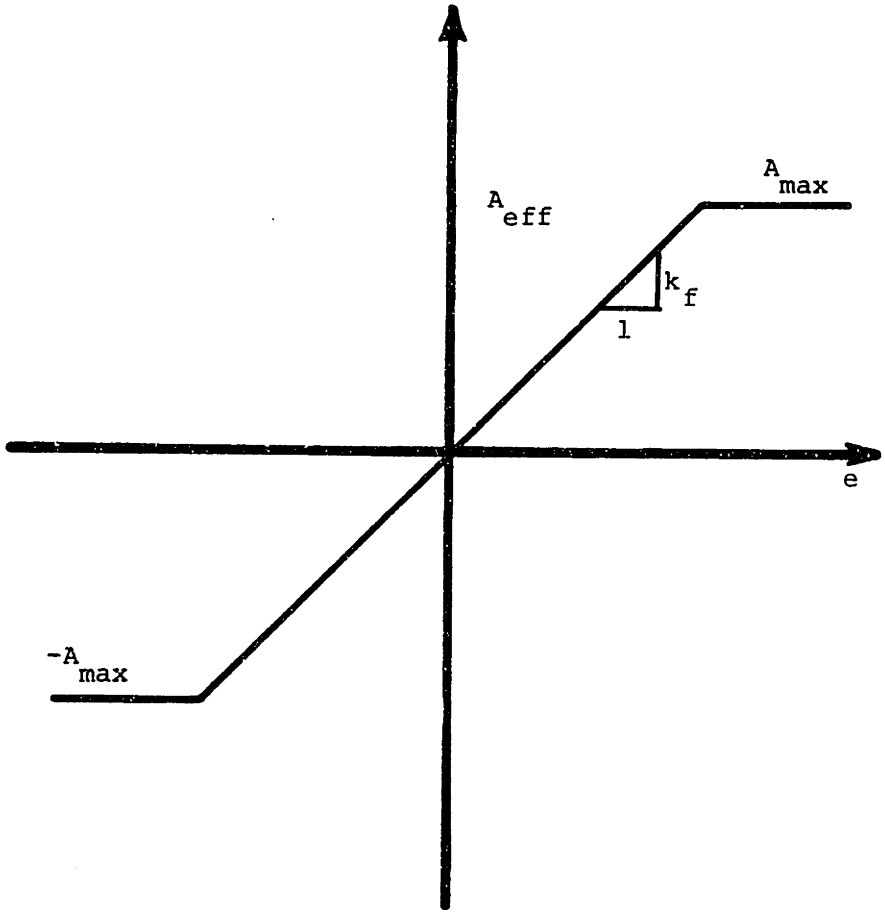

FIGURE 5.2.1: VALVE SATURATION

TABLE 5.2.1: SYSTEM PERFORMANCE WITH VALVE SATURATION (k_f = 0.0003 in^2/lb)

	MAXIMUM A_{eff} (in^2)	RMS Stroke (in)	RMS Accel. (g)	Average Flow Per Truck (lbm/sec//ft^3/min*)
(No Sat.)	0.14	.470	.0307	0.115 // 92
	0.11	.469	.0309	0.115 // 92
	0.09	.466	.0317	0.115 // 92
	0.07	.449	.0356	0.114 // 92
	Passive	.539	.0478	———

*Volume flow rates are given for air at an atmospheric pressure of 14.7 psi and at ambient temperature.

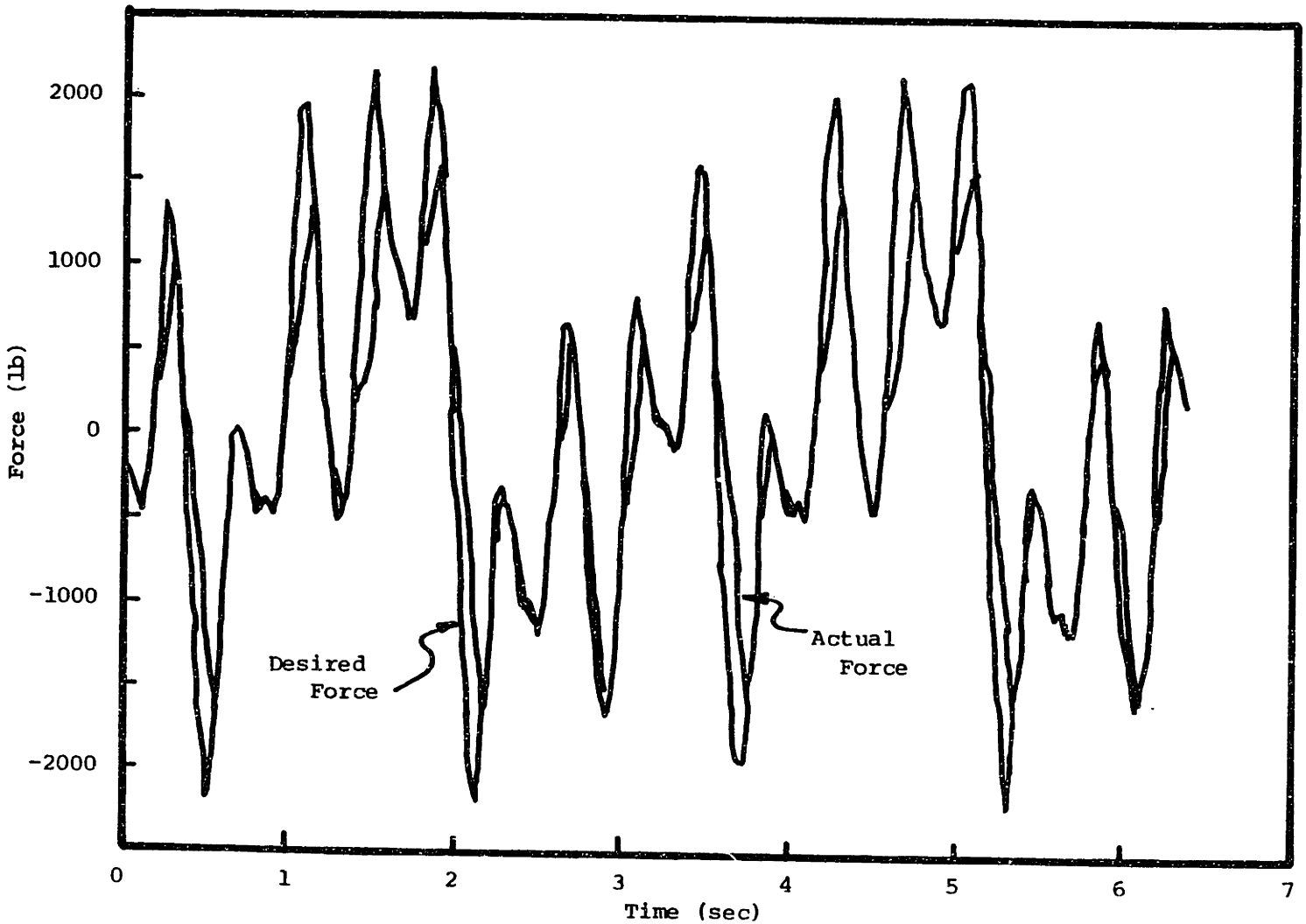

FIGURE 5.2.2: TIME TRACES FOR ACTUAL AND DESIRED ACTUATOR FORCES WITH 50% VALVE SATURATION

desired force and the actuator force for the simulation where A_{max} is equal to 0.07 in^2. Note the inability of the actuator to produce the larger forces.

5.3 Bang-Bang Control

A simple alternative to the linear spool valve is the nonlinear Bang-Bang controller. Implemented with a four-way solenoid valve, it opens in one direction when the actuator force error is positive, closes when it is zero, and opens the other direction if the error is negative (Figure 5.3.1).

The original simulations of the Bang-Bang controller showed good performance for an adequate size orifice (0.14 in^2, not for 0.07 in^2). However, these simulations allowed the value speed to match the time step of the simulation. This made the results time step dependent and also implied a very high response speed for the valve. For time steps of 0.001 and 0.004 seconds the rms accelerations were calculated to be 0.0284 and 0.0306 g, respectively.

Further simulations allowed the valve response speed to vary independently of the simulation's time increment. These simulations identified two problems associated with a Bang-Bang controller implementation: the high necessary valve speed and the flow demand.

A valve response speed of 0.03 seconds to open or close provided similar rms accelerations (0.0463g) to the passive suspension (0.0478g). Tripling the valve speed was necessary to provide 70% of the acceleration reduction of an ideal active suspension (0.028 g). A valve speed of 0.01 seconds yielded an rms acceleration of 0.0337 g. This requires a valve

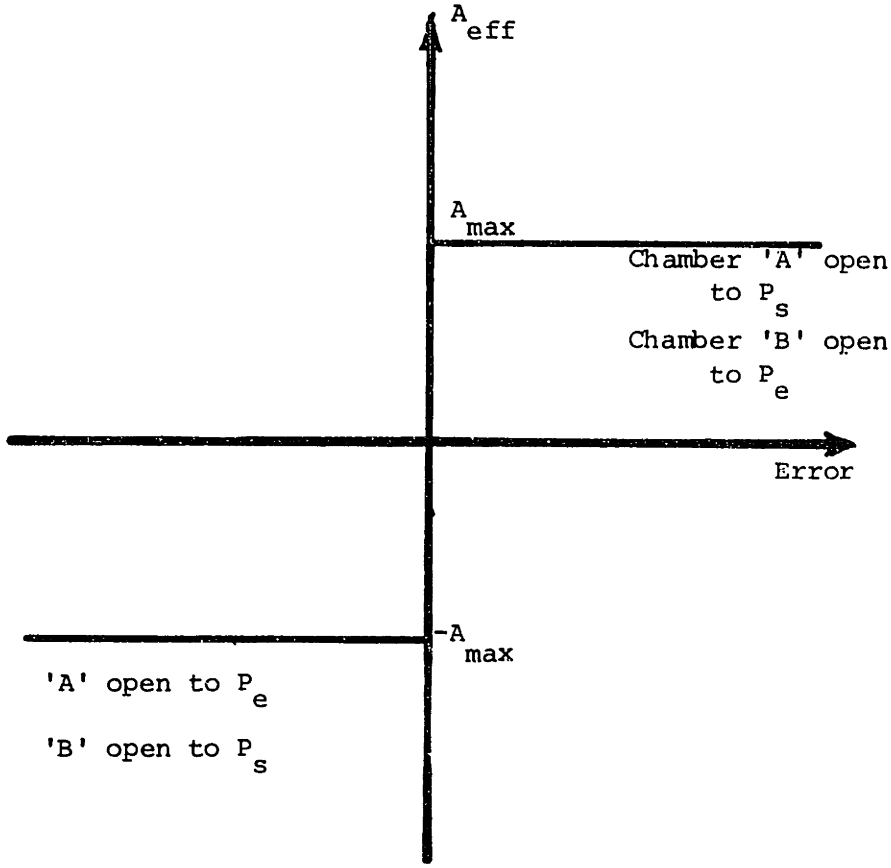

FIGURE 5.3.1: BANG-BANG CONTROLLER

capable of cycling at 50 hertz. Furthermore, since the actual force never exactly equaled to the desired force, the solenoid valve was always fully open in one direction or the other. This resulted in a very high flow demand. Simulations at both valve speeds (0.01 and 0.03 seconds) predicted average flows of 0.33 lbm/sec/truck (265 ft^3/min/truck), about three times that needed for a spool valve. The flow rate could be reduced some by introducing a dead zone (Figure 5.3.2) which would close the valve for a force error less than some threshold level; however, this would clearly slow the active system's response and reduce its accuracy.

The simulations show that the Bang-Bang controller is not an appropriate means of providing flow control for the pneumatic actuator. Even if a fast enough valve action could be provided, the flow demands are more than double that required for a continuous spool valve.

5.4 Chamber Pressure Feedback

The implementation of the pneumatic actuator system requires the measurement of the active force in order to close the force feedback loop around the actuator. One common method of determining the force in hydraulic cylinders is by measuring the cylinder pressure differential. The force is then simply this differential times the piston area, a constant.

With airsprings, however, the piston area varies with the actuator displacement. Knowledge of the effective piston area would require the additional measurement of the secondary stroke. The model was augmented to show the effect of approximating the force by measuring only the

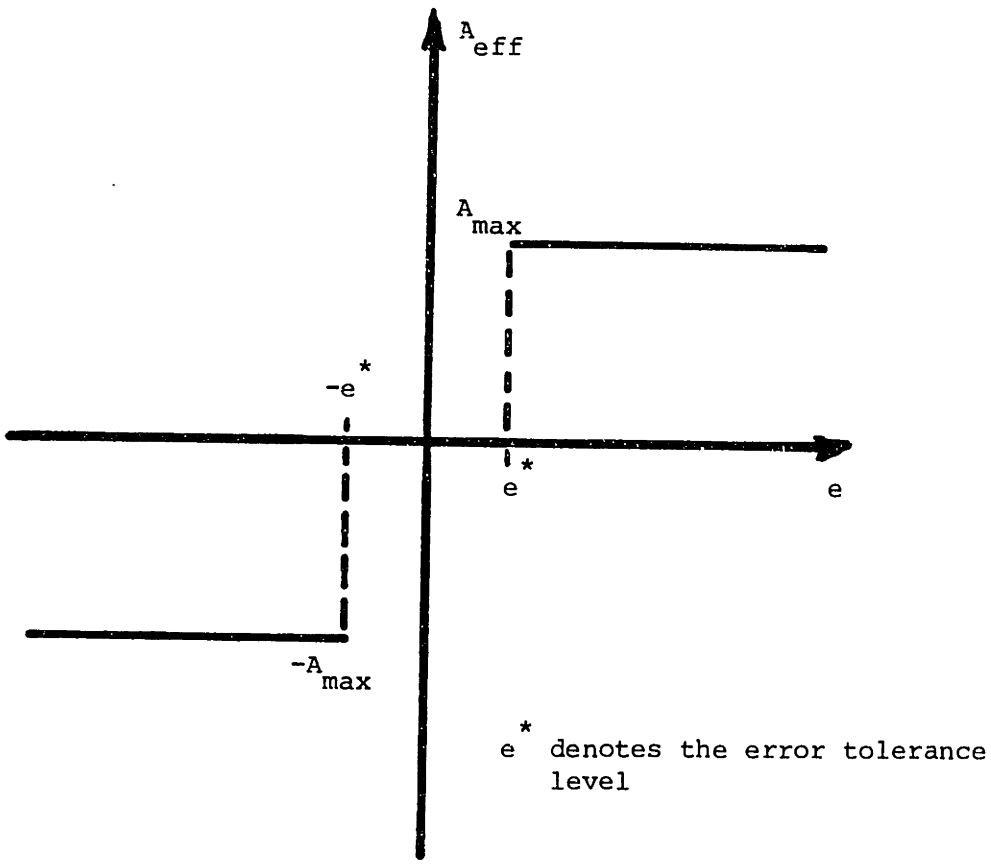

FIGURE 5.3.2: BANG-BANG CONTROLLER WITH DEAD ZONE

pressure differential and using a zeroeth order approximation of the piston area as being constant; thus, avoiding a costly stroke measurement. However, the model showed this to be a poor substitute for force feedback. The actuator was unable to track the desired force adequately, as shown in Figure 5.4.1. This resulted in an rms acceleration of 0.0351 only 74% of the reduction possible with an actual force measurement.

Force feedback should therefore be provided more directly, using force transducers such as strain gages, located on the actuator drive rods.

5.5 Active Power Consumption and Flow Limitation

Power Consumption

An apparent paradox between Chapters 3 and 4 is the vast difference in the active suspension power consumption estimates: Chapter 3 estimates 4.4 horsepower/car, while Chapter 4 estimates 27 to 38 horsepower/car. This difference is related to the use of a gas (air) as a working fluid (Chapter 4), rather than an incompressible working fluid (Chapter 3).

The study of pneumatic versus hydraulic actuator system power consumption starts with the power consumption equations presented in Chapter 4. The specific work equations are repeated here for reference:

Pneumatic - Isothermal

$$w = RT \ln \frac{P_s}{P_i} \tag{5.5.1}$$

- Adiabatic

$$w = \frac{k}{k-1} RT_i \left[\left(\frac{P_s}{P_i} \right)^{\frac{k-1}{k}} - 1 \right] \tag{5.5.2}$$

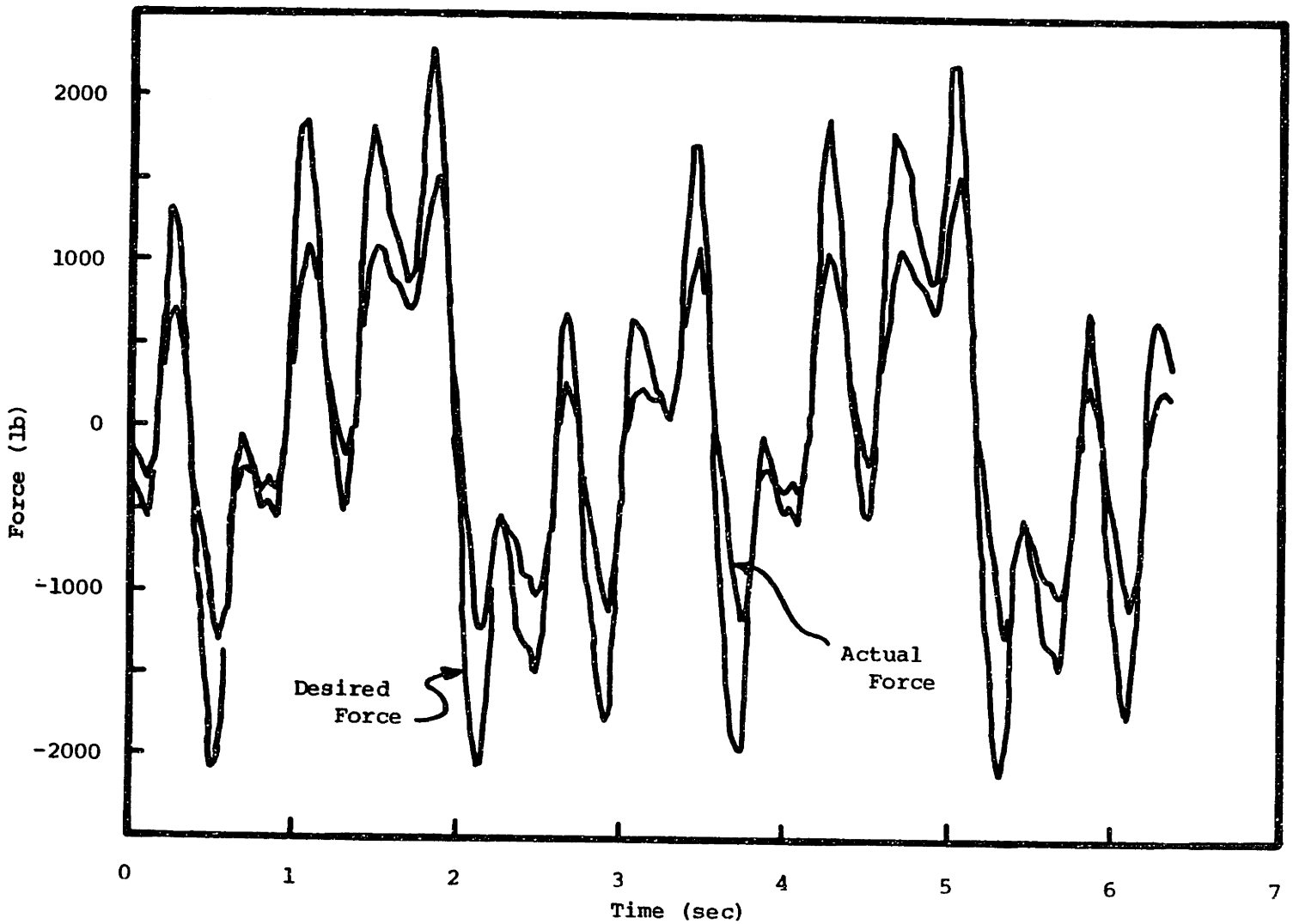

FIGURE 5.4.1: TIME TRACES FOR ACTUAL AND DESIRED ACTUATOR FORCE WITH PRESSURE FEEDBACK

Hydraulic

$$w = \frac{1}{\rho} (P_s - P_i). \qquad (5.5.3)$$

Recall that P_s is the maximum system pressure. The subscript "i" represents the initial conditions -- ambient pressure and temperature.

Assumptions used in the compression analyses are as follows:

Isothermal (Pneumatic) - constant temperature compression from P_i to P_s at temperature T_i.

Adiabatic (Pneumatic) - constant entropy (no heat transfer) compression from P_i and T_i to P_s and T_e (compressor exit temperature); further assumes constant pressure cooling from T_e back to T_i in the accumulator such that the valve is supplied with air at ambient temperature.

Hydraulic - constant density pressurization of a fluid; since ρ is constant, no assumptions need be made about the temperature change; pressure goes from P_i to P_s.

The mass flow for both systems can be given by

$$\dot{m} = \rho_n Q_n \qquad (5.5.4)$$

where Q_n is the volume flow rate for a mass flow, $\dot{m}$, with density, ρ_n. For pnematics the index, n, is used to match volume flow rates and densities, since a given mass occupies a different volume if its density changes. The density of hydraulic fluid is essentially constant relative to air's changing density; hence, the subscript is dropped for hydraulics.

Applying the ideal gas law to equation 5.5.4 and combining the specific work and mass flow equations yields:

$$\text{Power} = Q_n \cdot P_n \frac{T_i}{T_n} \ln \frac{P_s}{P_i}$$

(Isothermal Compression)

$$\text{Power} = Q_n \cdot P_n \cdot \frac{T_i}{T_n} \frac{k}{k-1} \left[\left(\frac{P_s}{P_i}\right)^{\frac{k-1}{k}} - 1\right]$$

(Adiabatic Compression) (5.5.5)

$$\text{Power} = Q(P_s - P_i)$$

(Hydraulic)

If the mean cylinder pressure and temperature are used to define the index, n, then the volume flow rates are comparable, although not equal, for the pneumatic and hydraulic systems. Therefore, P_n is set equal to 102.5 psig (117.2 psia), the nominal chamber pressure; T_n is set equal to T_i, as the average chamber temperature is assumed to be near the ambient temperature.

With the supply pressure and ambient pressure set at 144.7 psia and 14.7 psia, respectively, the power equations become

$$\text{Power} = \begin{cases} Q_n \cdot 268 \text{ psi} & \text{(Isothermal Compression)} \\ Q_n \cdot 378 \text{ psi} & \text{(Adiabatic Compression)} \\ Q \cdot 145 \text{ psi} & \text{(Hydraulic)} \end{cases} \quad (5.5.6)$$

This shows that for equal volumetric flows hydraulic power is 1.85 to 2.61 times more efficient. Because of the compressibility of air,

though, the required pneumatic volumetric flow, Q_n, is larger than that for the hydraulic system, as shown in the following example:

> Consider the system shown in Figure 5.5.1. A frictionless piston moves inside a cylinder. With the piston below the stops, the fluid pressure inside the chamber is constant at $P_i = W/A$, the pressure that assures equilibrium with the weight placed on the lid. As the lid rises against the stops, the pressure can increase, since the stops take on a load. Fluid, either gas or liquid, can be added from the source at constant pressure, P_s. For simplicity consider $P_s = 2P_i$.
>
> First consider the constant pressure doubling of volume from V_1 to V_2 as the lid raises from height "h" to height "2h", just touching the stops (Figure 5.5.1a). Since pressure and temperature are both constant, so is density. Thus, for pneumatics and hydraulics a constant pressure doubling of volume requires a doubling of mass. The pneumatic volume flow, $Q_i \cdot \Delta t$, related to the density ρ_i is equal to $Q \cdot \Delta t$, the hydralic flow rate times the allowed time increment. Both are equal to V_1, the constant pressure volume increase.
>
> Now consider a constant volume doubling of pressure from P_i to P_s as shown in Figure 5.5.1b. Since hydraulic fluid is essentially incompressible, only an infinitesimal mass increase is needed to double the pressure. Therefore, the hydraulic flow, $Q \cdot \Delta t$, is zero. However, the pneumatic system is governed by the linear ideal gas law such that doubling the pressure requires a doubling of the density (equivalently, a doubling of the mass). Thus, the air mass flow needed here is twice as large as in the first case (since the volume is now $2 \cdot h \cdot A$); the pneumatic volume flow measured in terms of air at ρ_i, the original density, is equal to V_2, the constant chamber volume.

Clearly, the volume flows for pneumatics and hydraulics are only equal for constant pressure volume increases. A pressure change at constant volume requires no hydraulic flow, while the pneumatic flow required is equal to the volume times the pressure change ratio,

$$\Delta V_i = V_i \cdot P_{final}/P_i. \qquad (5.5.7)$$

Since a pressure increase in the actuator takes flow from the supply, while a decrease exhausts air to the atmosphere, the overall effect is

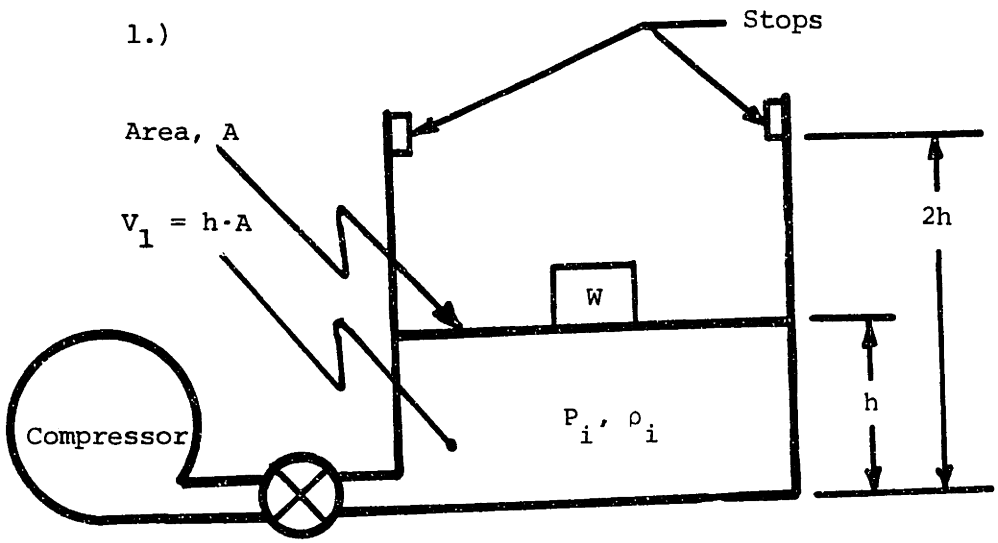

$$W = P_i \cdot A$$

Temperature = Constant

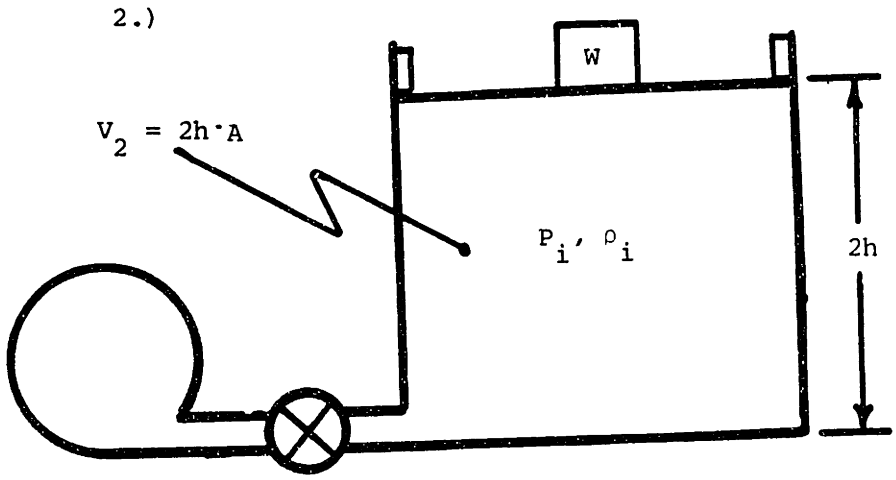

FIGURE 5.5.1a: CONTROL SURFACE WITH MOVING BOUNDARY--CONSTANT PRESSURE

1.)

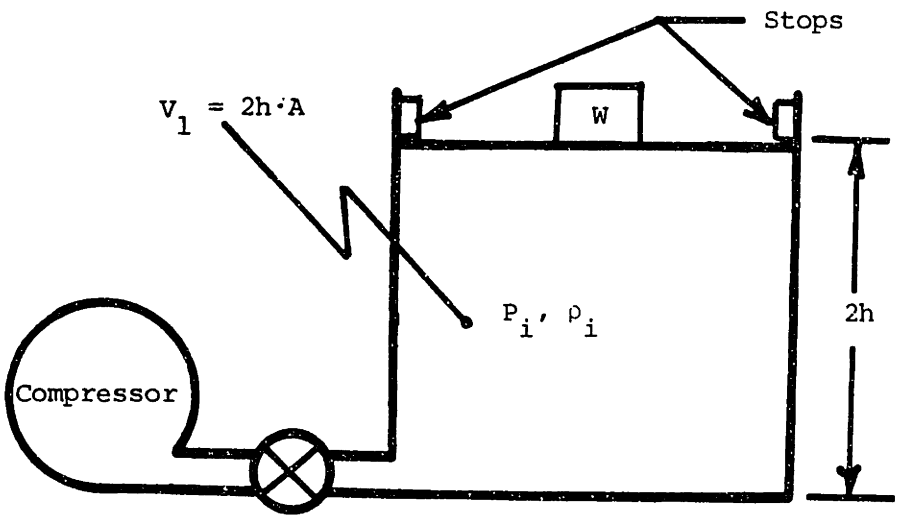

Volume = constant = $2L \cdot A$
Temperature = constant

2.)

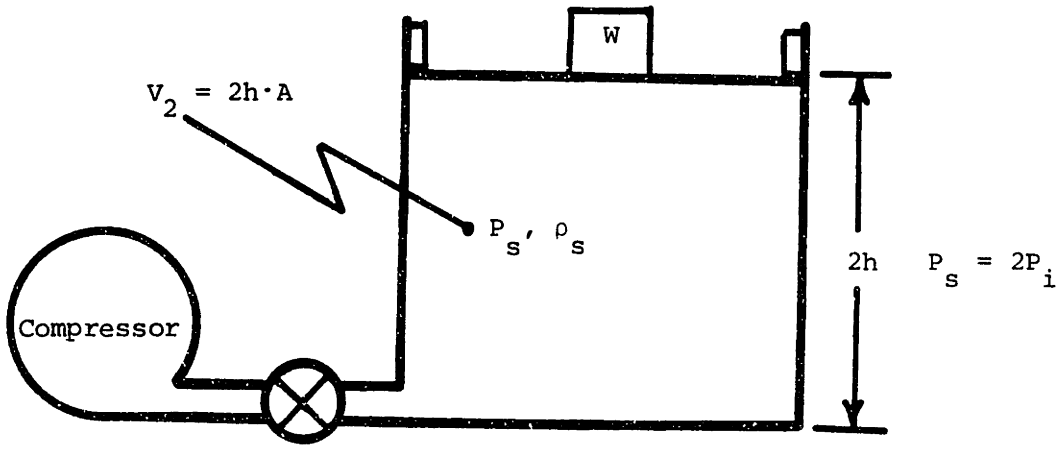

FIGURE 5.5.1b: CONTROL SURFACE WITH VARIABLE PRESSURE--CONSTANT VOLUME

unilateral: the pneumatic supply always provides a volume greater or equal to that needed for a hydraulic system.

Reduction of pneumatic flow consumption, and thereby power, can only be achieved by reducing the chamber volume. Three parameters must be considered: the piston area, the stroke, and the "dead volume". The piston area times the stroke approximately yields the working volume; this volume is necessary for the cylinder to provide the necessary travel (stroke) and the desired force (area). The dead volume is the result of many things; fittings, tubing, safety margins, and clearances all contribute to the dead volume.

With a piston area of 25 in^2 and a 1.5 inch peak stroke, the working volume for each airspring is only 37.5 in^3, leaving 112.5 in^3 of excess volume. Simulations of a pneumatic cylinder with a constant bore of 25 in^2 and only 2.5 in^2 of dead volume per chamber showed a reduction in average flow rate of about 65% (0.0512 lbm/sec), requiring a compressor power of 13 to 17 horsepower per car.

Two items should be noted: such a small dead volume does not allow for larger strokes that might occurs (no factor of safety is involved) or for the air volume between the actuator and the valve; furthermore, this flow rate, which is equivalent to 82 ft^3/min./car of 14.7 psia and 70°F, is still greater than is available for one car of a ten car consist using the present compression equipment.

Flow Limitation

The flow currently available from the AEM-7 locomotive is 135 ft^3/min.; from the F40, 254 ft^3/min. These flows must supply the entire train;

estimating the consist at about ten cars, the supply of air now available is about an order of magnitude below the demand predicted in Chapter 4 for an airspring actuator: 13 to 25 ft^3/min/car rather than 185 ft^3/min/car.

In an attempt to determine the level of active control that is possible with the limited flow, a simulation of a smaller actuator was performed. The volume and area parameters were scaled down to one tenth their actual values. To accommodate the reduced actuator area, the acceleration and velocity feedback coefficients were also reduced.

This system used one tenth as much flow as the larger system (0.012 lb/sec/truck) however, the active suspension made negligible improvements in ride quality. Root mean square acceleration was reduced only 5.2% from the passive level; rms stroke was reduced 4.7%.

Overall indications concerning power and flow are: the present air supply is not adequate to operate a continuously operating active suspension; all possible efforts must be made to limit the dead volume in the pneumatic actuator, including the use of more compact airsprings (same diameter, but shorter) or pneumatic cylinders.

5.6 Failure Analysis

A study of the actuator design was made to examine the possible failure modes and to determine system modifications that would lessen the harmful or wasteful effects of different failures. Active suspensions are capable of creating large forces; this potential must be controlled during system failures in order to avoid complete ride deter-

ioration. When a failure takes place, whether electrical or mechanical, the active system should exert as little force as possible on the carbody and truck, and flow loss must be minimized.

Figure 5.6.1 shows the actuator system with modifications made for failure protection. The use of two three-way servovalves (items 1 & 2) allows both actuator chambers to be closed off from the air supply at the same time. By using valves which both exhaust their chambers to atmosphere in the non-energized state, any electronically related valve failure results in the immediate exhausting of that valve's airspring to atmosphere. This position not only creates the least force on the vehicle, but also lessens flow leakage by closing off the supply.

Simulations comparing failures with both airsprings open to the supply, both open to atmosphere, and both closed off showed the closed off position to result in the worst ride quality. The maximum valve orifice was set at 0.11 square inches for the failure simulations. The sealed airsprings doubled the passive spring stiffness and nearly doubled the rms accelerations (0.088 g, as compared to the passive level of 0.048 g); exposing both chambers to the supply yielded accelerations of 0.065 g, while the exposure to atmospheric pressure was only slightly worse than the passive suspension at 0.049 g.

The major disadvantage of a normally-open to atmosphere valve is that constant energizing is needed during operation; however, in stations the electrical power could be shut off with relatively little air leakage. Normally-closed valves are more likely to leak due to overlap and wear.

1&2 - 3 way spool valves

3 - 2 way safety valve

4&5 - 3 way safety valves

6&7 - Airsprings

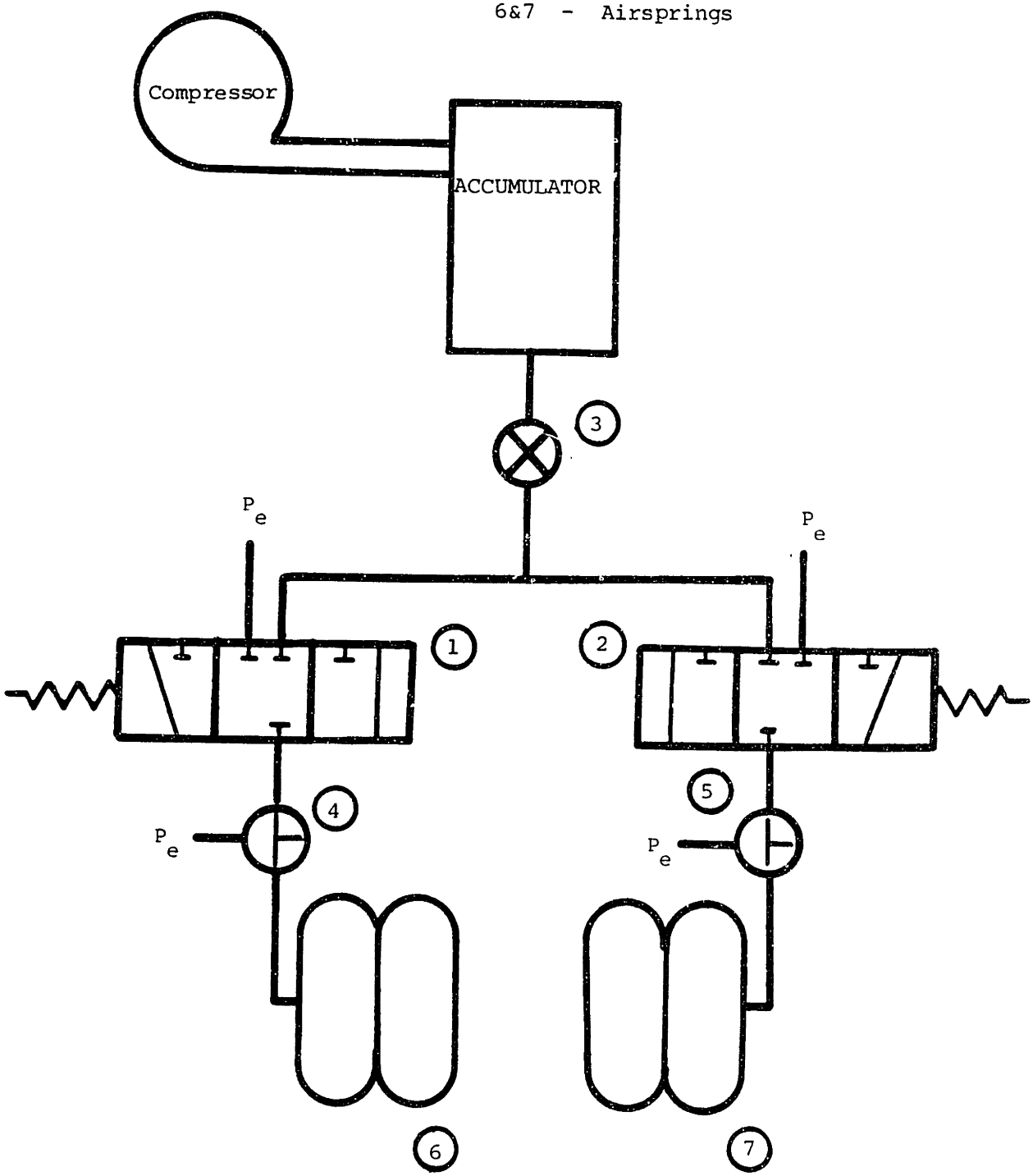

FIGURE 5.6.1: ACTUATOR SYSTEM - FAILURE PROTECTION MODIFICATIONS

Other potential electrical malfunctions, such as accelerometer failure, could result in a constant zero force command. The valves, then commanded only by the actuator's own force feedback loop, would continue to function, attempting to relieve all forces created by the stroking action of the airsprings. This would result in increased rms accelerations of 0.050 g and also require about 75% of the flow and power used during fully active operation. Once noticed, this problem could be remedied by shutting off the system such that the actuator chambers are exposed to the atmosphere.

Mechanical problems are not so easily solved. Either or both valves can stick closed, open to supply, or open to the atmosphere. The single degree of freedom vehicle simulation, with its linear passive springs shows the worst situation to result from both valves stuck closed. This is the same situation that could occur for an electrical failure with normally closed valves; however, mechanically (broken springs, etc.) it can happen with any type of valve. As stated previously, it would result in rms acceleration levels of 0.088 g, almost twice the passive level.

If one valve sticks open to the atmosphere, while the other sticks open to the atmosphere, another failure problem could arise. The pressure differential in the actuator would force the carbody over to one side, causing a mean stroke of 1.06 inches and increasing the frequency of bumpstop contacts. The resulting carbody acceleration would be higher than the 0.057 g level predicted by the single mass simulation, since it does not model the bumpstop.

Both of these failure modes would result in rough rides and require additional equipment to return the vehicle to near-passive ride quality. Extra valves must be placed in the design for use during mechanical failures. The two-way valve shown in Figure 5.6.1 at location 3 could cut off the air supply, while large T-valves (4&5) between the airsprings and the spool valves could exhaust the chambers to the atmosphere.

These additional valves need not be dynamically responsive and would be manually operated, either mechanically or electronically, since they would only be used in emergencies. Thus, a system failure of the worst kind (air trapped in the actuator chambers) would effectively increase the passive stiffness and double the rms accelerations over the passive vehicle levels. However, this problem could be relieved manually, restoring the system to its passive operating mode.

5.7 Power Sensitivity to Track Input Level

The analytical work presented thus far has used the analytical model for class-6 track presented in Chapters 2 and 3. However, data taken by ENSCO, Inc. indicates that track in the Northeast Corridor could be smoother than class-6; the Power Spectral Densities for both class-6 track and the ENSCO data are presented in Figures 2.4.3 a and b for a vehicle speed of 80 mph. This section investigates the sensitivity of the active system performance to the input level.

Comparison of the two track spectra shows the sample from the Northeast Corridor to be about an order of magnitude lower than the analytical class-6 model. For this reason, the input levels of the models

were adjusted such that the track input PSD's for alignment and cross-level were both ten times lower than the analytical class 6 model, but maintained the same break frequencies. Hence, the amplitudes of the six sinusoids used as an input to the single mass simulation were multiplied by $1/\sqrt{10}$.

Table 5.7.1 compares the performances of the passive and active suspensions at the lower input level with those representative of a class 6 track input. The active suspension used a force feedback loop gain of $k_f = 0.0003$ in^2/lbf. It should be noted that lowering the input PSD by one order of magnitude resulted in a nearly linear lowering of the root mean square performance levels; with the rms truck displacement lower by a factor of 0.32 ($1/\sqrt{10}$), the rms stroke, acceleration, force, and flow for the active suspension dropped by 0.32, 0.31, 0.32, and 0.34 times respectively.

Thus, the sensitivity of the active system is shown to vary almost linearly with the input level for input spectra lower than the class 6 spectra and of the same shape.

5.8 Summary

This chapter examined some of the problems related to implementation of the pneumatic actuator system designed in Chapter 4.

Section 5.2 showed that valve opening saturation at 50% of the desired peak orifice size seriously impairs system performance; however, a valve capable of 64% to 80% of the desired orifice area produces essentially the same performance as a non-saturating valve.

TABLE 5.7.1: SENSITIVITY OF PERFORMANCE TO INPUT LEVEL

PSD INPUT LEVEL	RMS STROKE (in)	RMS ACCELERATION (g)	RMS FORCE (lb_f)	AVERAGE FLOW (lb_m/sec/truck)//(ft^3/min/truck)	POWER (hp/car)
CLASS 6					
Passive	.54	.048	———	———	
Active	.47	.031	900	.115 // 92	27 to 38
$\frac{1}{10}$ CLASS 6					
Passive	.17	.015	———	———	
Active	.15	.0095	290	.039 // 31	9 to 13

The use of an on-off, or Bang-Bang, controller to implement the active control scheme was shown to be a poor substitute for a linear displacement spool valve. The Bang-Bang controller would require at least a 50 hertz solenoid valve and require more than twice the flow needed for a linear valve.

The force feedback control loop for the airspring actuator was shown to require a direct measurement of the force, possibly with strain gages. Estimation of the actuator force by measuring the chamber pressures and assuming a constant actuator area was shown to produce poor actuator performance. The actuator output had much difficulty following the desired force input signal as the stroke caused the airsprings' piston areas to change from their nominal sizes.

Reduction of actuator dead volume was shown to be the key to lower power consumption. Specially designed airsprings or pneumatic cylinders could produce the necessary forces with smaller volumes, but experimental work is needed to determine safe maximum stroke limits. Even with reduced dead volumes, pneumatic systems were shown to be less power efficient than hydraulic systems, and the flow rate required to generate the desired active forces was shown with a one degree of freedom model to be greater than that flow available from Amtrak's current pneumatic supplies. Lowering the acceleration and velocity feedback gains, C_a and C_v, and reducing the actuator size lowered the active power consumption to that level currently available, but the resulting performance was similar to that of the passive vehicle.

The failure analysis of Section 5.6 showed the worst rms accelerations to result from a failure that locked both valves closed, trapping the air inside the airspsrings. This caused rms accelerations to double, as the effective spring stiffness also doubled. Using two three-way spool valves that are both open to atmosphere in their non-energized states would help reduce the possibility of this type of lock-up. Having this happen with a pneumatic system is considerably less harmful than a hydraulic lock-up, where the suspension can become almost rigid. The same property, compressibility, which causes increased power consumption is an advantage in the case of a failure.

Section 5.7 showed that power consumption decreases proportionally with rms input level if the input spectrum maintains its characteristic shape. From a practical standpoint, this means lower power consumption than implied in Chapter 4 if the track is smoother than class-6 track. Data from ENSCO, Inc. showed track spectral densities representative of the Northeast Corridor to be an order of magnitude lower than the spectral densities for the class-6 track model. Thus, average power consumption could be on the order of 9 to 13 horsepower/car for the Northeast Corridor. More study is needed of the track condition to better estimate the average power usage of the active suspension.

CHAPTER 6

SUMMARY AND CONCLUSIONS

This thesis investigated the influence of limited bandwidth actuators on an active suspension for rail vehicles. The study included:

- ride quality testing and evaluation on a Northeast Corridor Amcoach vehicle to identify the ride quality problem
- implementation of an active control law to a linear 15 d.o.f. passive vehicle model corresponding to Amcoach dimensions with a well designed passive suspension using an infinite bandwidth actuator model
- evaluation of the active suspension using a finite bandwidth, first order lag actuator model and establishment of actuator performance requirements
- evaluation of active actuator system types
- design, modeling, and time domain simulation of a pneumatic actuator system
- analysis of actuator performance under system constraints such as valve saturation, pressure feedback, limited flow and power, and Bang-Bang controller implementation
- input level sensitivity and failure analyses

The results of the ride quality testing presented in Chapter 2 indicate that at higher speeds (80 mph), the lateral ride of the Amcoach vehicle is dominated by 0.5 to 1 Hz vibrations; these vibrations have been identified as corresponding to the lateral, roll, and yaw modes of the carbody on the secondary suspension. Thus, lateral ride improvement in this speed range was shown to be dependent on controlling the secondary suspension vibrations.

Parametric studies in Chapter 3 using a linear frequency domain vehicle model with class-6 level track input spectra showed a 3 hertz bandwidth actuation system to reduce rms accelerations of the vehicle by 50% over the passive vehicle, a reduction equal to the ideal actuator reduction, and to realize 75% of the stroke reductions predicted for the ideal system. The actuator system must be capable of generating 3000 lb/truck and actuators must have at least 3 inch strokes, peak to peak, and be capable of velocities of 1.5 ft/sec.

A survey of actuator systems showed a pneumatic actuator system to be preferred for the following reasons:

- Amtrak maintenance personnel are already familiar with pneumatic maintenance
- Pneumatic systems do not require return lines and cannot cause messy leaks as can hydraulics
- Hydraulic systems can become very stiff if the fluid is locked up inside the actuator; the compliance of air serves to soften the pneumatic system
- electro-magnetic systems have limited travel based on the need to maintain a small air gap

The actuator system designed in Chapter 4 consisted of four major parts: the compressor, the accumulator, the servovalve, and the actuator. The compressor must provide a flow of 0.115 lb/sec/truck (92 ft^3/min at 14.7 psia) at a supply pressure of 130 psig; one 3.0 cubic foot accumulator is needed per truck. The actuator design required a 25 in^2 piston area and, therefore, was modeled after the use of two Firestone 224 Airmount® Airstroke® airsprings mounted one on either side of the truck. Each pair of airsprings requires a pair

of synchronized 3-way linear spool valves (these function as a single 4-way valve, but are both normally open to atmosphere). These valves are driven by the error signal between the actual and desired forces.

The response speed of the actuator was adjusted by varying the gain on the error signal and was increased to provide the necessary bandwidth as well as to reject the stroke disturbance of the actuator. A gain level of 0.003 in^2/lb was selected; this allowed the pneumatic actuator to provide an acceleration level within 9.3% of the ideal active rms acceleration level.

Simulations showed the valves to need maximum effective orifice areas of 0.14 in^2 and predicted a pneumatic power consumption level of 27 to 38 horsepower per car. Assuming a ten car consist, pneumatic active control for the train would require 270 to 380 horsepower, less than 10% of the 4800 hp continuous power available at 100 mph from the AEM-7 locomotive [18]. However, the flow cannot be provided by the present air compressor which is limited to 137 ft^3/min. The active system would require an average flow rate of 1850 ft^3/min for the consist. Individual compressors could be used on each car or the locomotive's compressor could be replaced with a larger compressor as a central source.

Recommendations for further work are as follows:

- construction and testing of the valve-airspring assembly; examination of the effect of valve response speed on actuator performance
- full scale prototype testing on the Northeast Corridor to determine peak strokes and forces and to measure active performance

- re-designing to optimize component sizes; investigation of the use of pneumatic cylinders to reduce the dead volume of the actuators

REFERENCES

1. Sussman, D. and Wormley, D.N., "Measurement and Evaluation of Ride Quality in Advanced Ground Transportation Systems."

2. Hedrick, J.K., et al., "Performance Limits of Rail Passenger Vehicles: Evaluation and Optimization," Final Report, U.S. DOT Contract DOT-OS-70052, December 1979.

3. Wormley, D.N., et al., "Rail Passenger Vehicle Truck Design Methodology," U.S. DOT Final Report, Report No. FRA/ORD-81/11, January 1981.

4. Celniker, G.W., "The Application of Active Control to Rail Vehicles," S.M. Thesis, Department of Mechanical Engineering, M.I.T., January 1981.

5. Partridge, M.A., " The Effect of Suspension System Passive Modification on Rail Vehicle Lateral Dynamics," S.M. Thesis, Department of Mechanical Engineering, M.I.T., March 1982.

6. Jindai, K., Kasai, K., Terada, K., Kakehi, Y., Iwasaki, F., "Fundamental Study on Semi-Actively Controlled Pneumatic Servo Suspensions for Rail Cars," paper presented at the Joint ASME/IEEE Railroad Conference, Atlanta, Georgia, April 28-30, 1981.

7. Mauer, L., "Improvement of Railcar Vehicle Performance, State of the Art Report," U.S.-German Cooperation Project (MAN-MIT), EDS-022, October 16, 1979.

8. Goodall, R.M., Williams, R.A., and Lawton, A., "Practical Applications of Actively Controlled Suspensions to Railway Vehicles," presented at the 1979 ASME Winter Annual Meeting, New York, 1979.

9. Sinha, P.K., Wormley, D.N., and Hedrick, J.K., "Rail Passenger Vehicle Lateral Dynamic Performance Improvements through Active Control," ASME Journal of Dynamic Systems, Measurements and Control, Series G, Vol. 100, December 1978, pp. 270-283.

10. Jeffcoat, R.L., "Improvement of Rail Vehicle Lateral Dynamic Performance through Active Control," Vehicle Systems Dynamics, Vol. 4, No. 2-3, 1975, pp. 169-173.

11. Hedrick, J.K. and Wormley, D.N., "Active Control for Ground Transportation Vehicles: A State of the Art Review," ASME, AMD Monograph, Vol. 15, 1975.

12. Shapiro, S.M., "Engineering Data on Selected High Speed Passenger Trucks," Final Technical Report, Report No. 0391, The Budd Technical Center, Fort Washington, PA, May 1977.

13. Goodall, R.M., Williams, R.A., Lawton, A., and Harborough, P.R., "Railway Vehicle Active Suspensions in Theory and Practice."

14. "Airstroke® Actuators, Airmount® Isolators, Engineering Manual and Design Guide," Firestone Industrial Products Company, Noblesville, Indiana 46060.

15. Blackburn, et al., Fluid Power Control, M.I.T. Press, Cambridge, MA, 1960.

16. VanWylen, G.J., Sonntag, R.E., Fundamentals of Classical Thermodynamics, John Wiley & Sons, Inc., New York, 1976.

17. "DYSYS," M.I.T. Joint Computer Facility Library, 1980.

18. Ephraim, M., "The AEM-7 - A New High Speed, Light Weight Electric Passenger Locomotive," ASME Paper 82-RT-7, 1982.

APPENDIX A

EQUATIONS OF MOTION FOR PASSIVE VEHICLE

15 D.O.F. LATERAL MODEL EQUATIONS

Leading Wheelset Leading Truck

$$M_w \ddot{y}_{wl} = -\left[\frac{2f_{11}}{V} + 2c_{py} - \frac{c_{py} h_{tp} a_{11}}{a}\right]\dot{y}_{wl}$$

$$-2\left[k_{py} - \frac{f_{12}\Delta}{ar_o} + \frac{N}{2a}(a_{11} + \Delta) - \frac{k_{py} h_{tp} a_{11}}{2a}\right]y_{wl}$$

$$-\left[\frac{2f_{12}}{V} - \frac{VI_{wy} a_{11}}{ar_o}\right]\dot{\psi}_{wl} + 2f_{11}\psi_{wl}$$

$$+ \frac{c_{py} h_{tp} a_{11}}{a}\dot{y}_{w2} + \frac{k_{py} h_{tp} a_{11}}{a} y_{w2}$$

$$+ 2c_{py}\dot{y}_{tl} + 2k_{py} y_{tl} + 2c_{py} b\dot{\psi}_{tl} + 2k_{py} b\psi_{tl} + u_1$$

$$I_{wz}\ddot{\psi}_{wl} = \left[\frac{2f_{12}}{V} - \frac{VI_{wy} a_{11}}{ar_o}\right]\dot{y}_{wl} + \left[\frac{2f_{22}\Delta}{ar_o} - \frac{2af_{33}\lambda}{r_o}\right]y_{wl}$$

$$-\left[\frac{2f_{22}}{V} + \frac{2a^2 f_{33}}{V}\right] + 2c_{px} d_p^2\Big]\dot{\psi}_{wl}$$

$$-\left[2k_{px} d_p^2 - aN\delta_o + 2f_{12}\right]\psi_{wl}$$

$$+ 2c_{px} d_p^2\dot{\psi}_{tl} + 2k_{px} d_p^2\psi_{tl} + u_2$$

Trailing Wheelset Leading Truck

$$M_w\ddot{y}_{w2} = \frac{c_{py}h_{tp}a_{11}}{a}\dot{y}_{w1} + \frac{k_{py}h_{tp}a_{11}}{a}y_{w1} - [\frac{2f_{11}}{v} + 2c_{py} - \frac{c_{py}h_{tp}a_{11}}{a}]\dot{y}_{w2}$$

$$- 2[k_{py} - \frac{f_{12}\Lambda}{ar_o} + \frac{N}{2a}(a_{11} + \Delta) - \frac{k_{py}h_{tp}a_{11}}{2a}]y_{w2}$$

$$- 2[\frac{f_{12}}{v} - \frac{vI_{wy}a_{11}}{ar_o}]\dot{\psi}_{w2} + 2f_{11}\psi_{w2}$$

$$+ 2c_{py}\dot{y}_{t1} + 2k_{py}y_{t1} - 2c_{py}b\dot{\psi}_{t1} - 2k_{py}b\psi_{t1} + u_3$$

$$I_{wz}\ddot{\psi}_{w2} = [\frac{2f_{12}}{v} - \frac{vI_{wy}a_{11}}{ar_o}]\dot{y}_{w2} + [\frac{2f_{22}\Delta}{ar_o} - \frac{2af_{33}\lambda}{r_o}]y_{w2}$$

$$-[\frac{2f_{22}}{v} + \frac{2a^2f_{33}}{v} + 2c_{px}d_p^2]\dot{\psi}_{w2}$$

$$-[2k_{px}d_p^2 - aN\delta_o + 2f_{12}]\psi_{w2}$$

$$+ 2c_{px}d_p^2\dot{\psi}_{t1} + 2k_{px}d_p^2\psi_{t1} + u_4$$

Leading Truck

$$M_t\ddot{y}_{t1} = [2c_{py} - \frac{a_{11}}{a}(2c_{py}h_{tp} + c_{sy}h_{ts})]\dot{y}_{w1}$$

$$+ [2k_{py} - \frac{a_{11}}{a}(2k_{py}h_{tp} + k_{sy}h_{ts})]y_{w1}$$

$$+ [2c_{py} - \frac{a_{11}}{a}(2c_{py}h_{tp} + c_{sy}h_{ts})]\dot{y}_{w2}$$

$$+ [2k_{py} - \frac{a_{11}}{a}(2k_{py}h_{tp} + k_{sy}h_{ts})]y_{w2}$$

$$-[4c_{py} + 2c_{sy}]\dot{y}_{t1} - [4k_{py} + 2k_{sy}]y_{t1}$$

$$+2c_{sy}\dot{y}_c + 2k_{sy}y_c + 2c_{sy}\ell_s\dot{\psi}_c + 2k_{sy}\ell_s\psi_c$$

$$+2c_{sy}h_{cs}\dot{\phi}_c + 2k_{sy}h_{cs}\phi_c + u_5$$

$$I_{tz}\ddot{\psi}_{t1} = 2bc_{py}\dot{y}_{w1} + 2bk_{py}y_{w1} + 2d_p^2c_{px}\dot{\psi}_{w1} + 2d_p^2k_{px}\psi_{w1}$$

$$-2bc_{py}\dot{y}_{w2} - 2bk_{py}y_{w2} + 2d_p^2c_{px}\dot{\psi}_{w2} + 2d_p^2k_{px}\psi_{w2}$$

$$-[4c_{py}b^2 + c_{s\psi} + 4c_{px}d_p^2]\dot{\psi}_{t1}$$

$$-[4k_{py}b^2 + k_{s\psi} + 4k_{px}d_p^2]\psi_{t1}$$

$$+c_{s\psi}\dot{\psi}_c + k_{s\psi}\psi_c + u_6$$

Leading Wheelset, Trailing Truck

$$M_w\ddot{y}_{w3} = -[\frac{2f_{11}}{v} + 2c_{py} - \frac{c_{py}h_{tp}a_{11}}{a}]\dot{y}_{w3}$$

$$-2[k_{py} - \frac{f_{12}\Delta}{ar_o} + \frac{N}{2a}(a_{11} + \Delta) - \frac{k_{py}h_{tp}a_{11}}{2a}]y_{w3}$$

$$-[\frac{2f_{12}}{v} - \frac{vI_{wy}a_{11}}{ar_o}]\dot{\psi}_{w3} + 2f_{11}\psi_{w3}$$

$$+\frac{c_{py}h_{tp}a_{11}}{a}\dot{y}_{w4} + \frac{k_{py}h_{tp}a_{11}}{a}y_{w4}$$

$$+2c_{py}\dot{y}_{t2} + 2k_{py}y_{t2} + 2c_{py}b\dot{\psi}_{t2} + 2k_{py}b\psi_{t2} + u_7$$

$$I_{wz}\ddot{\psi}_{w3} = [\frac{2f_{12}}{v} - \frac{vI_{wy}a_{11}}{ar_o}]\dot{y}_{w3} + [\frac{2f_{22}\Delta}{ar_o} - \frac{2af_{33}\lambda}{r_o}]y_{w3}$$

$$-[\frac{2f_{22}}{v} + \frac{2a^2f_{33}}{v} + 2c_{px}d_p^2]\dot{\psi}_{w3}$$

$$-[2k_{px}d_p^2 - aN\delta_o + 2f_{12}]\psi_{w3}$$

$$+2c_{px}d_p^2\dot{\psi}_{t2} + 2k_{px}d_p^2\psi_{t2} + u_8$$

Trailing Wheelset, Trailing Truck

$$M_w\ddot{y}_{w4} = \frac{c_{py}h_{tp}a_{11}}{a}\dot{y}_{w3} + \frac{k_{py}h_{tp}a_{11}}{a}y_{w3} - [\frac{2f_{11}}{v} + 2c_{py} - \frac{c_{py}h_{tp}a_{11}}{a}]\dot{y}_{w4}$$

$$- 2[k_{py} - \frac{f_{12}\Delta}{ar_o} + \frac{N}{2a}(a_{11} + \Delta) - \frac{k_{py}h_{tp}a_{11}}{2a}]y_{w4}$$

$$-[\frac{2f_{12}}{v} - \frac{vI_{wy}a_{11}}{ar_o}]\dot{\psi}_{w4} + 2f_{11}\psi_{w4}$$

$$+ 2c_{py}\dot{y}_{t2} + 2k_{py}y_{t2} - 2c_{py}b\dot{\psi}_{t2} - 2k_{py}b\psi_{t2} + u_9$$

$$I_{wz}\ddot{\psi}_{w4} = [\frac{2f_{12}}{v} - \frac{vI_{wy}a_{11}}{ar_o}]y_{w4} + [\frac{2f_{22}\Delta}{ar_o} - \frac{2af_{33}\lambda}{r_o}]y_{w4}$$

$$- [\frac{2f_{22}}{v} + \frac{2a^2f_{33}}{v} + 2c_{px}d_p^2]\dot{\psi}_{w4}$$

$$- [2k_{px}d_p^2 - aN\delta_o + 2f_{12}]\psi_{w4}$$

$$+ 2c_{px}d_p^2\dot{\psi}_{t2} + 2k_{px}d_p^2\psi_{t2} + u_{10}$$

Trailing Truck

$$M_t\ddot{y}_{t2} = [2c_{py} - \frac{a_{11}}{a}(2c_{py}h_{tp} + c_{sy}h_{ts})]\dot{y}_{w3}$$

$$+ [2k_{py} - \frac{a_{11}}{a}(2k_{py}h_{tp} + k_{sy}h_{ts})]y_{w3}$$

$$+ [2c_{py} - \frac{a_{11}}{a}(2c_{py}h_{tp} + c_{sy}h_{ts})]\dot{y}_{w4}$$

$$+ [2k_{py} - \frac{a_{11}}{a}(2k_{py}h_{tp} + k_{sy}h_{ts})]y_{w4}$$

$$- [4c_{py} + 2c_{sy}]\dot{y}_{t2} - [4k_{py} + 2k_{sp}]y_{t2}$$

$$+ 2c_{sy}\dot{y}_c + 2k_{sy}y_c - 2c_{sy}\ell_s\dot{\psi}_c - 2k_{sy}\ell_s\psi_c$$

$$+ 2c_{sy}h_{cs}\dot{\phi}_c + 2k_{sy}h_{cs}\phi_c + u_{11}$$

$$I_{tz}\ddot{\psi}_{t2} = 2bc_{py}\dot{y}_{w3} + 2bk_{py}y_{w3} + 2d_p^2c_{px}\dot{\psi}_{w3} + 2d_p^2k_{px}\psi_{w3}$$

$$- 2bc_{py}\dot{y}_{w4} - 2bk_{py}y_{w4} + 2d_p^2c_{px}\dot{\psi}_{w4} + 2d_p^2k_{px}\psi_{w4}$$

$$- [4c_{py}b^2 + c_{s\psi} + 4c_{px}d_p^2]\dot{\psi}_{t2}$$

$$- [4k_{py}b^2 + k_{s\psi} + 4k_{px}d_p^2]\psi_{t2}$$

$$+ c_{s\psi}\dot{\psi}_c + k_{s\psi}\psi_c + u_{12}$$

Carbody

$$M_c\ddot{y}_c = -\frac{a_{11}h_{ts}c_{sy}}{a}\dot{y}_{w1} - \frac{a_{11}h_{ts}k_{sy}}{a}y_{w1} - \frac{a_{11}h_{ts}c_{sy}}{a}\dot{y}_{w2} - \frac{a_{11}h_{ts}k_{sy}}{a}y_{w2}$$

$$+ 2c_{sy}\dot{y}_{t1} + 2k_{sy}y_{t1} - \frac{a_{11}h_{ts}c_{sy}}{a}\dot{y}_{w3} - \frac{a_{11}h_{ts}k_{sy}}{a}y_{w3} - \frac{a_{11}h_{ts}c_{sy}}{a}\dot{y}_{w4}$$

$$- \frac{a_{11}h_{ts}k_{sy}}{a}y_{w4} + 2c_{sy}\dot{y}_{t2} + 2k_{sy}y_{t2} - 4c_{sy}\dot{y}_c - 4k_{sy}y_c$$

$$- 4h_{cs}c_{sy}\dot{\phi}_c - 4h_{cs}k_{sy}\phi_c + u_{13}$$

$$I_{cz}\ddot{\psi}_c = -\frac{h_{ts}\ell_s a_{11}c_{sy}}{a}\dot{y}_{w1} - \frac{h_{ts}\ell_s a_{11}k_{sy}}{a}y_{w1} - \frac{h_{ts}\ell_s a_{11}c_{sy}}{a}\dot{y}_{w2}$$

$$- \frac{h_{ts}\ell_s a_{11}k_{sy}}{a}y_{w2} + 2\ell_s c_{sy}\dot{y}_{t1} + 2\ell_s k_{sy}y_{t1} + c_{s\psi}\dot{\psi}_{t1}$$

$$+ k_{s\psi}\psi_{t1} + \frac{h_{ts}\ell_s a_{11}c_{sy}}{a}\dot{y}_{w3} + \frac{h_{ts}\ell_s a_{11}k_{sy}}{a}y_{w3}$$

$$+ \frac{h_{ts}\ell_s a_{11}c_{sy}}{a}\dot{y}_{w4} + \frac{h_{ts}\ell_s a_{11}k_{sy}}{a}y_{w4} - 2\ell_s c_{sy}\dot{y}_{t2}$$

$$- 2\ell_s k_{sy}y_{t2} + c_{s\psi}\dot{\psi}_{t2} + k_{s\psi}\psi_{t2}$$

$$- [4\ell_s^2 c_{sy} + 2c_{s\psi}]\dot{\psi}_c - [4\ell_s^2 k_{sy} + 2k_{s\psi}]\psi_c + u_{14}$$

$$I_{cy}\ddot{\phi}_c = \frac{a_{11}}{a}[d_s^2 c_{sz} - h_{cs}h_{ts}c_{sy}]\dot{y}_{w1} + \frac{a_{11}}{a}[d_s^2 k_{sz} - h_{cs}h_{ts}k_{sy}]y_{w1}$$

$$+ \frac{a_{11}}{a}[d_s^2 c_{sz} - h_{cs}h_{ts}c_{sy}]\dot{y}_{w2} + \frac{a_{11}}{a}[d_s^2 k_{sz} - h_{cs}h_{ts}k_{sy}]y_{w2}$$

$$+ 2h_{cs}c_{sy}\dot{y}_{t1} + 2h_{cs}k_{sy}y_{t1}$$

$$+ \frac{a_{11}}{a}[d_s^2 c_{sz} - h_{cs}h_{ts}c_{sy}]y_{w3} + \frac{a_{11}}{a}[d_s^2 k_{sz} - h_{cs}h_{ts}k_{sy}]y_{w3}$$

$$+ \frac{a_{11}}{a}[d_s^2 c_{sz} - h_{cs}h_{ts}c_{sy}]\dot{y}_{w4} + \frac{a_{11}}{a}[d_s^2 k_{sz} - h_{cs}h_{ts}k_{sy}]y_{w4}$$

$$+ 2h_{cs}c_{sy}\dot{y}_{t2} + 2h_{cs}k_{sy}y_{t2} - 4h_{cs}c_{sy}y_c - 4h_{cs}k_{sy}y_c$$

$$-[4h_{cs}^2 c_{sy} + 4d_s^2 c_{sz}]\dot{\phi}_c - [4h_{cs}^2 k_{sy} + 4d_s^2 k_{sz} - h_{cs}W]\phi_c + u_{15}$$

$$u_1 = \left[\frac{2r_o f_{11} a_{11}}{av} - \frac{c_{py} h_{tp} a_{11}}{a}\right]\dot{u}_a(t) - \frac{c_{py} h_{tp} a_{11}}{a}\dot{u}_a\left(t - \frac{2b}{v}\right)$$

$$+ 2\left[\frac{N}{2a}(a_{11} + \Delta) - \frac{f_{12}\Delta}{ar_o} - \frac{k_{py} h_{tp} a_{11}}{2a}\right]u_a(t)$$

$$- \frac{k_{py} h_{tp} a_{11}}{a} u_a\left(t - \frac{2b}{v}\right)$$

$$u_2 = -\left[\frac{2f_{12} a_{11} r_o}{av} - \frac{I_{wy} v a_{11}}{ar_o}\right]u_a(t) - 2\left[\frac{f_{22}\Delta}{ar_o} - \frac{af_{33}\lambda}{r_o}\right]u_a(t)$$

$$u_3 = -\frac{c_{py} h_{tp} a_{11}}{a}\dot{u}_a(t) + \left[\frac{2r_o f_{11} a_{11}}{av} - \frac{c_{py} h_{tp} a_{11}}{a}\right]\dot{u}_a\left(t - \frac{2b}{v}\right)$$

$$- \frac{k_{py} h_{tp} a_{11}}{a} u_a(t) + 2\left[\frac{N}{2a}(a_{11} + \Delta) - \frac{f_{12}\Delta}{ar_o} - \frac{k_{py} h_{tp} a_{11}}{2a}\right]u_a\left(t - \frac{2b}{v}\right)$$

$$u_4 = -\left[\frac{2f_{12} a_{11} r_o}{av} - \frac{I_{wy} v a_{11}}{ar_o}\right]\dot{u}_a\left(t - \frac{2b}{v}\right) - 2\left[\frac{f_{22}\Delta}{ar_o} - \frac{af_{33}\lambda}{r_o}\right]u_a\left(t - \frac{2b}{v}\right)$$

$$u_5 = \frac{a_{11}}{a}[2c_{py} h_{tp} + c_{sy} h_{ts}]\dot{u}_a(t) + \frac{a_{11}}{a}[2c_{py} h_{tp} + c_{sy} h_{ts}]\dot{u}_a\left(t - \frac{2b}{v}\right)$$

$$+ \frac{a_{11}}{a}[2k_{py} h_{tp} + k_{sy} h_{ts}]u_a(t) + \frac{a_{11}}{a}[2k_{py} h_{tp} + k_{sy} h_{ts}]u_a\left(t - \frac{2b}{v}\right)$$

$$u_6 = 0$$

$$u_7 = \left[\frac{2r_o f_{11} a_{11}}{av} - \frac{c_{py} h_{tp} a_{11}}{a}\right]\dot{u}_a\left(t - \frac{2\ell_s}{v}\right) - \frac{c_{py} h_{tp} a_{11}}{a}\dot{u}_a\left(t - \frac{2(\ell_s + b)}{v}\right)$$

$$+ 2\left[\frac{N}{2a}(a_{11} + \Delta) - \frac{f_{12}\Delta}{ar_o} - \frac{k_{py} h_{tp} a_{11}}{2a}\right]u_a\left(t - \frac{2\ell_s}{v}\right)$$

$$- \frac{k_{py} h_{tp} a_{11}}{a} u_a\left(t - \frac{2(\ell_s + b)}{v}\right)$$

$$u_8 = -\left[\frac{2f_{12} a_{11} r_o}{av} - \frac{I_{wy} v a_{11}}{a r_o}\right] \dot{u}_a\left(t - \frac{2\ell_s}{v}\right) - 2\left[\frac{f_{22}\Delta}{a r_o} - \frac{a f_{33}\lambda}{r_o}\right] u_a\left(t - \frac{2\ell_s}{v}\right)$$

$$u_9 = -\frac{c_{py} h_{tp} a_{11}}{a} \dot{u}_a\left(t - \frac{2\ell_s}{v}\right) + \left[\frac{2r_o f_{11} a_{11}}{av} - \frac{c_{py} h_{tp} a_{11}}{a}\right] \dot{u}_a\left(t - \frac{2(\ell_s + b)}{v}\right)$$

$$- \frac{k_{py} h_{tp} a_{11}}{a} u_a\left(t - \frac{2\ell_s}{v}\right) + 2\left[\frac{N}{2a}(a_{11} + \Delta) - \frac{f_{12}\Delta}{a r_o} - \frac{k_{py} h_{tp} a_{11}}{2a}\right]$$

$$\cdot u_a\left(t - \frac{2\ell_s + b}{v}\right)$$

$$u_{10} = -\left[\frac{2f_{12} a_{11} r_o}{av} - \frac{I_{wy} v a_{11}}{a r_o}\right] \dot{u}_a\left(t - \frac{2(\ell_s + b)}{v}\right)$$

$$-2\left[\frac{f_{22}\Delta}{a r_o} - \frac{a f_{33}\lambda}{r_o}\right] u_a\left(t - \frac{2(\ell_s + b)}{v}\right)$$

$$u_{11} = \frac{a_{11}}{a}[2c_{py} h_{tp} + c_{sy} h_{ts}] \dot{u}_a\left(t - \frac{2\ell_s}{v}\right)$$

$$+ \frac{a_{11}}{a}[2c_{py} h_{tp} + c_{sy} h_{ts}] \dot{u}_a\left(t - \frac{2(\ell_s + b)}{v}\right)$$

$$+ \frac{a_{11}}{a}[2k_{py} h_{tp} + k_{sy} h_{ts}] u_a\left(t - \frac{2\ell_s}{v}\right)$$

$$+ \frac{a_{11}}{a}[2k_{py} h_{tp} + k_{sy} h_{ts}] u_a\, t - \frac{2(\ell_s + b)}{v}$$

$$u_{12} = 0$$

$$u_{13} = \frac{a_{11} h_{ts} c_{sy}}{a}\left[\dot{u}_a(t) + \dot{u}_a\left(t - \frac{2b}{v}\right) + \dot{u}_a\left(t - \frac{2\ell_s}{v}\right) + \dot{u}_a\left(t - \frac{2\ell_s + b}{v}\right)\right]$$

$$+ \frac{a_{11} h_{ts} k_{sy}}{a}\left[u_a(t) + u_a\left(t - \frac{2b}{v}\right) + u_a\left(t - \frac{2\ell_s}{v}\right) + u_a\left(t - \frac{2(\ell_s + b)}{v}\right)\right]$$

$$u_{14} = \frac{h_{ts} \ell_s c_{sy} a_{11}}{a}\left[\dot{u}_a(t) + \dot{u}_a\left(t - \frac{2b}{v}\right) - \dot{u}_a\left(t - \frac{2\ell_s}{v}\right) - u_a\left(t - \frac{2(\ell_s + b)}{v}\right)\right]$$

$$+ \frac{h_{ts} \ell_s k_{sy} a_{11}}{a}\left[u_a(t) + u_a\left(t - \frac{2b}{v}\right) - u_a\left(t - \frac{2\ell_s}{v}\right) - u_a\left(t - \frac{2(\ell_s + b)}{v}\right)\right]$$

$$u_{15} = -\frac{a_{11}}{a}\left[d_s^2 c_{sz} - h_{ts} c_{sy}\right]\left[\dot{u}_a(t) + \dot{u}_a\left(t - \frac{2b}{v}\right) + \dot{u}_a\left(t - \frac{2\ell_s}{v}\right) + \dot{u}_a\left(t - \frac{2(\ell_s + b)}{v}\right)\right]$$

$$- \frac{a_{11}}{a}\left[d_s^2 k_{sz} - h_{ts} k_{sy}\right]\left[u_a(t) + u_a\left(t - \frac{2b}{v}\right) + u_a\left(t - \frac{2\ell_s}{v}\right) + u_a\left(t - \frac{2(\ell_s + b)}{v}\right)\right]$$

CROSSLEVEL INPUTS

$$u_1 = + \frac{r_o M_w}{2a} \ddot{u}_c(t) + [\frac{r_o C_{py}}{a} + \frac{C_{py} h_{tp}}{2a}] \dot{u}_c(t) + \frac{C_{py} h_{tp}}{2a} \dot{u}_c(t - \frac{2b}{v})$$

$$+ [\frac{r_o k_{py}}{a} + \frac{k_{py} h_{tp}}{2a}] u_c(t) + \frac{k_{py} h_{tp}}{2a} u_c(t - \frac{2b}{v})$$

$$u_2 = - \frac{I_{wy} v}{2ar_o} \dot{u}_c(t)$$

$$u_3 = + \frac{r_o M_w}{2a} \ddot{u}_c(t - \frac{2b}{v}) + \frac{C_{py} h_{tp}}{2a} \dot{u}_c(t) + [\frac{r_o C_{py}}{a} + \frac{C_{py} h_{tp}}{2a}] \dot{u}_c(t - \frac{2b}{v})$$

$$+ \frac{k_{py} h_{tp}}{2a} u_c(t) + [\frac{r_o k_{py}}{a} + \frac{k_{py} h_{tp}}{2a}] u_c(t - \frac{2b}{v})$$

$$u_4 = - \frac{I_{wy} v}{2ar_o} \dot{u}_c(t - \frac{2b}{v})$$

$$u_5 = [\frac{-r_o c_{py}}{a} - \frac{1}{4a} (4C_{py} h_{tp} + 2C_{sy} h_{ts})] \dot{u}_c(t)$$

$$+ [\frac{-r_o c_{py}}{a} - \frac{1}{4a} (4C_{py} h_{tp} + 2C_{sy} h_{ts})] \dot{u}_c(t - \frac{2b}{v})$$

$$+ [\frac{-r_o k_{py}}{a} - \frac{1}{4a} (4k_{py} h_{tp} + 2k_{sy} h_{ts})] u_c(t)$$

$$+ [\frac{-r_o k_{py}}{a} - \frac{1}{4a} (4k_{py} h_{tp} + 2k_{sy} h_{ts})] u_c(t - \frac{2b}{v})$$

$$u_6 = -hr_o C_{py} \dot{u}_c(t) + hr_o C_{py} \dot{u}_c(t - \frac{2b}{v})$$

$$-hr_o k_{py} u_c(t) + hr_o k_{py} u_c(t - \frac{2b}{v})$$

$$u_7 = + \frac{r_o M_w}{2a} \ddot{u}_c(t - \frac{2\ell_s}{v}) + [\frac{r_o C_{py}}{a} + \frac{C_{py} h_{tp}}{2a}] \dot{u}_c(t - \frac{2\ell_s}{v})$$

$$+ \frac{C_{py} h_{tp}}{2a} \dot{u}_c(t - \frac{2(\ell_s + b)}{v}) + [\frac{r_o k_{py}}{a} + \frac{k_{py} h_{tp}}{2a}] u_c(t - \frac{2\ell_s}{v})$$

$$+ \frac{k_{py} h_{tp}}{2a} u_c(t - \frac{2(\ell_s + b)}{v})$$

$$u_8 = - \frac{I_{wy} V}{2ar_o} \dot{u}_c(t - \frac{2\ell_s}{v})$$

$$u_9 = + \frac{r_o M_w}{2a} \ddot{u}_c(t - \frac{2(\ell_s + b)}{v} + \frac{C_{py} h_{tp}}{2a} \dot{u}_c(t - \frac{2\ell_s}{v})$$

$$+ [\frac{r_o C_{py}}{a} + \frac{C_{py} h_{tp}}{2a}] \dot{u}_c(t - \frac{2(\ell_s + b)}{v} + \frac{k_{py} h_{tp}}{2a} u_c(t - \frac{2\ell_s}{v})$$

$$+ [\frac{r_o k_{py}}{a} + \frac{k_{py} h_{tp}}{2a}] u_c(t - \frac{2(\ell_s + b)}{v})$$

$$u_{10} = - \frac{I_{wy} v}{2ar_o} u_c(t - \frac{2(\ell_s + b)}{v})$$

$$u_{11} = [- \frac{r_o C_{py}}{a} - \frac{1}{4a}(4C_{py} h_{tp} + 2C_{sy} h_{ts})] \dot{u}_c(t - \frac{2\ell_s}{v})$$

$$+ [- \frac{r_o C_{py}}{a} - \frac{1}{4a}(4C_{py} h_{tp} + 2C_{sy} h_{ts})] u_c(t - \frac{2(\ell_s + b)}{v})$$

$$+ [- \frac{r_o k_{py}}{a} - \frac{1}{4a}(4k_{py} h_{tp} + 2k_{sy} h_{ts})] u_c(t - \frac{2\ell_s}{v})$$

$$+ [- \frac{r_o k_{py}}{a} - \frac{1}{4a}(4k_{py} h_{tp} + 2k_{sy} k_{ts})] u_c(t - \frac{2(\ell_s + b)}{v})$$

$$u_{12} = -\frac{h_{ro}C_{py}}{2a}\left[\dot{u}_c\left(t-\frac{2\ell_s}{v}\right) - \dot{u}_c\left(t-\frac{2(\ell_s+b)}{v}\right)\right]$$

$$-\frac{h_{ro}k_{py}}{2a}\left[u_c\left(t-\frac{2\ell_s}{v}\right) - u_c\left(t-\frac{2(\ell_s+b)}{v}\right)\right]$$

$$u_{13} = -\frac{h_{ts}C_{sy}}{2a}\left[\dot{u}_c(t) + \dot{u}_c\left(t-\frac{2b}{v}\right) + \dot{u}_c\left(t-\frac{2\ell_s}{v}\right) + \dot{u}_c\left(t-\frac{2(\ell_s+b)}{v}\right)\right]$$

$$-\frac{h_{ts}k_{sy}}{2a}\left[u_c(t) + u_c\left(t-\frac{2b}{v}\right) + u_c\left(t-\frac{2\ell_s}{v}\right) + u_c\left(t-\frac{2(\ell_s+b)}{v}\right)\right]$$

$$u_{14} = -\frac{h_{ts}\ell_s C_{sy}}{2a}\left[\dot{u}_c(t) + \dot{u}_c\left(t-\frac{2b}{v}\right) - \dot{u}_c\left(t-\frac{2\ell_s}{v}\right) - \dot{u}_c\left(t-\frac{2(\ell_s+b)}{v}\right)\right]$$

$$-\frac{h_{ts}\ell_s k_{sy}}{2a}\left[u_c(t) + u_c\left(t-\frac{2b}{v}\right) - u_c\left(t-\frac{2\ell_s}{v}\right) - u_c\left(t-\frac{2(\ell_s+b)}{v}\right)\right]$$

$$u_{15} = -\frac{1}{2a}\left[ds^2 C_{sz} - C_{sy}h_{cs}h_{ts}\right]\left[\dot{u}_c(t) + \dot{u}_c\left(t-\frac{2b}{v}\right) + \dot{u}_c\left(t-\frac{2\ell_s}{v}\right)\right.$$

$$\left. + u_c\left(t-\frac{2(\ell_s+b)}{v}\right)\right]$$

$$+\frac{1}{2a}\left[ds^2 k_{sz} - k_{sy}h_{cs}h_{ts}\right]\left[u_c(t) + u_c\left(t-\frac{2b}{v}\right) + u_c\left(t-\frac{2\ell_s}{v}\right)\right.$$

$$\left. + u_c\left(t-\frac{2(\ell_s+b)}{v}\right)\right]$$

APPENDIX B

ACTIVE FORCES MATRICES

The active forces vector $\underline{f}$ is a four element vector containing the total active lateral force and torque on each truck:

$$\underline{f} = \begin{bmatrix} f_1 \\ f_2 \\ \tau_1 \\ \tau_2 \end{bmatrix}$$

with f_j and τ_j equal to the active force and torque, respectively, on the j^{th} truck.

The desired forces vector, $\underline{f}_i$, serves as the input to the actuators and is determined the following feedback law:

$$\underline{f}_i = \bar{\underline{K}}_m \ddot{\underline{x}} + \bar{\underline{K}}_c \dot{\underline{x}} + \bar{\underline{K}}_k \underline{x}.$$

If $\underline{x}$, the displacement vector, is given by

$$\begin{bmatrix} \psi_{w1} \\ \psi_{w1} \\ y_{w2} \\ \psi_{w2} \\ y_{T1} \\ \psi_{T1} \\ y_{w3} \\ \psi_{w3} \\ y_{w4} \\ \psi_{w4} \end{bmatrix}$$

(first wheelset lateral displacement)
(first wheelset yaw displacement)
(second wheelset lateral displacement)
(second wheelset yaw displacement)
(front truck lateral displacement)
(front truck yaw displacement)
(third wheelset lateral displacement)
(third wheelset yaw displacement)
(fourth wheelset lateral displacement)
(fourth wheelset yaw displacement)

$$\begin{bmatrix} y_{T2} \\ \psi_{T2} \\ y_c \\ \psi_c \\ \Phi_c \end{bmatrix}$$

(rear truck lateral displacement)

(rear truck yaw displacement)

(carbody lateral displacement)

(carbody yaw displacement)

(carbody roll displacement)

then the feedback matrices $\bar{\underline{K}}_m$, $\bar{\underline{K}}_c$, and $\bar{\underline{K}}_k$ for the local controller are given as follows:

$$\bar{\underline{K}}_m^{-1} = \begin{bmatrix} 0 & 0 & 0 & 0 \\ 0 & 0 & 0 & 0 \\ 0 & 0 & 0 & 0 \\ 0 & 0 & 0 & 0 \\ 0 & 0 & 0 & 0 \\ 0 & 0 & 0 & 0 \\ 0 & 0 & 0 & 0 \\ 0 & 0 & 0 & 0 \\ 0 & 0 & 0 & 0 \\ 0 & 0 & 0 & 0 \\ 0 & 0 & 0 & 0 \\ -C_a & -C_a & 0 & 0 \\ -C_a \cdot \ell_s & C_a \cdot \ell_s & 0 & 0 \\ -C_a \cdot h_{cs} & -C_a \cdot h_{cs} & 0 & 0 \end{bmatrix}$$

$$\underline{\underline{K}}_c^{-1} = \begin{bmatrix} 0 & 0 & 0 & 0 \\ 0 & 0 & 0 & 0 \\ 0 & 0 & 0 & 0 \\ 0 & 0 & 0 & 0 \\ 0 & 0 & 0 & 0 \\ 0 & 0 & 0 & 0 \\ 0 & 0 & 0 & 0 \\ 0 & 0 & 0 & 0 \\ 0 & 0 & 0 & 0 \\ 0 & 0 & 0 & 0 \\ 0 & 0 & 0 & 0 \\ -C_v & -C_v & 0 & 0 \\ -C_v \cdot \ell_s & C_v \cdot \ell_s & 0 & 0 \\ -C_v \cdot h_{cs} & -C_v \cdot h_{cs} & 0 & 0 \end{bmatrix}$$

The local controller uses only carbody acceleration and velocity feedbacks, so the displacement feedback matrix is the null matrix. Furthermore, the control scheme uses only lateral forces on the trucks; for this reason the third and fourth columns of the transposed matrices are all zeroes.

The active forces distribution matrix, $\underline{\underline{D}}$, is generalized for all four actuation efforts given by $\underline{f}_o$, the actual forces vector.

$$\underline{\bar{D}} = \begin{bmatrix} 0 & 0 & 0 & 0 \\ 0 & 0 & 0 & 0 \\ 0 & 0 & 0 & 0 \\ 0 & 0 & 0 & 0 \\ 0 & 0 & 0 & 0 \\ 1 & 0 & 0 & 0 \\ 0 & 0 & 1 & 0 \\ 0 & 0 & 0 & 0 \\ 0 & 0 & 0 & 0 \\ 0 & 0 & 0 & 0 \\ 0 & 0 & 0 & 0 \\ 0 & 0 & 0 & 0 \\ 0 & 1 & 0 & 0 \\ 0 & 0 & 0 & 1 \\ -1 & -1 & 0 & 0 \\ -\ell_s & \ell_s & -1 & -1 \\ -h_{cs} & -h_{cs} & 0 & 0 \end{bmatrix}$$

In this form control laws that utilize torque actuators on the trucks can be simulated by adding the appropriate terms to the feedback matrices.

APPENDIX C

VALVE.FOR

```
C
C       This subroutine is run with DYSYS and shows the
C       response of a pneumatic actuator-valve assembly
C       to either a step or sinusoidal command.
C
        SUBROUTINE EQSIM
        COMMON T,DT,Y(30),F(30),STIME,FTIME,NEWDT,NEWRUN,N,
        1      IPR,ICK,ICN,TBREAK,PNEXT,TBACK
        REAL MC,KSY
        REAL kf,k
        REAL KD(3)
        EQUIVALENCE (Y(1),Pa),(Y(2),Pb),(Y(3),Aeff),(Y(4),Wa),(Y(5),Wb),
        1       (Y(6),Force)
C
*
        IF (NEWDT .EQ.  0)GOTO 35
        IF (NEWDT .NE. -1)GOTO 20
C
C
C*************************************************************************
*
                READ(8,100)NDUM
                READ(8,2020) MC
*
C                                       READ SUSPENSION PARAMETERS
                READ(8,100)NDUM
                READ(8,2020)KSY
*
                READ(8,100)NDUM
                READ(8,2020)CSY
*
                READ(8,100)NDUM
                READ(8,2020)KD(1),KD(2),KD(3)
*
                READ(8,100)NDUM
                READ(8,2020)kf
C
                READ(8,100)NDUM
                READ(8,2020)k,R,Ts,g,Vo,Avo,Apo,Cap
*
                READ(8,100)NDUM
                READ(8,2020)Pe,Ps,Pai,Pbi,Amax,Fp,Freq
*
C
C
                WRITE(5,105)MC
                WRITE(5,105)KSY,CSY
```

```
                WRITE(5,105)KD(1),KD(2),KD(3)
                WRITE(5,105)kf
                WRITE(5,105)k,R,Ts,g,Vo,Avo,Apo,Cap
                WRITE(5,105)Pe,Ps,Pai,Pbi,Amax,Fp,Freq
C
  100   FORMAT(8I4)
 2020   FORMAT(8G15.5)
  105   FORMAT(1X,/,1X,8G10.2)
C
C
                                        !       Yc      =       0.0
                                        !       Yt      =       0.0
        Pa      =       Pai
        Pb      =       Pbi
        H       =       R*Ts/g          !       These terms and variables
        WF      =       2*3.14*Freq     !       have no meaning in this
  20    CONTINUE                        !       program, since they don't
c                                       !       change!
*****************************************************************************
c
        Apa     =       Apo             !       + Cap*(Yc-Yt)
        Apb     =       Apo             !       - Cap*(Yc-Yt)
        Force = Pa*Apa - Pb*Apb
c
        IF(T .GE. 0.0)GOTO 25
                Aeff = 0.0
          GOTO 30
C
  25    Fi      =       Fp * cos (WF * T)
        Aeff    =       kf * (Fi - Force)
C
  30    IF(Aeff .GE. 0.0)then
          If(Aeff .GT. Amax)Aeff = Amax
                Wa2 = 0.0
                Wb1 = 0.0
           Call Flow(Pa,Ps,Aeff,Ts,Wa1)
           Call Flow(Pe,Pb,Aeff,Ts,Wb2)
        ENDIF
c
        IF(Aeff .LT. 0.0) THEN
          If(Aeff .LT. -Amax)Aeff = -Amax
                Aeffn = - Aeff
                Wa1 = 0.0
                Wb2 = 0.0
           Call Flow(Pe,Pa,Aeffn,Ts,Wa2)
           Call Flow(Pb,Ps,Aeffn,Ts,Wb1)
        ENDIF
c
```

```
                Wa      =       Wa1 - Wa2
                Wb      =       Wb1 - Wb2
c
                Va      =       Vo
                Vb      =       Vo
c
   35           F(1)    =       k/Va * (H*Wa)
                F(2)    =       k/Vb * (H*Wb)
c
C
        RETURN
        END
        SUBROUTINE FLOW(Pd,Pu,Aeff,Ts,W)
        REAL k
c       This program calculates the compressible flow through
c       an orifice.
c
c       Pu                                      !       psia
c       Aeff                                    !       in**2
c       Ts                                      !       R
c       W                                       !       lbf/sec
        C1 = 2.06                               !       sqrt(R)/sec
        C2 = 0.532                              !       sqrt(R)/sec
        k = 1.4
c
        If(Pd/Pu .LE. 0.528) GOTO 10
c
        If(Pd .GT. Pu)GOTO 5
        W  =  Aeff * C1 * Pu / Ts**0.5  * (Pd/Pu)**(1./k)
        1 *( 1. - (Pd/Pu)**((k-1)/k) )**0.5
        RETURN
    5   Pu5 = Pd
        Pd5 = Pu
        W  = - Aeff * C1 * Pu5 / Ts**0.5  * (Pd5/Pu5)**(1./k)
        1 *( 1. - (Pd5/Pu5)**((k-1)/k) )**0.5
        RETURN
c
   10   W  =  Aeff * C2 * Pu / Ts**0.5
c
        return
        end
```

APPENDIX D
STROKE.FOR

```
C
C       This program runs with DYSYS and provides a time
C       domain simulation of the disturbance response of a
C       pneumatic actuator-valve assembly for sinusoidal
C       stroke disturbances.
C
        SUBROUTINE EQSIM
        COMMON T,DT,Y(30),F(30),STIME,FTIME,NEWDT,NEWRUN,N,
        1      IPR,ICK,ICN,TBREAK,PNEXT,TBACK
        REAL MC,KSY
        REAL kf,k
        REAL KD(3)
        EQUIVALENCE (Y(1),Yac),(Y(2),Pa),(Y(3),Pb),
        1       (Y(4),Aeff),(Y(5),Wa),(Y(6),Wb),
        1       (Y(7),Force),(Y(8),Vac),
        1       (Y(9),Apa),(Y(10),Apb)
C
*
        IF (NEWDT .EQ.  0)GOTO 35
        IF (NEWDT .NE. -1)GOTO 20
C
C
C*************************************************************************
*
                READ(8,100)NDUM
                READ(8,2020) MC
*
C                                       READ SUSPENSION PARAMETERS
                READ(8,100)NDUM
                READ(8,2020)KSY
*
                READ(8,100)NDUM
                READ(8,2020)CSY
*
                READ(8,100)NDUM
                READ(8,2020)KD(1),KD(2),KD(3)
*
                READ(8,100)NDUM
                READ(8,2020)kf
C
                READ(8,100)NDUM
                READ(8,2020)k,R,Ts,g,Vo,Avo,Apo,Cap
*
                READ(8,100)NDUM
                READ(8,2020)Pe,Ps,Pai,Pbi,Amax,Fp,Freq,Vp
*
C
```

```
C
                WRITE(5,105)MC
                WRITE(5,105)KSY,CSY
                WRITE(5,105)KD(1),KD(2),KD(3)
                WRITE(5,105)kf
                WRITE(5,105)k,R,Ts,g,Vo,Avo,Apo,Cap
                WRITE(5,105)Pe,Ps,Pai,Pbi,Amax,Fp,Freq,Vp
C
  100   FORMAT(15I4)
 2020   FORMAT(15G15.5)
  105   FORMAT(1X,/,1X,15G10.2)
C
C
        Yac     =       0.0
        Pa      =       Pai
        Pb      =       Pbi
        H       =       R*Ts/g
        WF      =       2.*3.14*Freq
c
*******************************************************************************
c
c       This section runs once a time step.
c
c
c
  20    Apa     =       Apo     +       Cap*Yac
        Apb     =       Apo     -       Cap*Yac
        Force   =       Pa*Apa  -       Pb*Apb
c
        IF(T .GE. 0.0)GOTO 25
                  Vac  = 0.0
                  GOTO 30
C
c
  25    Vac     =       Vp * cos (WF * T)
C
c
c
  30    Aeff    =       kf * (Fp - Force)
        IF(Aeff .GE. 0.0)then
          If(Aeff .GT. Amax)Aeff = Amax
                Wa2 = 0.0
                Wb1 = 0.0
           Call Flow(Pa,Ps,Aeff,Ts,Wa1)
           Call Flow(Pe,Pb,Aeff,Ts,Wb2)
           ENDIF
c
        IF(Aeff .LT. 0.0) THEN
```

```
          If(Aeff .LT. -Amax)Aeff = -Amax
                Aeffn = - Aeff
                Wa1 = 0.0
                Wb2 = 0.0
           Call Flow(Pe,Pa,Aeffn,Ts,Wa2)
           Call Flow(Pb,Ps,Aeffn,Ts,Wb1)
           ENDIF
c
                Wa      =       Wa1 - Wa2
                Wb      =       Wb1 - Wb2
c
                Va      =       Vo      +       Yac*Avo
                Vb      =       Vo      -       Yac*Avo
c
**************************************************************************
c
c       This section runs 4 times every time step.
c
c
   35           F(1)    =       Vac
                F(2)    =       k/Va * (H*Wa - Pa*Avo*Vac)
                F(3)    =       k/Vb * (H*Wb + Pb*Avo*Vac)
c
C
        RETURN
        END
        SUBROUTINE FLOW(Pd,Pu,Aeff,Ts,W)
        REAL k
c       This program calculates the compressible flow through
c       an orifice.
c
c       Pu                                      !       psia
c       Aeff                                    !       in**2
c       Ts                                      !       R
c       W                                       !       lbf/sec
        C1 = 2.06                               !       sqrt(R)/sec
        C2 = 0.532                              !       sqrt(R)/sec
        k = 1.4
c
        If(Pd/Pu .LE. 0.528) GOTO 10
c
        If(Pd .GT. Pu)GOTO 5
        W  =  Aeff * C1 * Pu / Ts**0.5  * (Pd/Pu)**(1./k)
        1 *( 1. - (Pd/Pu)**((k-1)/k) )**0.5
        RETURN
    5   Pu5 = Pd
        Pd5 = Pu
        W  = - Aeff * C1 * Pu5 / Ts**0.5  * (Pd5/Pu5)**(1./k)
```

```
      1 *( 1. - (Pd5/Pu5)**((k-1)/k) )**0.5
      RETURN
c
   10 W  =  Aeff * C2 * Pu / Ts**0.5
c
      return
      end
```

APPENDIX E

AIRMASS.FOR

```
C
C       This subroutine is run with DYSYS and simulates a
C       single D.O.F. mass with a pneumatic suspension.
C
        SUBROUTINE EQSIM
        COMMON T,DT,Y(30),F(30),STIME,FTIME,NEWDT,NEWRUN,N,
        1      IPR,ICK,ICN,TBREAK,PNEXT,TBACK
        REAL MC,KSY
        REAL kf,k
        REAL KD(3)
        EQUIVALENCE (Y(1),Yc),(Y(2),Vc),(Y(3),Pa),(Y(4),Pb),(Y(5),Yt),
        1       (Y(6),Vt),(Y(7),Aeff),(Y(8),Wa),(Y(9),Wb),
        1       (Y(10),Force),(Y(11),Apa),(Y(12),Apb),(Y(13),Stroke),
        1       (Y(14),Accel),(Y(15),Fi)
C
*
        IF (NEWDT .EQ.  0)GOTO 35
        IF (NEWDT .NE. -1)GOTO 20
C
C
C*************************************************************************
*
                READ(8,100)NDUM
                READ(8,2020) MC
*
C                                       READ SUSPENSION PARAMETERS
                READ(8,100)NDUM
                READ(8,2020)KSY
*
                READ(8,100)NDUM
                READ(8,2020)CSY
*
                READ(8,100)NDUM
                READ(8,2020)KD(1),KD(2),KD(3)
*
                READ(8,100)NDUM
                READ(8,2020)kf
C
                READ(8,100)NDUM
                READ(8,2020)k,R,Ts,g,Vo,Avo,Apo,Cap
*
                READ(8,100)NDUM
                READ(8,2020)Pe,Ps,Pai,Pbi,Amax
*
                READ(8,100)NDUM
                READ(8,2020)Yt1,Yt2,Yt3,Yt4,Yt5,Yt6
*
```

```
                READ(8,100)NDUM
                READ(8,2020)Freq1,Freq2,Freq3,Freq4,Freq5,Freq6
*
C
C
                WRITE(5,105)MC
                WRITE(5,105)KSY,CSY
                WRITE(5,105)KD(1),KD(2),KD(3)
                WRITE(5,105)kf
                WRITE(5,105)k,R,Ts,g,Vo,Avo,Apo,Cap
                WRITE(5,105)Pe,Ps,Pai,Pbi,Amax
                WRITE(5,105)Yt1,Yt2,Yt3,Yt4,Yt5,Yt6
                WRITE(5,105)Freq1,Freq2,Freq3,Freq4,Freq5,Freq6
C
  100   FORMAT(15I4)
 2020   FORMAT(15G15.5)
  105   FORMAT(1X,/,1X,15G10.2)
C
C
        Yc      =       0.
        Yt      =       0.
        Vc      =       0.
        Vt      =       0.
        Pa      =       Pai
        Pb      =       Pbi
        A       =       Ksy/Mc
        B       =       Csy/Mc
        D       =       Ap/Mc
        H       =       R*Ts/g
        WF1     =       2.*3.14*Freq1
        WF2     =       2.*3.14*Freq2
        WF3     =       2.*3.14*Freq3
        WF4     =       2.*3.14*Freq4
        WF5     =       2.*3.14*Freq5
        WF6     =       2.*3.14*Freq6
c
        Ncount          =       0.0
        SumYc           =       0.0
        SumYc2          =       0.0
        SumVact         =       0.0
        SumVact2        =       0.0
        SumYt           =       0.0
        SumYt2          =       0.0
        SumAeff         =       0.0
        SumAeff2        =       0.0
        SumFrc          =       0.0
        SumFrc2         =       0.0
        SumAc           =       0.0
```

```
      SumAc2          =       0.0
      SumStr          =       0.0
      SumStr2         =       0.0
      SumW            =       0.0
      SumW2           =       0.0
c
c
c*************************************************************************
c
  20  CONTINUE
c
c                     This section is processed only if the first time
c                     in the time step.
c
c
            Yt        =       Yt1 * sin (WF1*T+1.)    +
     1                        Yt2 * sin (WF2*T+4.)    +
     1                        Yt3 * sin (WF3*T+3.)    +
     1                        Yt4 * sin (WF4*T+6.)    +
     1                        Yt5 * sin (WF5*T+2.)    +
     1                        Yt6 * sin (WF6*T)
c
            Vt        =       WF1 * Yt1 * cos (WF1*T+1.)      +
     1                        WF2 * Yt2 * cos (WF2*T+4.)      +
     1                        WF3 * Yt3 * cos (WF3*T+3.)      +
     1                        WF4 * Yt4 * cos (WF4*T+6.)      +
     1                        WF5 * Yt5 * cos (WF5*T+2.)      +
     1                        WF6 * Yt6 * cos (WF6*T)
c
            Apa       =       Apo     +       Cap*(Yc-Yt)
            Apb       =       Apo     -       Cap*(Yc-Yt)
c
            Force     =       Pa*Apa  -       Pb*Apb
            Stroke    =       Yc      -       Yt
            Vact      =       Vc      -       Vt
c
c
      IF(T .GE. 0.0)GOTO 25
            Yt        =       0.0
            Vt        =       0.0
c
c
c
  25        Fi        =       KD(2) * Vc   +
     1                        KD(3) * (A*(Yt - Yc) + B*(Vt-Vc) + Force/Mc)
c
            Accel     =       A*(Yt - Yc) + B*(Vt-Vc) + Force/Mc
c
```

```
c
 30             Aeff    =       kf * (Fi - Force)
                IF(Aeff .GE. 0.0)then
                    IF(Aeff .GT. Amax) Aeff=Amax
                        Wa2 = 0.0
                        Wb1 = 0.0
                        Call Flow(Pa,Ps,Aeff,Ts,Wa1)
                        Call Flow(Pe,Pb,Aeff,Ts,Wb2)
                ENDIF
c
                IF(Aeff .LT. 0.0) THEN
                    IF(Aeff .lt. -Amax)Aeff = -Amax
                        Aeffn = - Aeff
                        Wa1 = 0.0
                        Wb2 = 0.0
                        Call Flow(Pe,Pa,Aeffn,Ts,Wa2)
                        Call Flow(Pb,Ps,Aeffn,Ts,Wb1)
                ENDIF
c
                Wa      =       Wa1 - Wa2
                Wb      =       Wb1 - Wb2
c
                Va      =       Vo + (Yc-Yt)*Avo
                Vb      =       Vo - (Yc-Yt)*Avo
c
        Ncount          =       Ncount          +       1
*
        SumYc           =       SumYc           +       Yc
        SumYc2          =       SumYc2          +       Yc**2
*
        SumYt           =       SumYt           +       Yt
        SumYt2          =       SumYt2          +       Yt**2
*
        SumVact         =       SumVact         +       Vact
        SumVact2        =       SumVact2        +       Vact**2
*
        SumAeff         =       SumAeff         +       Aeff
        SumAeff2        =       SumAeff2        +       Aeff**2
*
        SumFrc          =       SumFrc          +       Force
        SumFrc2         =       SumFrc2         +       Force**2
*
        SumAc           =       SumAc           +       Accel
        SumAc2          =       SumAc2          +       Accel**2
*
        SumStr          =       SumStr          +       Stroke
        SumStr2         =       SumStr2         +       Stroke**2
*
```

```
      SumW          =     SumW          +     Wa1
      1                                 +     Wb1
      SumW2         =     SumW2         +     Wa1**2
      1                                 +     Wb1**2
*
      IF(T .GE. FTIME)THEN
*
        AYc         =     SumYc   / Ncount
        VYc         =     ((SumYc2-SumYc**2/Ncount) / (Ncount-1))
*
        AYt         =     SumYt   / Ncount
        VYt         =     ((SumYt2-SumYt**2/Ncount) / (Ncount-1))
*
        AVact       =     SumVact / Ncount
        VVact       =     ((SumVact2-SumVact**2/Ncount) / (Ncount-1))
*
        AAeff       =     SumAeff / Ncount
        VAeff       =     ((SumAeff2-SumAeff**2/Ncount) / (Ncount-1))
*
        AFrc        =     SumFrc  / Ncount
        VFrc        =     ((SumFrc2-SumFrc**2/Ncount) / (Ncount-1))
*
        AAc         =     SumAc   / Ncount
        VAc         =     ((SumAc2-SumAc**2/Ncount) / (Ncount-1))
*
        AStr        =     SumStr  / Ncount
        VStr        =     ((SumStr2-SumStr**2/Ncount) / (Ncount-1))
*
        AW          =     SumW    / Ncount
        VW          =     ((SumW2-SumW**2/Ncount) / (Ncount-1))
*
      Write(5,301)
 301  FORMAT(//22X,'Mean',19X,'Variance'//)
*
      Write(5,302)AYc,VYc
      Write(5,303)AYt,VYt
      Write(5,309)AVact,VVact
      Write(5,304)AAeff,VAeff
      Write(5,305)AFrc,VFrc
      Write(5,306)AAc,VAc
      Write(5,307)AStr,VStr
      Write(5,308)AW,VW
*
 302  FORMAT(1X,'Yc',15X,E10.3,11X,E10.3/)
 303  FORMAT(1X,'Yt',15X,E10.3,11X,E10.3/)
 304  FORMAT(1X,'Aeff',13X,E10.3,11X,E10.3/)
 305  FORMAT(1X,'Force',12X,E10.3,11X,E10.3/)
 306  FORMAT(1X,'Accel',12X,E10.3,11X,E10.3/)
```

```
 307     FORMAT(1X,'Stroke',11X,E10.3,11X,E10.3/)
 308     FORMAT(1X,'Flow',13X,E10.3,11X,E10.3/)
 309     FORMAT(1x,'Vact',13X,E10.3,11X,E10.3/)
*
         endif
*
*****************************************************************
c        This section runs every time.

   35            F(1)    =       Vc
*
                 F(2)    =       A*(Yt - Yc) + B*(Vt-Vc) +
         1                       (Pa*Apa - Pb*Apb)/Mc
*
                 F(3)    =       k/Va * (H*Wa - Pa*Avo*(Vc-Vt))
*
                 F(4)    =       k/Vb * (H*Wb + Pb*Avo*(Vc-Vt))
*
*
         RETURN
         END
*****************************************************************************
*****************************************************************************
         SUBROUTINE FLOW(Pd,Pu,Aeff,Ts,W)
         REAL k
c        This program calculates the compressible flow through
c        an orifice.
c
c        Pu                                !       psia
c        Aeff                              !       in**2
c        Ts                                !       R
c        W                                 !       lbf/sec
         C1 = 2.06                         !       sqrt(R)/sec
         C2 = 0.532                        !       sqrt(R)/sec
         k = 1.4
c
         If(Pd/Pu .LE. 0.528) GOTO 10
c
         If(Pd .GT. Pu)GOTO 5
         W  =  Aeff * C1 * Pu / Ts**0.5  * (Pd/Pu)**(1./k)
         1 *( 1. - (Pd/Pu)**((k-1)/k) )**0.5
         RETURN
    5    Pu5 = Pd
         Pd5 = Pu
         W  = - Aeff * C1 * Pu5 / Ts**0.5  * (Pd5/Pu5)**(1./k)
         1 *( 1. - (Pd5/Pu5)**((k-1)/k) )**0.5
         RETURN
c
```

```
   10    W  =  Aeff * C2 * Pu / Ts**0.5
c
         return
         end
```